Observations on the Directional Development Of Wind-Waves in Mixed Seas

by Dung Nguy

Technical Report
APL-UW TR9802
March 1998

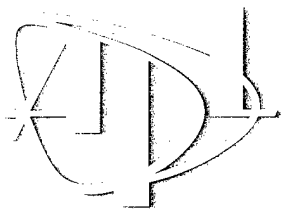

Applied Physics Laboratory University of Washington
Seattle, Washington 98105-6698

Contracts N00039-91-C-0072 and N00014-96-1-0325

Observations on the Directional Development
of
Wind-Waves in Mixed Seas

by

Dung Nguy

A thesis submitted in partial fulfillment
of the requirements for the degree of

Master of Science in Mechanical Engineering

University of Washington

1998

Approved by Peter H Dahl
Chairman of Supervisory Committee

Program Authorized
to Offer Degree Mechanical Engineering

Date March 16, 1998

In presenting this thesis in partial fulfillment of the requirements for a Master's degree at the University of Washington, I agree that the Library shall make its copies freely available for inspection. I further agree that extensive copying of this thesis is allowable only for scholarly purposes, consistent with "fair use" as prescribed in the U.S. Copyright Law. Any other reproduction for any purposes or by any means shall not be allowed without my written permission.

Signature 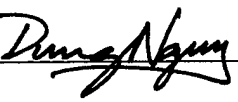

Date March 13, 1998

FOREWORD

This report is a duplication of the thesis submitted in partial fulfillment of the requirements for the Master of Science in Mechanical Engineering degree at the University of Washington in March 1998. Dr. Peter H. Dahl was the chairperson of the supervisory committee.

University of Washington
Abstract

Observations on the Directional Development
of Wind-Waves in Mixed Seas

By Dung K. Nguy

Chairman of Supervisory Committee
Professor Peter H. Dahl
Department of Mechanical Engineering

Sea surface measurements recorded by a Directional Waverider buoy, deployed in the Gulf of Mexico, served as the basis of this investigation into the evolution of wind-waves in mixed seas. Five events of mixed seas were selected and examined in detail. These events chronicled the growth of new wind-seas in the presence of background swell during periods of high wind forcing. Under sufficiently high wind forcing, the wind-sea system developed similarly to cases of pure wind-waves. Wind-wave systems under wind action were found to grow at an angle to the wind vector and away from the mean direction of the low frequency wave system. Under low winds, the wind-sea evolution was dominated by interactions with swell. Situations of mixed seas showed that coupling between wave systems had a stabilizing effect of reducing a multimodal energy spectrum to a unimodal wave spectrum. Coupling between wave systems was observed to occur over local frequencies as predicted by the weakly nonlinear wave-wave interaction theory, and also over a wider frequency range. In cases where the energy spectrum of swell and wind-sea was distinctly bimodal, an equivalent wind-sea was partitioned from the long wave components to allow for a comparison with the growth of pure wind-waves. The directionality of the wind-sea and swell systems was found to influence the development of wind-waves. The directional spread distribution of mixed seas exhibited features different from those of pure wind-seas. The minimum angular spread of wind-seas was generally located at or above the wind-wave peak frequency. Finally, this modest collection of data supported the current hypothesis that opposed swell intensifies wind-wave growth, whereas an aligned swell attenuates wave growth.

Table of Contents

List of Figures

List of Tables

Acknowledgments

I would like to thank Professors Bruce Adee and Jim Riley for serving on the supervisory committee, and Dr. Bill Plant and Professor Peter Dahl for deterring me from my original route. I wish express my sincere gratitude to Professor Dahl for his guidance and patience. This thesis work was funded by the Office of Naval Research Code 3210A, via contract number N00039-91-C-0072 and grant number N00014-96-1-0325.

1. Background

1.1 Introduction

Beyond being a challenging academic interest, the study of ocean waves offers practical applications in coastal engineering, ship design, ship routing, and offshore structural engineering. The development of an ocean wave field driven by a steady, uniform wind field has been investigated at length, and extensive studies of fetch-limited wave growth have uncovered many mysteries associated with the evolution of pure wind-waves. However, wave evolution in the open ocean commonly consists of complex conditions. Meteorological conditions encountered at sea are often neither steady nor uniform; the sea state is often a mixture of wind-waves generated by a local wind field and swells propagating from a distant generation source. Such mixed seas of swell and wind-waves result in a multimodal wave field and the development of this multi-system field remains to be explored.

In researching the development of pure wind-waves, and the evolution of their energy spectrum, many studies, such as Hasselmann et al. (1973) and Donelan et al. (1985), generally omit multimodal spectra of coexisting wave systems from their final analysis. Studies on coexisting swell and wind-waves have been largely limited to laboratory experiments. Results from these experiments indicate that complex interactions exist between the wave systems. These simple, devised experiments provide us with a clue of what is to be expected in the open sea. Until recently, the effects of background swell on the development of wind-seas have not been investigated. In this observational study, some characteristics of the development of wind-waves in the presence of a swell system will be analyzed.

Before discussing the experiment and the field observations of mixed swell and wind-seas, basic forms of the wave spectrum, as well as the results of previous mixed seas studies, are briefly reviewed in the remainder of Section 1. Next, the experiment is described in Section 2; preliminary results, in the first part of Section 3. Five mixed seas cases are presented in the second part of Section 3. The collection of wave spectra in Sections 3.3 and 3.4 is arranged chronologically, allowing the reader to follow the development of the wave field. The reader is advised to keep in mind that, *in Sections 3 and 4, reference to the wave spectra will be dictated by the discussion of the wave growth characteristics, and not by the chronology of the events.*

1.2 Omnidirectional Wave Spectrum

Since the 1950s, spectral analysis has been an indispensable tool in studying the ocean surface. By representing the sea surface as a superposition of many component *sine* waves, the spectral method transforms a random-looking surface into a comprehensible description of the sea state, as a function dependent on the wave-number or the wave frequency. Whereas the wavenumber energy spectrum can be obtained by a Fourier transform of the spatial correlation of the sea surface, the frequency energy spectrum is reconstructed by a Fourier transform of the temporal correlation. A simple conversion from frequency space to wavenumber space can be approximated using the dispersion relation obtained from the linear theory for deep-water waves, $\omega^2 = gk$, where ω is the angular wave frequency, k is the wavenumber and g is the gravitational acceleration. (See Appendix.) In this study,

the energy density spectrum is represented in frequency space, so further discussion of the wavenumber spectrum is limited.

The wave energy spectrum has a directional and a non-directional representation. When the directional information of a sea state is not considered, the resulting spectrum describes only the wave amplitude of each frequency component and is referred to as an omnidirectional or one-dimensional frequency spectrum, $\Phi(f)$. Although the shape and magnitude of the spectrum depend on numerous variables, such as wind speed, wind direction, fetch distance, and wind duration, most spectral models are valid for simple conditions, subject to one or two variables, i.e. wind speed and fetch distance. Although many spectral forms have been presented over the years, two models are considered classical works and only these two unimodal forms will be summarized here.

Early omnidirectional spectral models are based on empirical fits for specific wind fields. For a steady wind, Pierson and Moskowitz (1964) proposed a forecast wave model for fully developed seas. The Pierson-Moskowitz spectrum (henceforth referred to as the P-M spectrum) predicts a mature wave field under the action of a steady wind, over a long fetch distance and over a long duration. In a fully developed sea, a quasi-equilibrium state is achieved and the wave spectrum can be defined by one variable--the wind speed. Although wind conditions at sea are rarely ideal, the P-M spectral formula is generally accepted as a measure of a fully developed, or near fully developed, sea. The P-M spectrum is a function of the frequency range and the peak frequency of the wind-sea:

$$\Phi(f) = \frac{\alpha g^2}{(2\pi)^4} f^{-5} \exp\left[-\beta\left(\frac{f_p}{f}\right)^4\right] \qquad \text{Eq. 1a}$$

where coefficients $\alpha = 0.081$ and $\beta = 0.74$, and where the peak frequency parameter, f_p, is dependent on $U_{19.5}$, the wind speed measured at 19.5 m (Pierson, 1964)

$$f_p = \frac{0.88\, g}{2\pi U_{19.5}}. \qquad \text{Eq. 1b}$$

Whereas the P-M shape is a one-variable, one-parameter spectrum, the JONSWAP spectral form is a two-variable, five-parameter formulation. The extensive JONSWAP (Joint North Sea Wave Project) study investigated the development of wind-seas under quasi-steady wind conditions with a fetch variable dependency. From the JONSWAP database, Hasselmann et al. (1973) proposed a fetch-limited spectrum of the form

$$\Phi(f) = \frac{\alpha g^2}{(2\pi)^4} f^{-5} \exp\left[\frac{-5}{4}\left(\frac{f_p}{f}\right)^4\right] \cdot G(f) \qquad \text{Eq. 2a}$$

where

$$f_p = \frac{3.5g}{U}\left(\frac{gX}{U^2}\right)^{-0.33}$$

$$\alpha = 0.076\left(\frac{Xg}{U^2}\right)^{-0.22} \qquad \text{Eq. 2b}$$

$$G(f) = \gamma^{\exp\left(\frac{(f-f_p)^2}{2\sigma f_p^2}\right)}$$

$$\sigma = \begin{cases} \sigma_a & \text{for} \quad f < f_p \\ \sigma_b & \text{for} \quad f > f_p \end{cases}$$

and X is the fetch distance, $G(f)$ is the peak enhancement term, and U is the wind speed taken at the standard height of 10 m. The five parameters consist of two scale parameters and three shape parameters: respectively, peak frequency f_p, fetch dependent coefficient α, peak enhancement factor γ, left peak width σ_a, and right peak width σ_b. From the large number of wave measurements, Hasselmann et al. (1976) determined the average values of the shape parameters to be

$\gamma = 3.3$

$\sigma_a = 0.07$ Eq. 2c

$\sigma_b = 0.09.$

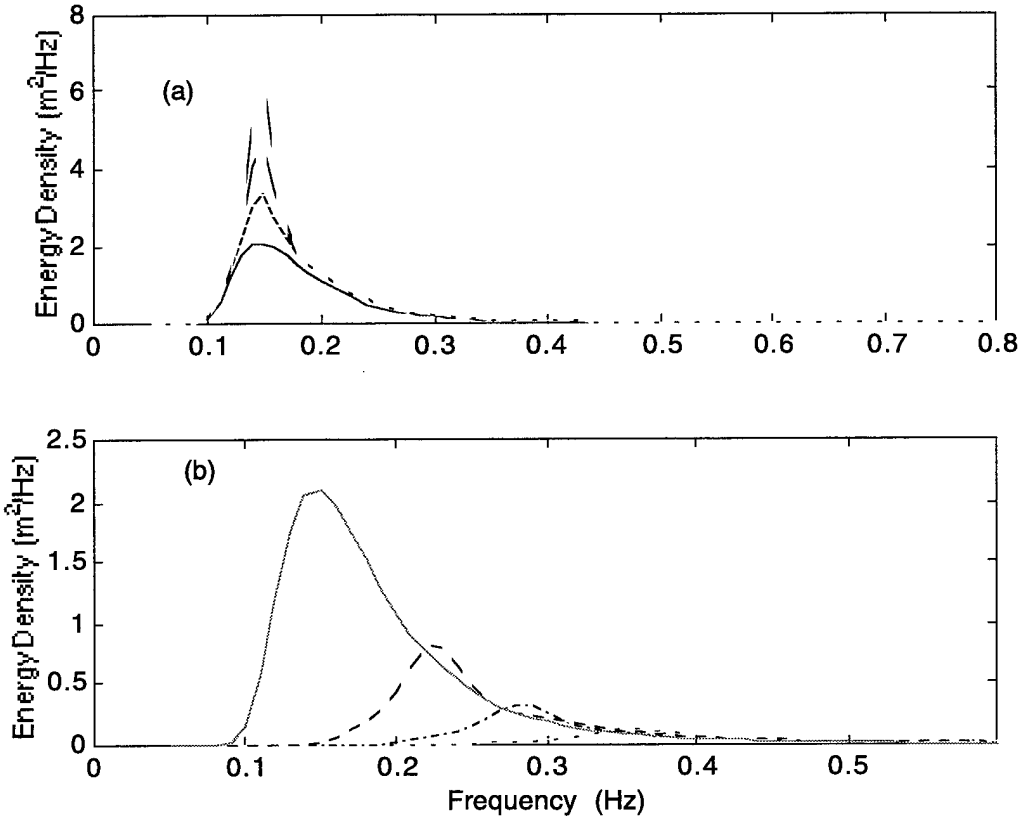

Figure 1. Examples of unimodal spectra. P-M and JONSWAP spectra for U=10 m/s (a) P-M (f) and JONSWAP with different peak enhancement factors: γ =1.4 (--), γ =2.0 (-.-), γ =2.8 (). (b) P-M (f) and JONSWAP at different fetch distances: F=10 km (..), F=20 km (-.-), F=40 km (--).

With the values of Eq. 2c, and an estimate of the coefficient α, the JONSWAP spectrum simplifies to a one-parameter model dependent on two variables, the wind speed U and the fetch distance X. The JONSWAP spectrum is similar to the P-M spectrum, but modified to include an overshoot effect characterized by the peak enhancement factor γ. The overshoot phenomenon has been identified as part of the

wind-wave generation process, occurring in the transition regime between the initial growth stage and the equilibrium or developed stage (Barnett and Sutherland, 1968). The peak enhancement factor approaches 1 as the fetch increases and the spectrum further develops toward the P-M form. As illustrated in Figure 1a, the JONSWAP spectrum approaches the P-M form as $\gamma \to 1$. A comparison of the JONSWAP and the P-M unimodal spectra is illustrated in Figure 1b, driven by a wind of 10 m/s.

While there are numerous parametric models of unimodal wave fields, there are very few models of multimodal wave fields. Multimodal seas are caused by distant swell systems propagating into a region of local wind-wave generation or by transient atmospheric conditions, such as storms and rapidly changing winds. Ochi and Hubble (1976) proposed a six-parameter model designed to forecast the wave field in stormy seas. The six-parameter spectrum was developed to represent most stages of wave development during a storm. The spectrum consists of one narrow frequency domain for swells, and another for wind-waves. Each domain is characterized by three spectral parameters: a spectral shape factor λ, a peak frequency ω_p, and a significant wave height ζ. The complete spectrum is attained by a superposition of the swell and wind-sea regimes

$$\Phi(\omega) = \frac{1}{4} \sum_{j=1,2} \frac{\left(\frac{4\lambda_j + 1}{4} \omega_{pj}\right)^{\lambda_j}}{\Gamma(\lambda_j)} \frac{\zeta_j^2}{4\lambda_j + 1} \exp\left[-\left(\frac{4\lambda_j + 1}{4}\right) \cdot \left(\frac{\omega_{pj}}{\omega}\right)^4 \right] \qquad \text{Eq. 3}$$

where j denotes the low (swell) and high (wind-sea) frequency domains. The Ochi and Hubble (1976) study categorized the wave measurements into different development stages, for which the six spectral parameters were numerically determined for best agreement with their collection of data. In the early stages of wave growth, the high frequency wind-sea peak constitutes a prominent contribution to the

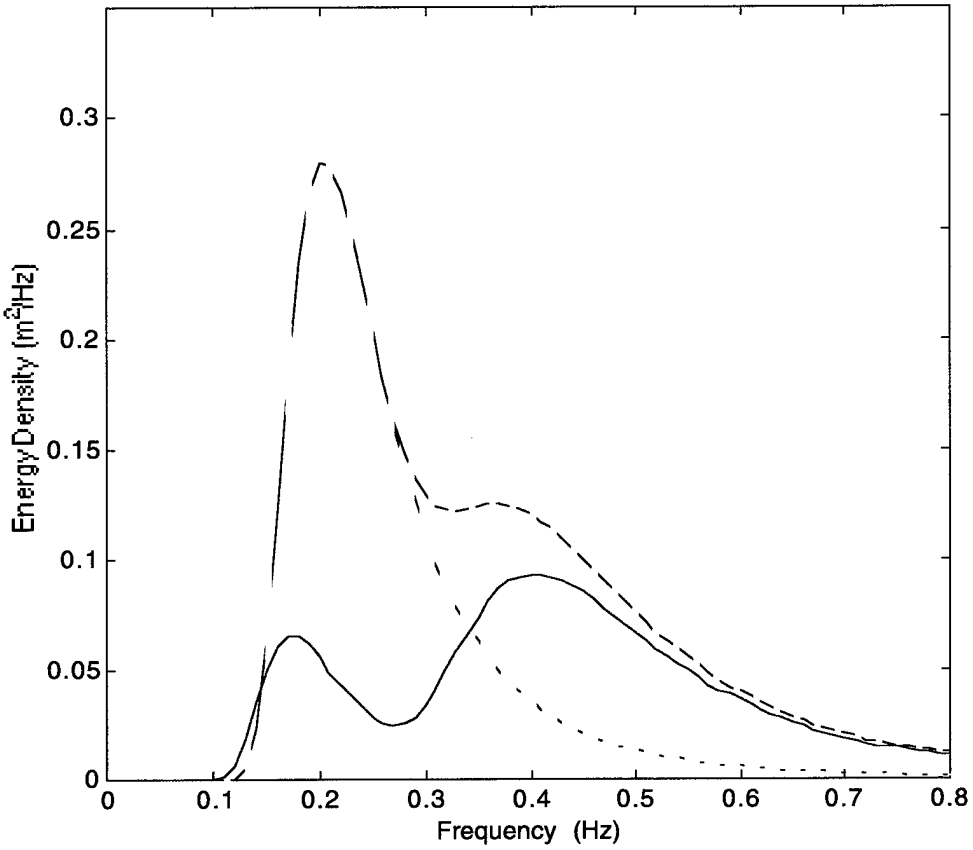

Figure 2. Ochi and Hubble (1976) spectrum with low frequency peak (f_{p1}) at 0.15 Hz and a second peak (f_{p2}) at 0.3 Hz, with shape factors: $\gamma_1 = 2, \gamma_2 = 4$ (*f*); $\gamma_1 = 4$, $\gamma_2 = 4$ (--); $\gamma_1 = 4$, $\gamma_2 = 2$ (..).

total wave energy. In cases of older, more developed seas, the six-parameter spectrum reduces to a form equivalent to a unimodal spectrum discussed above. If the presence of swell persists, the low frequency swell peak dominates the energy spectrum as the transient storm fades and the wind-wave system degenerates. Examples of double-peaked spectra for various spectral shape factors are given in Figure 2.

1.3 Directional Wave Spectrum

The one-dimensional spectral forms described in Section 1.2 offer no information on the directionality of a wave field. For a more complete representation of the sea surface, the directional information of each wave component must be incorporated into the omnidirectional spectrum to form a directional or two-dimensional energy spectrum. The directional data of a wave component consist of a mean direction of propagation, $\theta_m(f)$, and a directional spread about the mean wave direction, $\sigma(f)$. The directional wave spectrum is defined as

$$\Phi(f,\theta) = \Phi(f)D(f,\theta) \qquad \text{Eq. 4}$$

where the directional spreading function, $D(f,\theta)$, satisfies the following condition

$$\int_{-\pi}^{\pi} D(f,\theta)d\theta = 1. \qquad \text{Eq. 5}$$

Thus it follows that the directional spectrum can be reduced to a marginal frequency spectrum by integrating over all directions

$$\Phi(f) = \int_{-\pi}^{\pi} \Phi(f,\theta)d\theta \qquad \text{Eq. 6}$$

where $\Phi(f)$ is the omnidirectional spectrum discussed in the previous section. The angular distribution function $D(f,\theta)$ models the diffusion of the one-dimensional energy spectrum about the mean propagation directions. The directional distribution of wave energy is commonly modeled by a cos^{2s} or a $sech^2\beta$ function.

An early directional model of the cos^{2s} form proposed by Mitsuyasu et al. (1975) is dependent on the wave age of the wind-sea and the peak frequency

$$D(f,\theta) = \frac{2^{2s-1}}{\pi}\frac{\Gamma^2(s+1)}{\Gamma(s+1)}cos^{2s}\left(\frac{(\theta-\theta_m)}{2}\right) \qquad \text{Eq. 7}$$

and the spread parameter s is

$$s = \begin{cases} s_p \left(\dfrac{f}{f_p} \right)^{5} & \text{for} \quad f < f_p \\ s_p \left(\dfrac{f}{f_p} \right)^{-2.5} & \text{for} \quad f > f_p \end{cases} \qquad \text{Eq. 8}$$

where the angular spread at the peak, s_p, was determined empirically to be

$$s_p = 11.5 \left(\frac{U}{C_p} \right)^{-2.5} .$$

The term s_p depends on a wave age parameter, defined as the ratio of the phase speed of the peak wind-sea frequency to the wind speed at the standard 10-m height, C_p/U.

The wave age parameter is similar to the fetch distance in that it is an indicator of the development stage of wind-generated waves. For a young wind-sea, the phase speed of a peak frequency is slower than the wind speed, thus wave age $C_p/U < 1$. As the wind-sea evolves, the spectral peak migrates toward lower frequencies, which propagate at increased phase speeds. The wave age of a fully developed P-M sea corresponds to 1.2, with U taken at 10 m; hence, for a sea with a wave age greater than 1.2, the local wind field has little direct influence on the mature wind-waves. Similar to the JONSWAP fetch parameter X, the wave age parameter, or its inverse U/C_p, has been shown to be an effective measure of wind-wave development (Donelan et al., 1985).

As indicated by the dependence of the spread parameter s on the inverse wave age (Eq. 8), Mitsuyasu et al. (1975) believed that the stage of wave growth affects the directional spreading of wave energy. Their results indicate that younger seas have broader angular spreading than do older seas. On the contrary, Hasselmann et al. (1980) suggested that the spread parameter s is a function of both the wave age and

the frequency of wave components relative to the modal frequency f/f_p, but with dependence mainly on the latter. Hasselmann et al. (1980) proposed the spread parameter to be

$$s = \begin{cases} s_p\left(\frac{f}{f_p}\right)^{4.06} & \text{for} \quad f < f_p \\ s_p\left(\frac{f}{f_p}\right)^{-2.33-1.45\left(U/C_p-1.17\right)} & \text{for} \quad f > f_p \end{cases} \qquad \text{Eq. 9}$$

where

$$s_p = \begin{cases} 6.97 & \text{for} \quad f < f_p \\ 9.77 & \text{for} \quad f > f_p \end{cases}.$$

The dependency on inverse wave age in Eq. 9 determined by Hasselmann et al. (1980) is relatively weak, and thus is often excluded when this formula is implemented. Both Mitsuyasu et al. (1975) and Hasselmann et al. (1980) models predict that the minimum angular spread corresponds with the peak frequency. This is illustrated in Figure 4.

The Donelan et al. (1985) collection of data showed that the minimum spread did not coincide with the maximum energy frequency, but with a lower frequency, at approximately $0.95 f_p$. Donelan et al. (1985) accounted for this characteristic in their directional model of the $sech^2\beta$ form. As will be seen in the field data presented in Section 3, the narrowest spreading for the low frequency system is generally found below the peak frequency, and not at the peak frequency. Donelan et al. (1985) determined the directional distribution to depend only on the relative frequency

$$D(f,\theta) = \beta\, sech^2\left[\beta(\theta-\theta_m)\right], \qquad \text{Eq. 10}$$

where the spread parameter β is dependent on the component frequency and the modal frequency

$$\beta = \begin{cases} 2.61\left(f/f_p\right)^{1.3} & \text{for } 0.56 < f/f_p < 0.95 \\ 2.28\left(f/f_p\right)^{-1.3} & \text{for } 0.95 < f/f_p < 1.6 \\ 1.24 & \text{otherwise} \end{cases} \qquad \text{Eq. 11a}$$

and the mean wave direction is also a function of frequency, $\theta_m = \theta_m(f)$. Because the Donelan et al. (1985) study focused on a narrow frequency range around the peak frequency ($0.56 f_p \le f \le 1.6 f_p$), applying this parameterization of the spread function to frequencies above $1.6 f_p$ induces error in the directional distribution. Banner (1990) modified the spread parameter to extend beyond the $1.6 f_p$ limit

$$\beta = 10^{\left(-0.4+0.839\exp\left[-0.567\log\left(f/f_p\right)^2\right]\right)} \qquad \text{for } f/f_p > 1.6 \qquad \text{Eq. 11b}$$

(expressed by Banner in *k*-space).

Once the directional distribution is obtained using of one of the models described, the directional spread of each wave component can be computed. For a symmetric distribution, the directional spread can be defined as the "rms angular deviation of energy from the mean direction" of propagation (Longuet-Higgins et al., 1963). This measure of angular spread, $\sigma(f)$, is calculated from the second moment of the directional distribution as

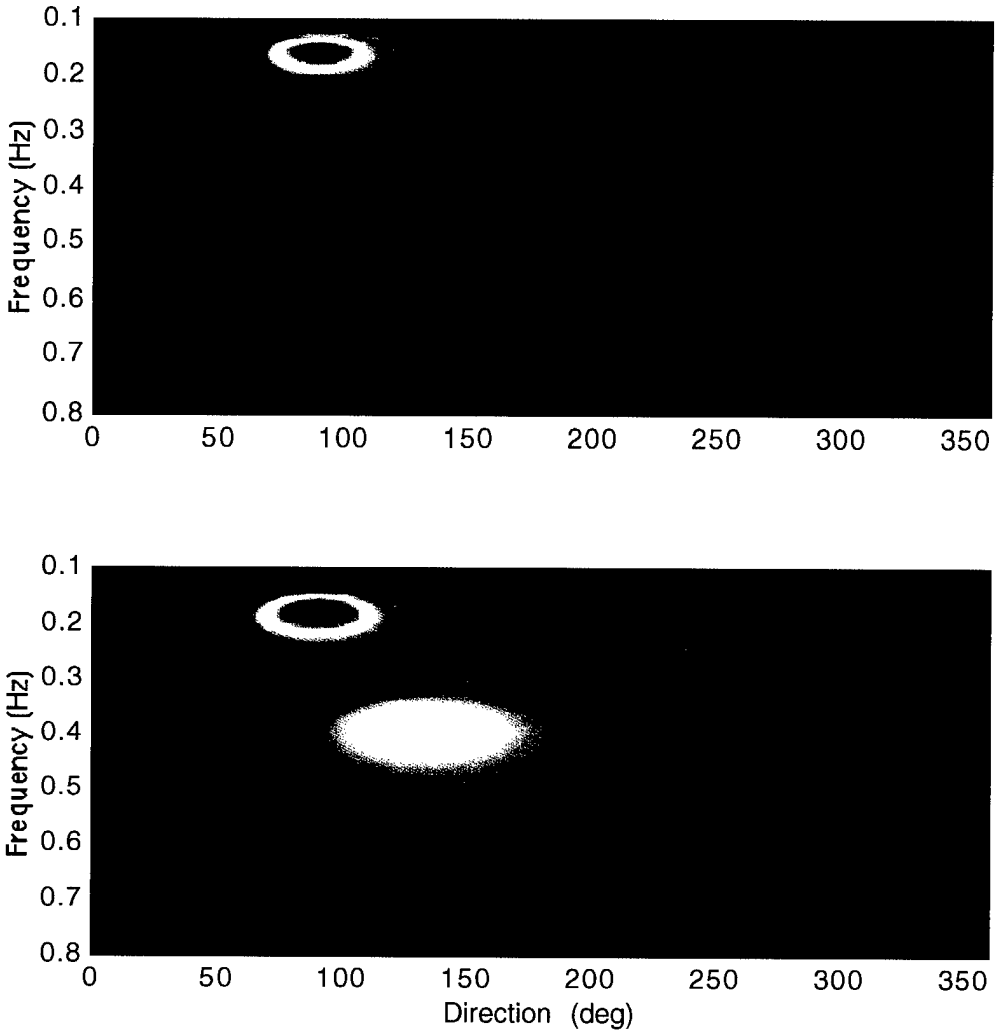

Figure 3. (a) Directional model for P-M spectrum of Figure 1, using Donelan et al. (1985), with all components propagating at 90°. (b) Bimodal spectrum with wind-sea superimposed at 135°, using Ochi and Hubble (1976).

$$\sigma_m(f) = \left[\int_{-\pi}^{\pi} (\theta - \theta_m)^2 \tilde{D}(f,\theta) d\theta\right]^{1/2} \qquad \text{Eq. 12}$$

where $\tilde{D}(f,\theta)$ is the normalized directional distribution, such that its integral equals 1. As an example, the directional wave spectrum and angular spread for the P-M model of Figure 1b are illustrated in Figures 3 and 4. The directional spectra in Figure 3 are computed using Eq. 4, where the distribution function $D(f,\theta)$ is the $sech^2\beta$

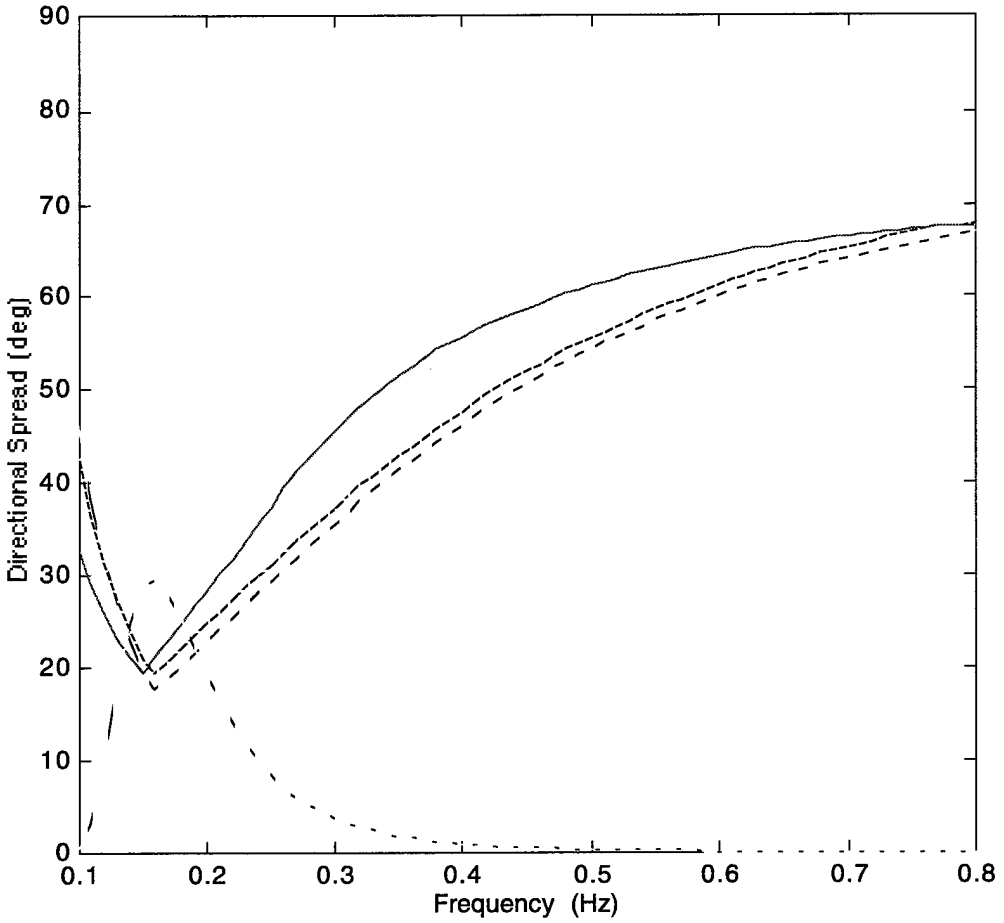

Figure 4. Example of directional spread for Donelan et al. (f), Hasselmann et al. (--), and Mitsuyasu et al.(-.-) distributions, with superimposed plot of P-M spectrum from Figure 1 (P-M*20).

formula of Eqs. 10 and 11. The directional spread is then determined using Eq. 12. As shown in Figure 4, wind-generated waves have a minimum angular spread around the spectral peak frequency, indicating that most of the energy of these components is concentrated in the mean direction of propagation. Away from the minimum, particularly in the high frequency range, the angular spread broadens, indicating that the energy of these components has a greater dispersion in direction than for longer

waves. Again the similarity between the Mitsuyasu et al. (1975) and the Hasselmann et al. (1980) forms can be seen for the case of a developed wave field.

Previous studies have focused on the directional spectrum and angular spread of pure wind-wave cases. For the case of coexisting swell and wind-waves, the directional spectrum gives a more informative account of possible interactions between the two systems than an omnidirectional spectrum does. Observed directional spectra of mixed seas exhibit complex interactions resulting in some interesting spectral features, which will be later discussed in Sections 3 and 4. Proposed mechanisms of interactions between swell and wind-sea remain speculative. One possible mechanism responsible for the interplay between systems is the nonlinear interactions among individual wave components. Since the JONSWAP investigation, these weakly nonlinear wave-wave interactions have been recognized to play an important role in the evolution of wind waves; for this reason, wave-wave interactions are believed to also play an important role in the development of mixed seas.

1.4 Transport Equation

The field of wave forecasting has evolved from simple diagnostic wave models, such as the P-M and the JONSWAP, to more complex numerical models, capable of predicting the evolution of a wave field under a variety of conditions. The framework of wave prediction models is based on the numerical integration of the transport equation

$$\frac{\partial F}{\partial t} + C_g \nabla F = S \qquad \text{Eq. 13}$$

where C_g is the wave group propagation velocity in deep water, S is the net source function, and $F(f,\theta)$ is the two-dimensional wave spectrum. The net source function is the summation of three expressions, each describing a dynamical process important to the development of a wave field:

$$S = S_{in} + S_{nl} + S_{ds} \qquad \text{Eq. 14}$$

where the terms S_{in}, S_{nl}, and S_{ds} represent, respectively, energy input by wind, nonlinear wave-wave energy transfer, and energy dissipation due to wave breaking. Eqs. 13 and 14 describe the spectral evolution of a wave system in deep water, with no current. Solving these equations has proven to be a difficult task, due to the complex source functions. Of the three functions, the wind input and nonlinear energy transfer terms have been well documented; the dissipation term remains the least understood. The challenge for numerical wave modelers continues to be the nonlinear and the dissipation source functions. The nonlinear interaction function is a very complex expression, which renders it computationally costly and time consuming to solve. The JONSWAP (Hasselmann et al., 1973) study concluded that resonant wave-wave interactions have a stabilizing effect on the spectral shape, driving the wave spectrum to a self-similar unimodal form. (See Figure 1.) The nonlinear transfer function is also responsible for the evolution of the spectral peak toward lower frequencies. Because of its importance to wave evolution, researchers are continually trying to find more efficient integration methods and more accurate parameterizations of the nonlinear energy transfer function.

Despite uncertainties in the dissipation term and complexities in the nonlinear term, numerical studies have produced interesting results in cases of bimodal seas, e.g. Young et al. (1987) and Masson (1993). Laboratory studies, such as Mitsuyasu (1966, 1992) and Donelan (1987), have also produced interesting findings concerning the effects of long, low frequency waves on the development of short, high frequency

waves. Numerical wave modeling and laboratory studies are important in that they can examine the significance of isolated factors contributing to the evolution of multi-system seas.

1.5 Mixed Seas Studies

Previous studies suggest that the effects of long waves on short waves result from one or more competing source mechanisms of Eq. 14. An early laboratory study by Mitsuyasu (1966) showed that when both systems propagate in the same direction, short wind-waves are attenuated by long waves. Later laboratory experiments, such as Donelan (1987) and Chu et al. (1992), have also observed this reduction of wind-wave energy for the situation of aligned long and short waves. Phillips and Banner (1974) proposed that the attenuation of short waves in the presence of long waves is caused by an augmentation of the surface wind drift, which induces premature breaking of wind-waves. This enhanced dissipation mechanism interferes with the balance of the competing source functions of the pure wind-wave case, resulting in reduced wave amplitudes. Further studies argued that the drift-enhanced dissipation hypothesis does not adequately predict the degree of wind-wave attenuation. Wright (1976) and Plant and Wright (1977) argued that the hypothesis overpredicts the observed level of wind-wave attenuation in cases of aligned seas. In the case of coexisting long waves and short waves propagating in opposite directions, the enhanced dissipation hypothesis also predicts a decrease of energy in the high frequency waves. However, laboratory observations have shown otherwise. Mitsuyasu (1992) and Reid (1995) found that the presence of opposing long waves intensifies, rather than attenuates, the spectral energy of short waves. In a field study

of mixed seas in the Gulf of Alaska, Hanson (1996) concluded that coexisting swell had no significant effect on wind-wave growth.

Donelan (1987) examined the role of the wind input source mechanism, S_{in}, for the pure wind-wave case and for the aligned swell and wind-sea case. Donelan (1987) concluded that the presence of long waves had an insignificant effect on the rate of wind energy input to wind-waves. Citing the insensitivity of the wind input source function to the existence of long waves and the inadequacy of the drift-enhanced dissipation hypothesis, Donelan (1987) conjectured that nonlinear wave-wave interactions act to transfer energy from one system to another. Hatori et al. (1981) and Toba et al. (1983) also support the speculation that "strong" nonlinear wave interactions are responsible for the reduction of wind-wave amplitudes, by extracting energy from high frequency components and transferring it to low frequency components. They argued that the weakly nonlinear transfer function, S_{nl}, is too localized in wavenumber, or frequency, to account for the interactions observed between the long wave and short wave systems distant in the frequency space. Although details of an alternative mechanism were not presented, Hatori et al. (1981) conjectured that only "strong" nonlinear interactions can contribute to the coupling between wave systems and to the modulation of wind-wave growth by coexisting long waves. Hatori et al. (1981) also argued that Hasselmann's (1963) calculations of the weakly nonlinear transfer function for mixed swell and wind-wave systems predicted interactions opposite to those observed.

A numerical study on the role of the weakly nonlinear interaction function by Masson (1993) obtained results different from the Hasselmann (1963) calculations. Masson (1993) found that coupling between swell and wind-waves increased as the wind-wave peak frequency of a bimodal spectrum approached the swell peak frequency. Masson (1993) also found that the weakly nonlinear interactions played an

important role in smoothing a bimodal spectrum into a unimodal spectrum; this stabilizing effect of the S_{nl} agrees with findings of the JONSWAP study, as noted in Section 1.4.

In addition to the aforementioned findings, other investigations have attempted to characterize the effects of swell on wind-sea in multimodal systems; unfortunately, results have often been inconclusive or contradictory. The lack of understanding of the development and interaction of coexisting wave systems is reflected in current numerical wave models. Current models treat mixed swell and wind-wave systems as a superposition of the two systems. It has been demonstrated (e.g. Mason, 1993) that the development of the a bimodal spectrum is not merely the development of the component wave systems, as parameterized by the Ochi and Hubble (1976) model. If the development of wind-seas in the presence of background swells can be understood, a new generation of wave forecast models accounting for the nonlinear coupling between wave systems would be more accurate in reconstructing wave systems found in nature and in predicting ocean wave conditions.

1.6 Research Objectives

Considering the complexity of ocean waves, a comprehensive investigation into the effects of coexisting swells on wind-waves would be a tremendous endeavor; the goal of this study is not so ambitious. This study examines several events of multiple system seas observed during a field experiment. The evolution of wind-wave systems in mixed seas is discussed, focusing on the directional characteristics of the wind-generated waves and the role of swells on their development. The results of this study are then discussed in parallel with those of previous studies. In the events

selected, interaction between swell and wind-seas is observed and described in Sections 3 and 4. However, an explanation for the interaction mechanism is beyond the scope of this observational analysis; that is left for future investigations.

2. Field Experiment

The experiment site was located near the Dry Tortugas Island in the Gulf of Mexico, at 24° 36.7' N, 82° 50.7' W. The experiment was conducted by Dahl et al. (1995) during the week of February 9-17, 1995. Atmospheric conditions were generally mild; sea and air temperatures ranged between 19° C and 23° C and wind velocities did not exceed 8 m/s. Wind measurements were taken at a 7-meter height by a propeller anemometer mounted onboard the *R/V Seaward Explorer*. The anemometer (WeatherPak) measured the wind speed, wind direction and air temperature at 10-minute intervals. Wind anemometers generally have resolutions of 1-5° for directional readings and about ± 0.1 m/s for wind speeds. The wind speeds encountered during the experiment were well within the operating range of a typical anemometer.

Surface wave measurements were made by a heave-pitch-roll buoy deployed in waters of 25-meter depth. Instrument components of the 0.9-meter diameter Directional Waverider buoy (Datawell) included one vertical accelerometer and two horizontal accelerometers for measuring wave motion, a temperature sensor for recording sea surface temperature, and an onboard micro-processor for computing the spectral energy density and the directional information. The wave buoy has a resolution of 1 cm for vertical surface displacement and 1.5° for wave directions (Directional Waverider Buoy Manual, Datawell). The mean wave direction, as well as the wind direction, is given in degrees clockwise, with 0° corresponding to the north direction. For each of the three accelerometers, the buoy recorded acceleration readings for 200 seconds, at a sampling rate of 1.28 Hz, producing time series of 256 data points. For every half-hour, an ensemble of eight time series was processed to

transform the raw information into its equivalent frequency spectrum. Wave energy spectra were produced, on average, every 1 hour or 1 1/2 hours. (See Appendix for computation of the wave spectra.) The spectral bandwidth ranges from 0.025 Hz to 0.58 Hz, with a resolution of 0.005 Hz up to 0.1 Hz and a resolution of 0.01 Hz for frequencies between 0.1 Hz and 0.58 Hz.

In this analysis, the effective frequency range is 0.08-0.58 Hz. The low frequency cutoff of 0.08 Hz results in no crucial loss of information because (1) the observed energy spectra contain relatively short swells, with modal frequencies greater than 0.13 Hz, and (2) the wave measurements below 0.1 Hz were deemed to be noise. Also, the water depth of 25 meters is considered to be sufficient to qualify the frequency components above 0.13 Hz to be deep-water waves. In strict definition, waves below 0.13 Hz are depth-dependent. However, the energy-containing region of the spectrum lies above this frequency limit. Since no significant energy is carried by waves in the depth-dependent or shallow-water regimes, the wave data are treated as deep-water measurements in this analysis.

3. Results

3.1 Response to Wind

As discussed in Section 1.5, the development of the sea surface is dictated by three dynamical processes, one of which being the energy transfer at the air-sea interface. In the wave generation process, shorter waves respond quickly to changes in the wind field. However, long waves with phase speeds faster than the wind speed are not wind-driven, and consequently these components are decoupled from the wind field. One way of measuring the response of waves to wind is to compare the energy variance of the wave spectrum to the wind speed. The total energy variance of the wave spectrum is

$$E = \int_{f_1}^{f_2} \Phi(f) df \qquad \text{Eq. 15}$$

where the effective lower limit $f_1 = 0.08$ Hz and the upper cut-off frequency $f_2 = 0.58$ Hz, as mentioned in Section 2. A history of the field data taken from February 11 to 17 is shown in Figure 5. The wave energies for the intermediate frequency range and the high frequency range are calculated in the same manner, but with lower limits of 0.3 Hz and 0.45 Hz, respectively. The changes in high frequency variance (Figure 5c) can be seen to follow closely with the changes in wind. The correlation coefficient between the short wave variance and the wind speed is 0.84, with a temporal lag of 1.5 hours. The intermediate range has a correlation C = 0.63, with a slower relaxation to wind of 2.4 hours (Figure 5b). Including low frequency swell components, the total energy variance has little dependence on the

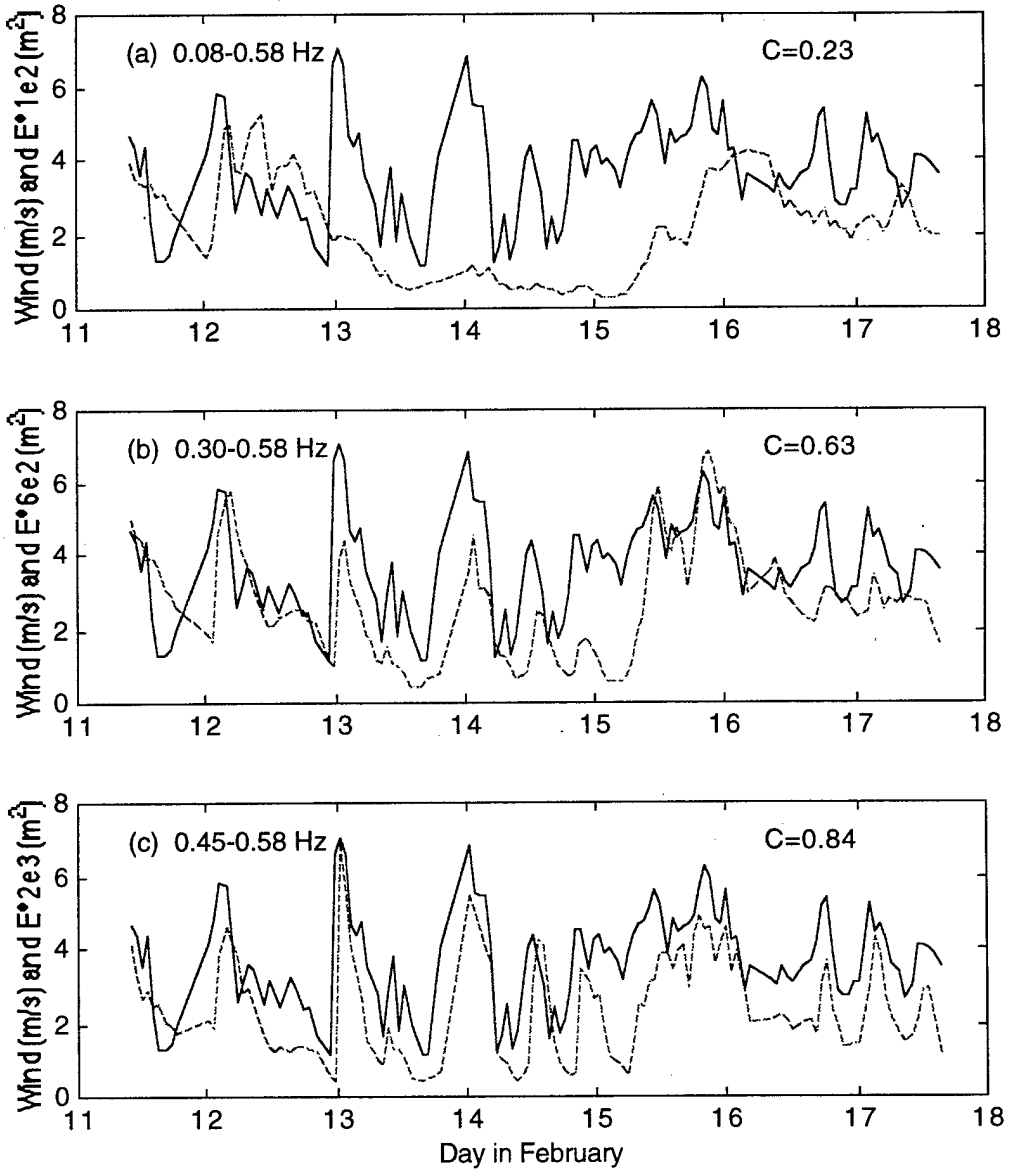

Figure 5. History of wave variance E (--) at three frequency regimes and the wind speed (–): (a) entire spectrum, (b) intermediate range and (c) high frequency range. Correlation coefficient is given as C.

wind field (Figure 5a). For general seas, unimodal or multimodal, the variance E is an ineffective parameter in describing the wave field, with respect to the wind field.

For a diagnosis of the wave field in response to wind, the root-mean-square wave slope has a higher correlation than the energy variance. The rms wave slope, defined as a measure of the fourth moment of the energy spectrum, is weighted toward the higher frequencies. As small waves are sensitive to changes in the wind field, the wave slope is also sensitive to changes in wind conditions. The rms wave slope is

$$\alpha_{rms} = \left[\frac{(2\pi)^4}{g^2} \int_{f_1}^{f_2} f^4 \Phi(f) df \right]^{1/2} \qquad \text{Eq. 16}$$

where f_1 and f_2 are the same frequency limits as those used to calculate the wave variance, for the same three frequency ranges. As plotted in Figure 6, the wave slope variations closely follow the wind speed fluctuations. Comparison of Figures 5a and 6a shows that the total rms wave slope has a higher correlation with the wind than does the total energy variance, since the variance of the long waves is independent of the local wind field. The results for the intermediate and high frequency regions are given in Figures 6b and 6c. Instead of using the integrated rms slope parameter in this analysis, the wave slope spectrum, $\Psi(f)$, is computed for each energy spectrum. Similar to Eq. 16, the normalized slope spectrum is

$$\Psi(f) = \frac{(2\pi)^4}{g^2} f^4 \Phi(f). \qquad \text{Eq. 17}$$

The slope spectrum allows for a direct comparison of the steepness of long waves and short waves, and also gives an indication of the wave breaking activity; this point will be revisited in Section 4.

Low frequency components are not associated with the local wind conditions, thus one would expect little or no correlation between wave propagation directions and

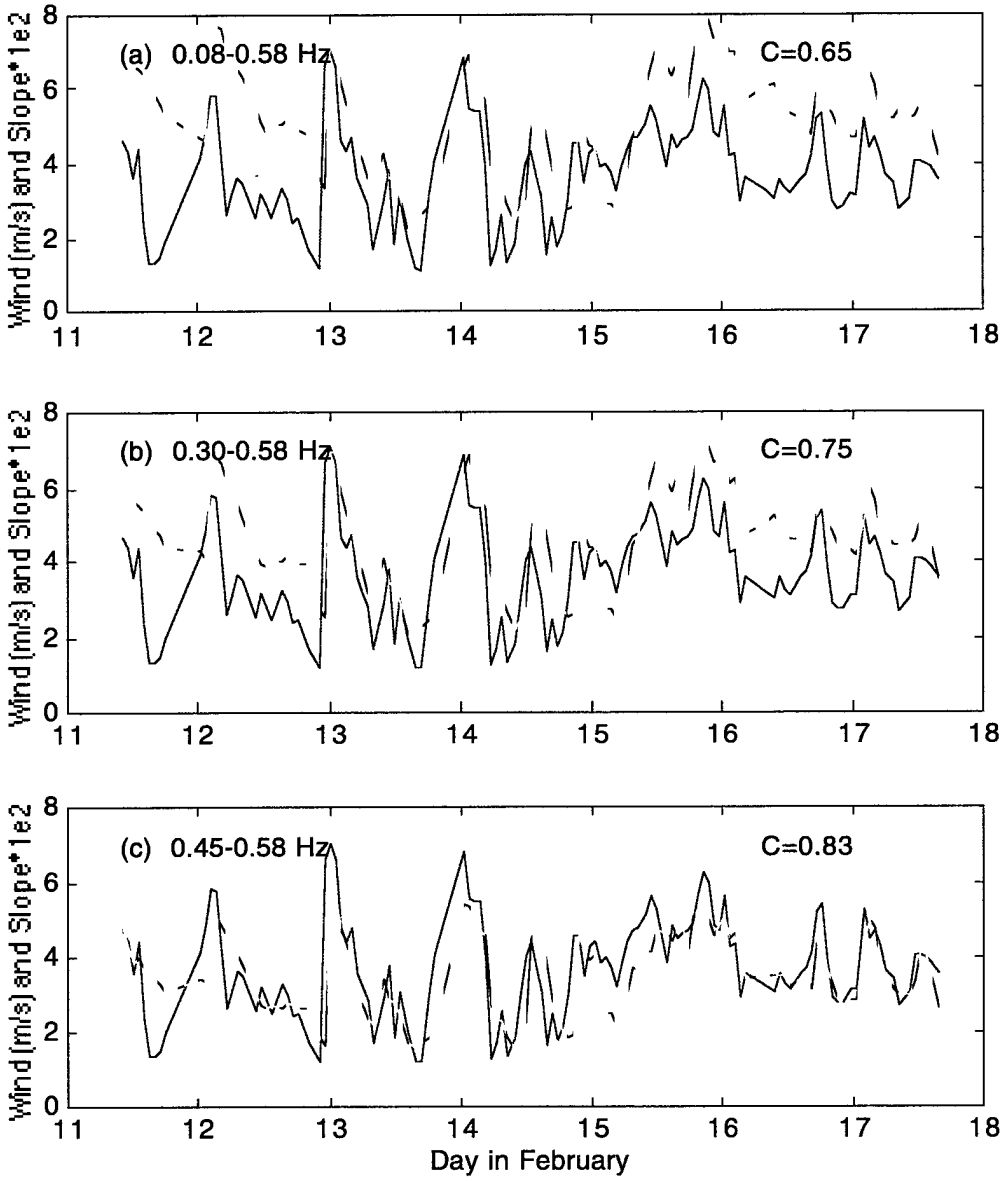

Figure 6. History of rms wave slope (--) for three frequency regimes and wind speed (–), showing higher correlation than wave variance E of Figure 5. Again, correlation is given as C.

wind directions. So in a turning wind, the low frequency waves would not respond to a change in wind direction. Such a situation of veering wind can be found in Figure 7a, where long waves travel in directions different from the wind vector. On February 12-13, the increase in wind speed is accompanied by a change in direction, approximately from 225° to 65°. (Wind and wave are given as directions of *approaching from*.) The wind change occurs over a one-hour period, while the wave direction of 0.15 Hz waves (6.6 second waves) remains unchanged at 225° until the long waves attenuate and align with the wind vector, about two days later. The directions of smaller waves at 0.30 Hz (3.3 second waves) and at 0.45 Hz (2.2 second waves) show better comparison with the wind measurements. Intuition would suggest that smaller wind-driven waves travel in a direction aligned with the wind vector. However it is interesting to observe that in many cases, the smaller waves travel at an angle to the wind, as from February 13-16 in Figure 7c. The wind-wave directions are generally 20° to 50° off of the wind vector. This offwind development has been observed by several fetch-limited wind-wave studies, e.g. Donelan et al. (1985) and Long et al. (1994). This and other directional features of wave growth in mixed seas will be described in the next section, where several cases of bimodal seas are examined.

3.2 Description of Data

In laboratory studies of mixed seas, four stages of wave development have been observed (Imai et al., 1981). But in a broader description of ocean wave growth, the sea state can be classified into three general groups. One group, Stage I, is the generation of young wind-waves in the presence of one or more low frequency

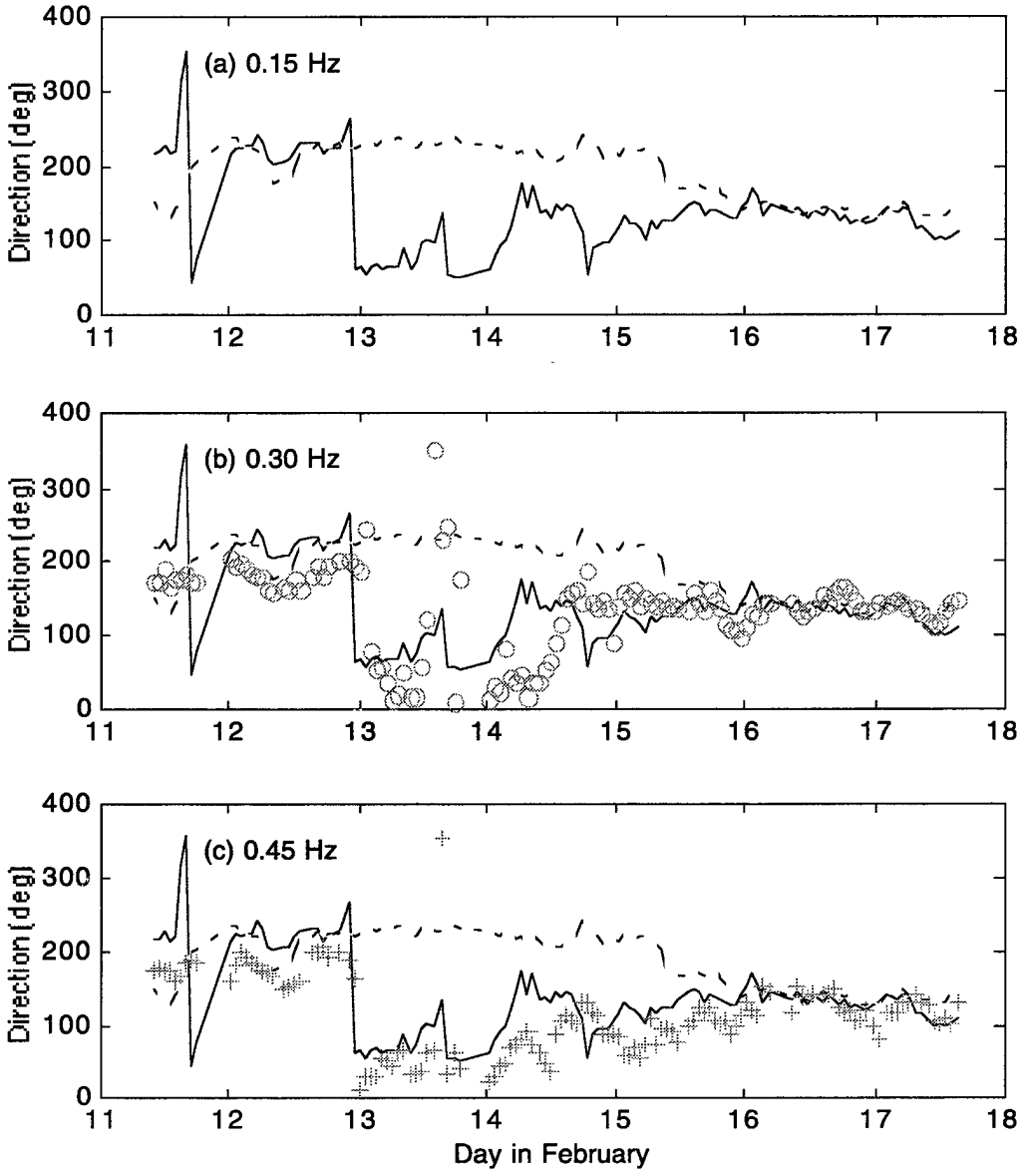

Figure 7. History of mean wave direction at three frequency components and wind direction (–): (a) 0.15 Hz (-.-), (b) 0.30 Hz (o), and (c) 0.45 Hz (+).

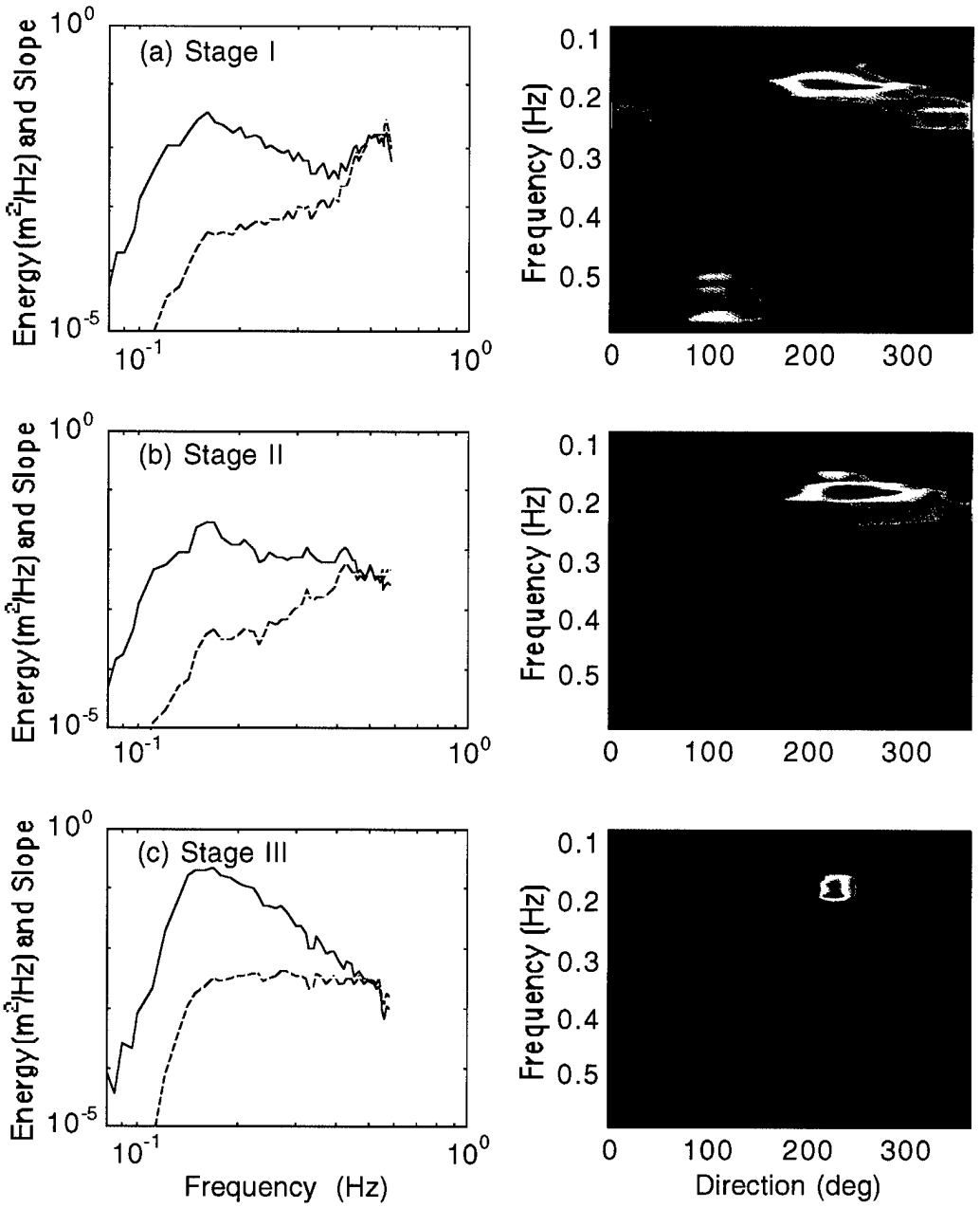

Figure 8. Omnidirectional (left) and directional spectra (right) of three stages of wave development: (a) young sea in presence of older sea; (b) interaction stage; (c) mature sea. The wave slope spectrum (red dashed) is also plotted with the energy density spectrum (blue solid).

wave systems, which commonly results in a spectrum with distinct multimodal peaks. Stage II is marked by a transition regime where the wind-wave peak is difficult to distinguish, suggesting a stage of interaction between the swell system and the wind-wave system. Stage III consists of more mature seas, in which low frequency waves dominate the energy spectrum. Examples of observed omnidirectional and directional wave spectra of each group are illustrated in Figure 8. Although this classification is neither rigorous nor definitive, it serves to help identity the cases of swell and wind-wave seas described below. The five cases selected from the experiment database are described in the next section. These events chronicle the evolution of the wave field during a more global event, caused by a sudden turn in the wind vector away from the original developed wind-sea. The first event (A) begins late on February 12, when the wind direction veers abruptly (Figures 7a and 9b). The three following events (B, C, and D) consist of an initially rising, followed by a decaying wind. (See Figure 9a.) The last event (E) terminates with the relaxation of the low frequency components to the wind vector (February 15-16 of Figure 7a), also marking the conclusion of the larger event begun on February 13. Next, the offwind wave development and the directional distribution of mixed seas are described in some detail for the selected events.

3.3 Offwind Wave Development

Field experiments, such as Donelan et al. (1985) and Long et al. (1994), have observed that wind-driven waves can be generated at an angle to the wind direction. In these fetch-limited studies, wind-waves were found to propagate up to 50° off of the wind vector. This phenomenon was also observed during the experiment. To

examine offwind wave growth in mixed seas, four of the five selected events will be analyzed in detail.

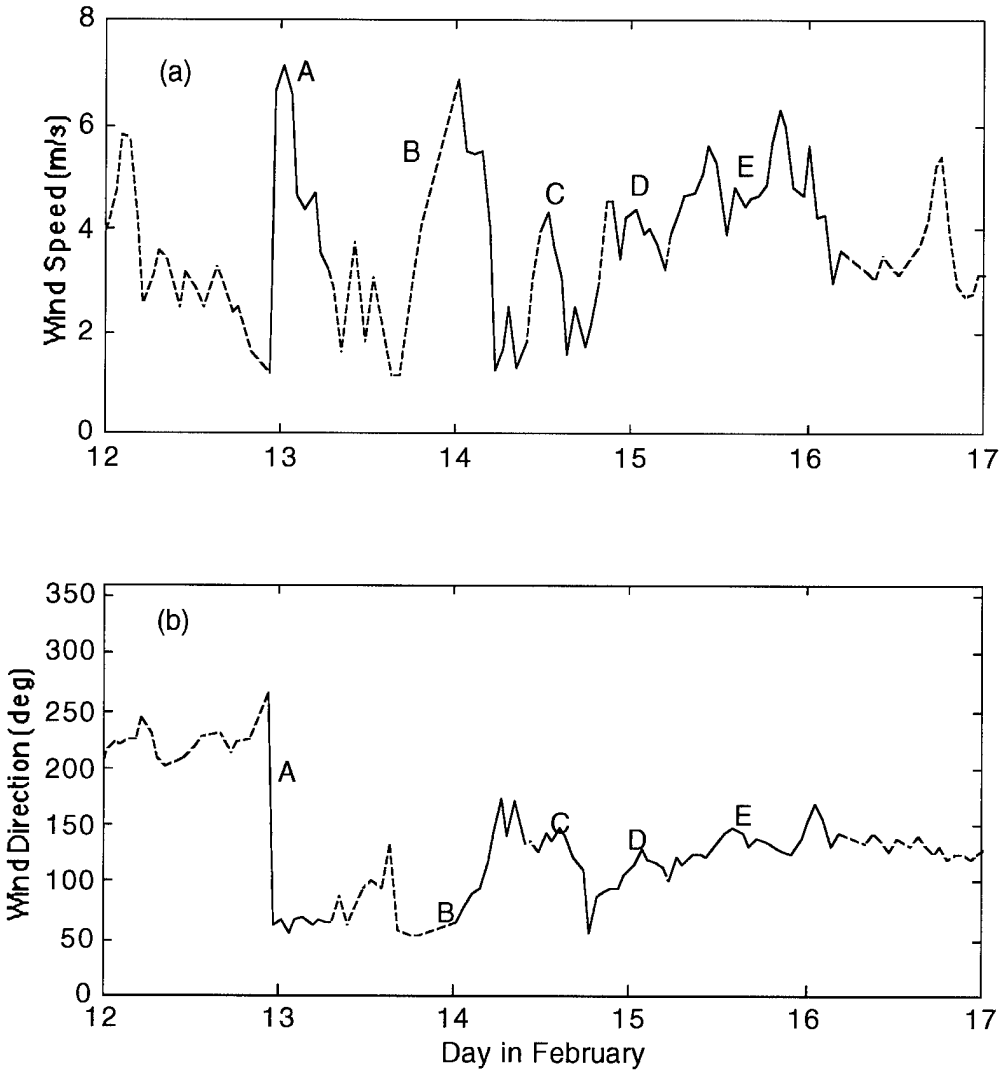

Figure 9. Wind data (dashed) for Events A, B, C, D and E (solid segments): (a) wind speed and (b) wind direction.

Table 1. **Event A**--Wind speed and direction, wave direction for low and high frequencies, and wave energy spread.

Time ddmm-hour	U_7 m/s	∂_w deg	θ_{m1} deg	θ_{m2} deg	σ_{min} deg
12Feb-2341	6.63	61	225	—	—
13Feb-0041*	7.07	67	223	17	36
13Feb-0141*	6.60	55	233	28	43
13Feb-0241	4.63	66	236	35	46
(13Feb-0341)	4.37	70	230	48	45
13Feb-0441	4.70	62	237	56	44
(13Feb-0541)	3.57	67	240	54	51
13Feb-0641	3.23	65	244	45	53

* classified as Stage I sea
( ) spectrum not included in figures
U_7 wind speed at 7 m, averaged over half-hour
∂_w wind direction, averaged over half-hour
θ_{m1} low-frequency peak direction, averaged over seven frequencies
θ_{m2} high-frequency peak direction, averaged over seven frequencies, (for Stage II seas, averaged at same frequencies of last Stage I sea)
σ_{min} average minimum wave spread

The development of waves at an angle to the wind can be clearly observed in Event A (Table 1). The prelude to Event A is characterized by a lull of 1-2 m/s winds coming from the general direction of west/southwest. A representative wave energy spectrum on February 12 at the time of 23:41 (hereafter denoted as 12Feb-2341) resembles a developed, Stage III sea propagating in a mean direction of 225°. Event A

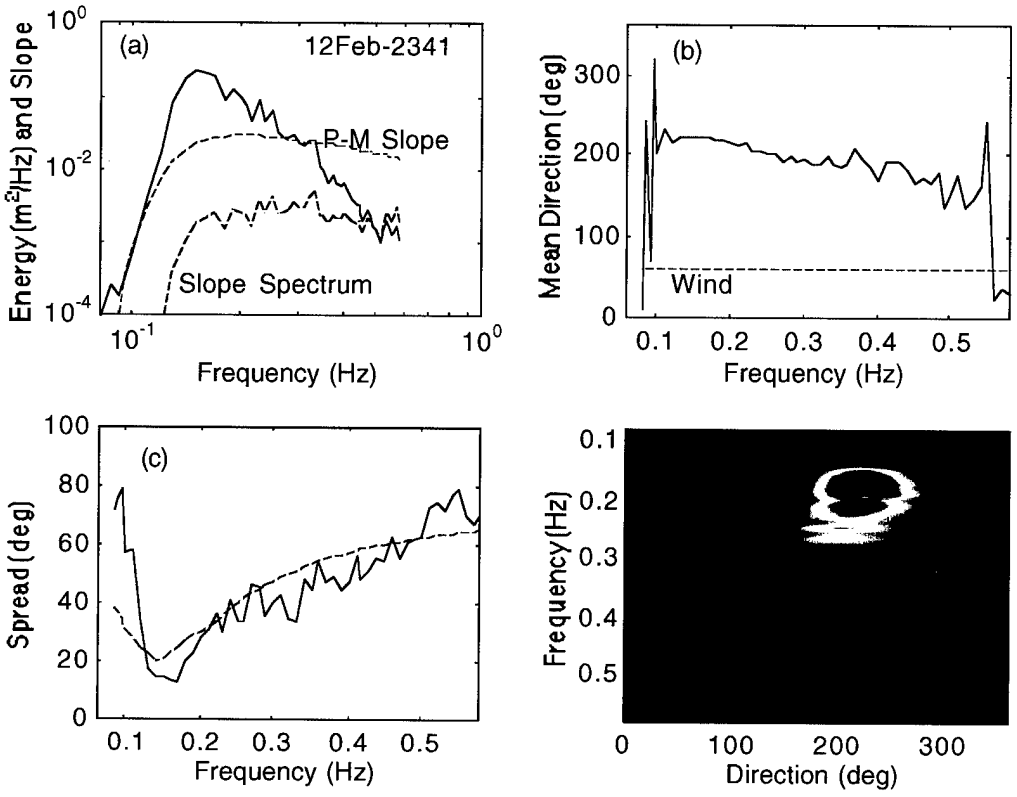

Figure 10. **Event A**--12Feb-2341. (a) Wave energy spectrum (blue solid), wave slope spectrum (red dashed), and P-M slope spectrum for a developed sea with modal frequency of 0.15 Hz (green dashed). (b) Mean wave (blue solid) and wind (red dashed) directions. (c) Wave spread (blue solid) and Donelan et al. (1985) spread model (green dashed). (d) Directional wave energy spectrum.

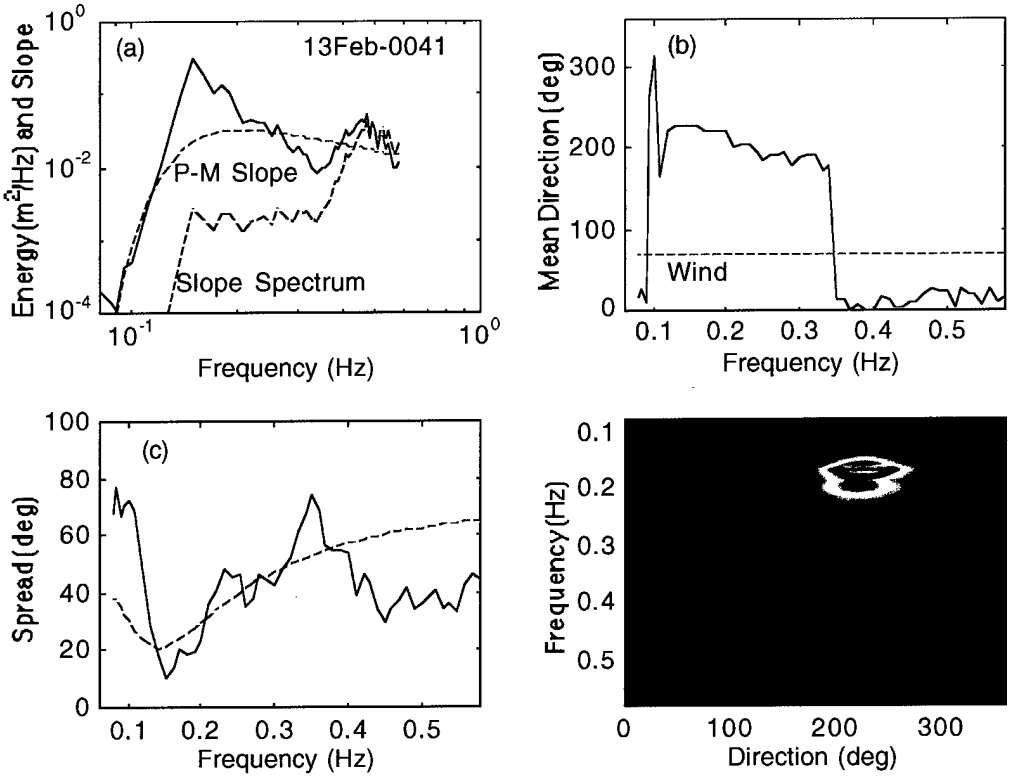

Figure 11. **Event A**--13Feb-0041. (See Figure 10 for legend.)

occurs at the onset of a change in the wind velocity; the wind speed rises from 1.4 m/s to 6.6 m/s over a period of 30 min and the wind direction shifts from west to east-northeast, at 61°. As seen early on Feb. 13 (Figure 9a), the wind remains at about 7 m/s for about 1.5 hours; after which, the wind speed decays gradually over the next 7 hours to about 3 m/s. Meanwhile, the wind direction remains at approximately 65°,

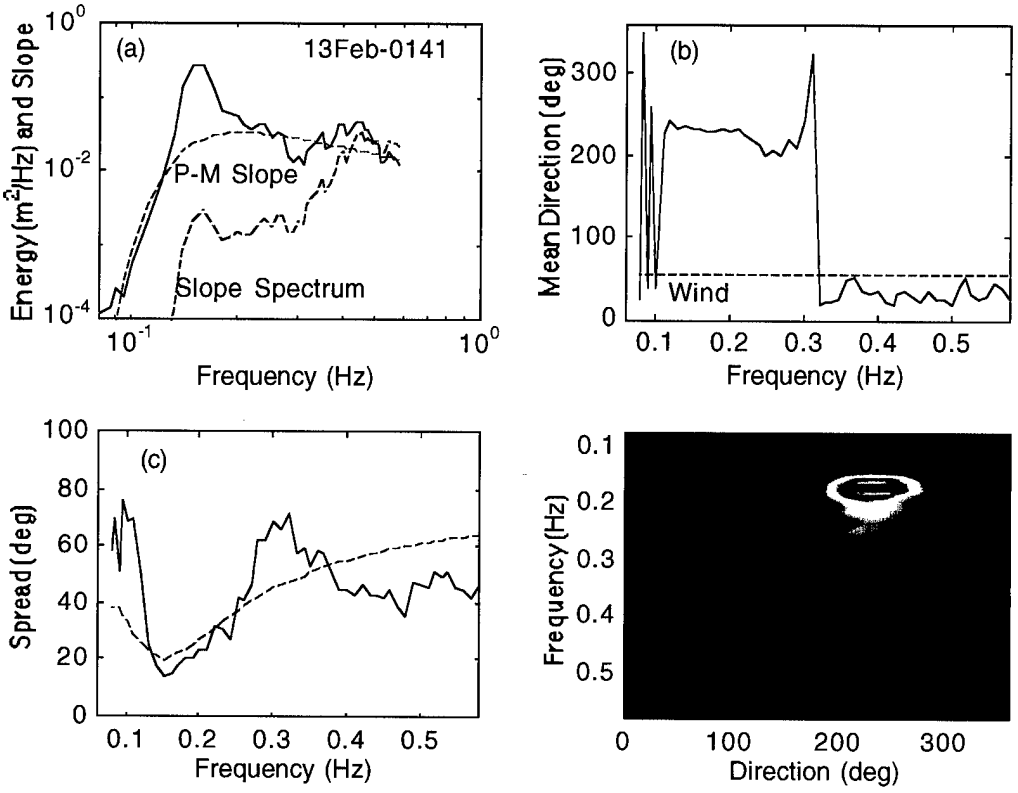

Figure 12. **Event A**--13Feb-0141. (See Figure 10 for legend.)

with maximum fluctuations of ±15°. The development of the omnidirectional and directional wave spectra can be seen from 12Feb-2341 to 13Feb-0241 (Figures 10-13). At 12Feb-2341 the 6.6 m/s wind has been blowing for a duration of only one half hour, therefore wind-generated waves are still too short to be observed in the current spectral frequency range. However after 1.5 hours, at 13Feb-0041, a small

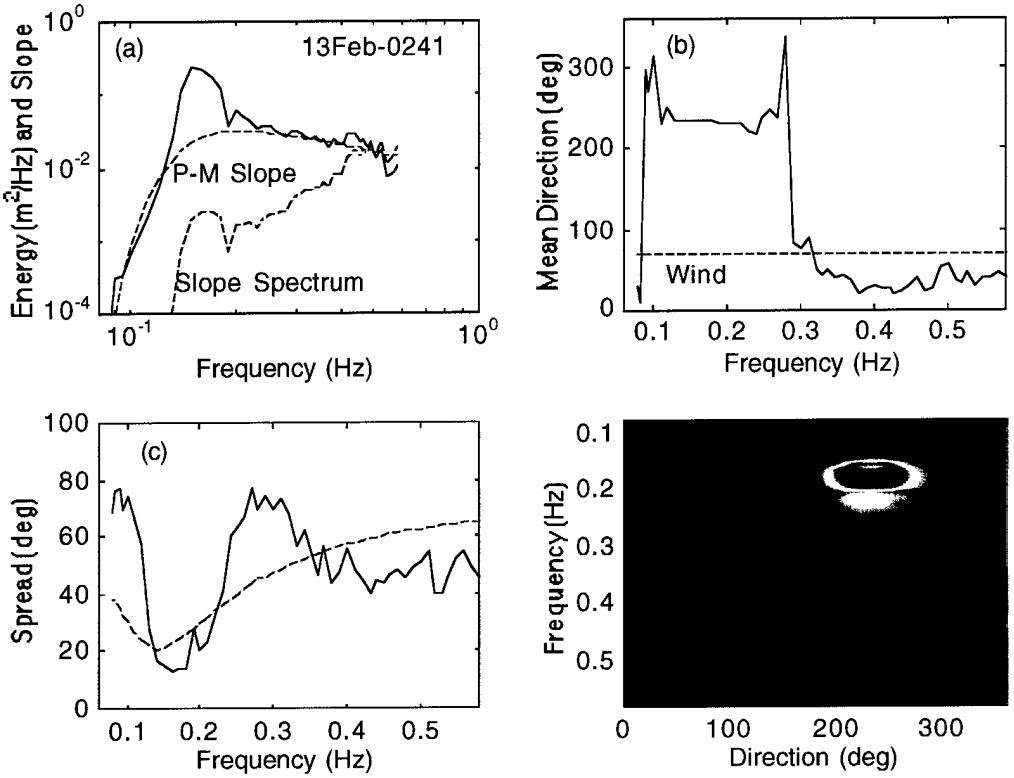

Figure 13. **Event A**--13Feb-0241. (See Figure 10 for legend.)

but distinct wind-wave system with a peak at about 0.46 Hz appears in the spectrum. The low frequency system at 0.15 Hz, in the direction of 223°, has become a swell system traveling in a direction almost opposite to the wind (approximately 160°). Although the wind is at 67°, the wind-wave system initially appears at about 17°, at 13Feb-0041. Then the wind-sea system progresses toward the lower frequencies and enters Stage II of wave development. From 13Feb-0241 to 0641, the wind field

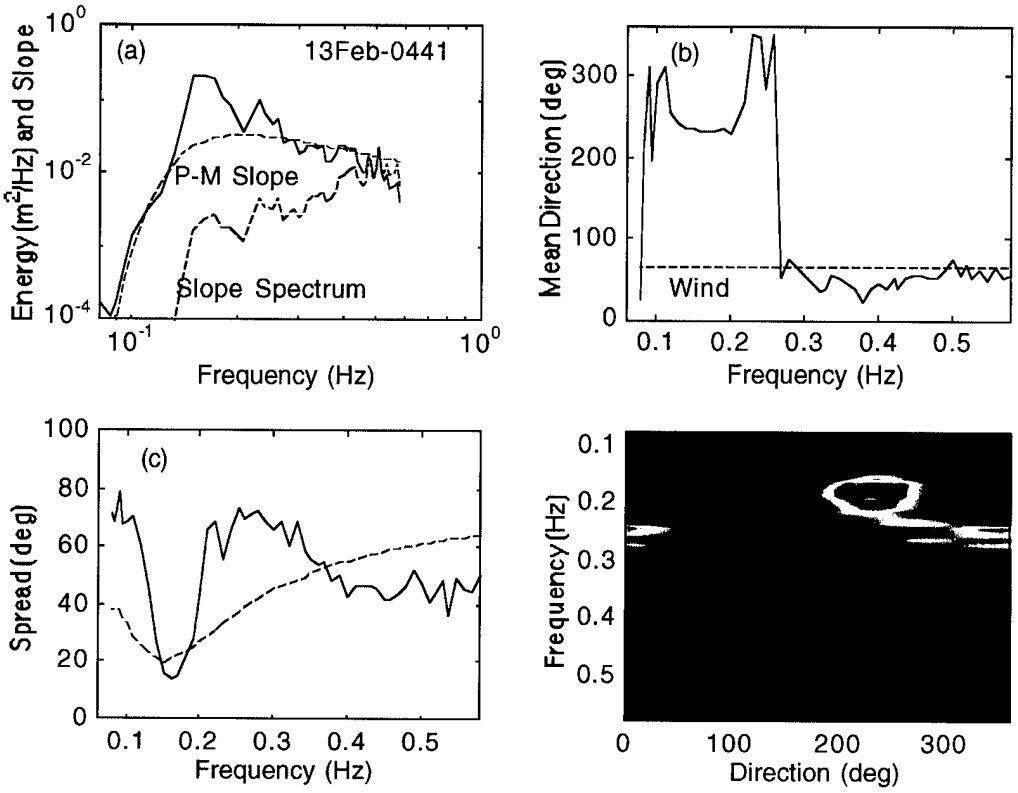

Figure 14. **Event A**--13Feb-0441. (See Figure 10 for legend.)

decays and the young waves slowly approach the wind vector. At 13Feb-0641, the low wind of 3.2 m/s has little influence on waves of frequencies below 0.45 Hz. This essentially marks the end of Event A.

Like the first event, Event B (Table 2) also consists of opposing wind and swell, and its growth characteristics are similar to those of Event A. Event B will be described in further detail in a later discussion of the directional spread of mixed seas.

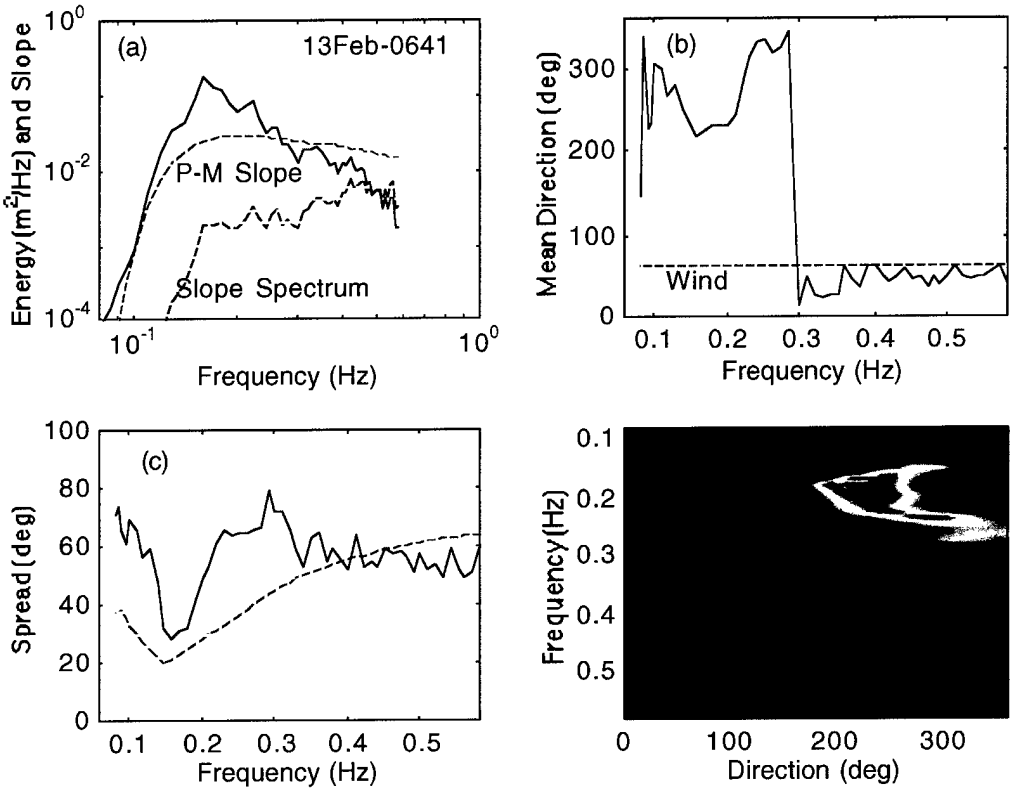

Figure 15. **Event A**--13Feb-0641. (See Figure 10 for legend.)

In the next events, wave growth in conditions of opposing/perpendicular and closely aligned wind and swell will be examined. In Event C, the case of wind and swell in an oblique direction between opposing and perpendicular directions shows that wind-waves develop at an angle to the wind direction in a manner similar to that observed in Event A. Before Event C, the wind fluctuates between 1 m/s and 2.5 m/s, and

Table 2. **Event B**--Wind speed and direction, wave direction for low and high frequencies, and wave energy spread.

Time ddmm-hour	U_7 m/s	∂_w deg	θ_{m1} deg	θ_{m2} deg	σ_{min} deg
14Feb-0041*	6.83	63	224	24	35
14Feb-0141*	5.50	80	228	27	37
14Feb-0241*	5.43	91	224	40	44
14Feb-0341	5.45	97	224	38	45
14Feb-0441	4.00	118	231	46	47
(14Feb-0541)	1.23	145	233	63	55
14Feb-0641	1.70	175	228	76	53
(14Feb-0741)	2.53	143	230	77	55
(14Feb-0841)	1.30	173	225	80	55
14Feb-0941	1.80	135	224	66	57

* classified as Stage I sea
( ) spectrum not included in figures
U_7 wind speed and ∂_w wind direction--same as Table 1
θ_{m1} low-frequency peak direction, θ_{m2} high-frequency peak direction, and σ_{min} average minimum wave spread--same as Table 1

between 100° and 200° for several hours, then increases to roughly 4 m/s. At 14Feb-1141 of Event C (Figure 23), the wind increases to 4.0 m/s, coming from 129°, while the young wind-waves propagate from 50°. At 14Feb-1241, the wind-sea has adjusted to 100° and a secondary wave peak around 0.5 Hz becomes visible. At 14Feb-1341 (Figure 25), the wind-wave system dominates the swell system located at 0.15 Hz and the wind-wave components travel from 107°. Although the wind begins

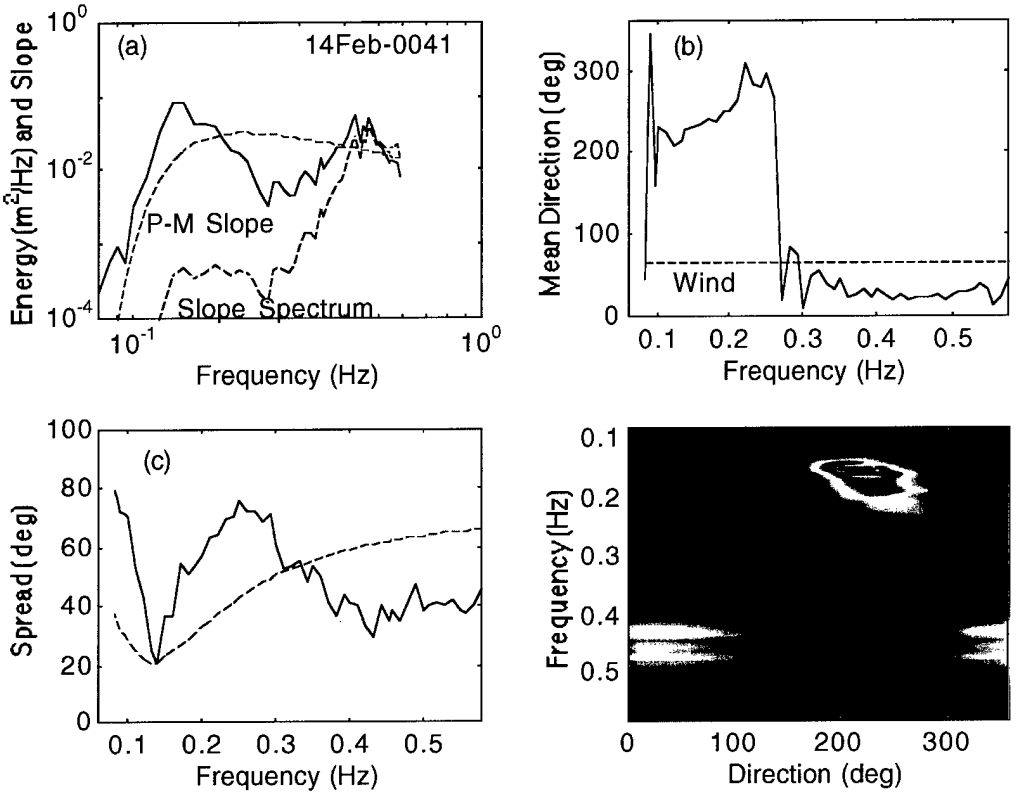

Figure 16. **Event B**--14Feb-0041. (a) Wave energy spectrum (blue solid), wave slope spectrum (red dashed), and P-M slope spectrum for a developed sea with modal frequency of 0.15 Hz (green dashed). (b) Mean wave (blue solid) and wind (red dashed) directions. (c) Wave spread (blue solid) and Donelan et al. (1985) spread model (green dashed). (d) Directional wave energy spectrum.

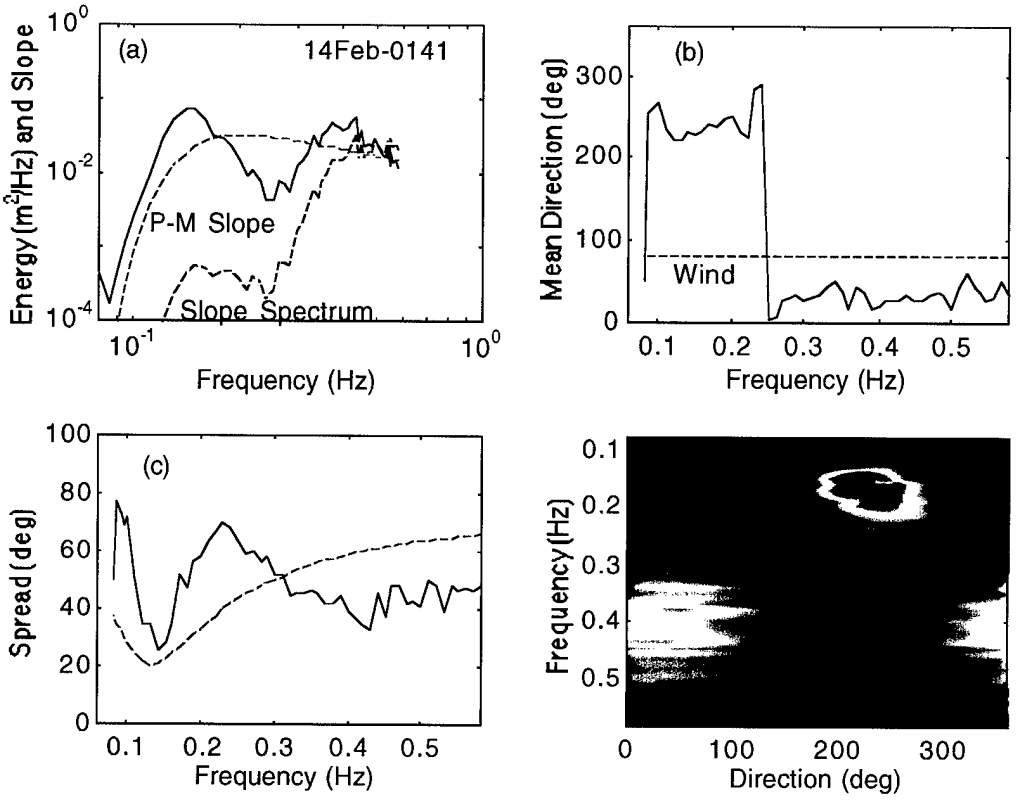

Figure 17. **Event B**--14Feb-0141. (See Figure 16 for legend.)

to decrease, the wind-sea at 0.43 Hz continues to dominate the energy spectrum, apparently edging closer to the wind vector. From 14Feb-1541 to 1741 one can observe not only the progression of the wind-wave system toward the wind direction (Table 3), but also the progression of the wind peak down the frequency space in the one-dimensional spectra (Figures 26a-28a), and the progression of the interaction

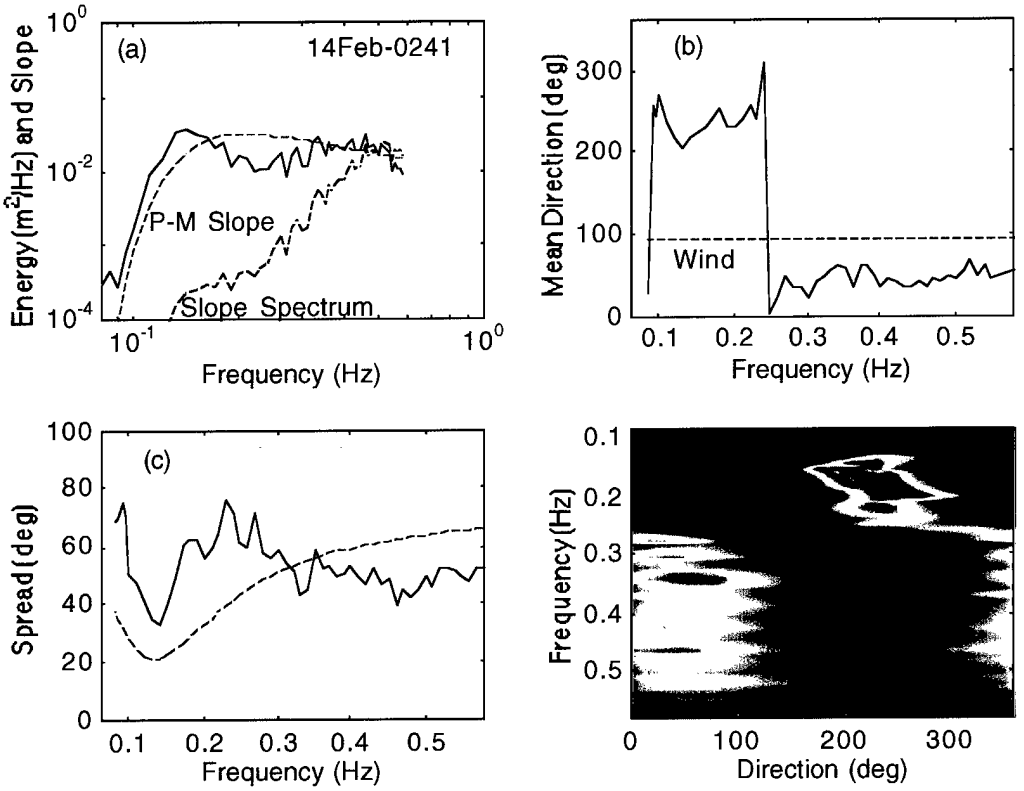

Figure 18. **Event** B--14Feb-0241. (See Figure 16 for legend.)

"bridge" between the swell and wind-wave system in the direction-frequency space of the two-dimensional spectra (Figures 26d-28d).

The end of Event C is followed immediately by an increase in wind, from 3.0 m/s to 4.5 m/s, marking the beginning of Event D. (See Events C and D of Figure 9.) In the hour from 14Feb-1841 to 1941, the wind veers from 55° to 88° (Table 3 of Event C), then later in Event D, stabilizing at approximately 120°. Determining the

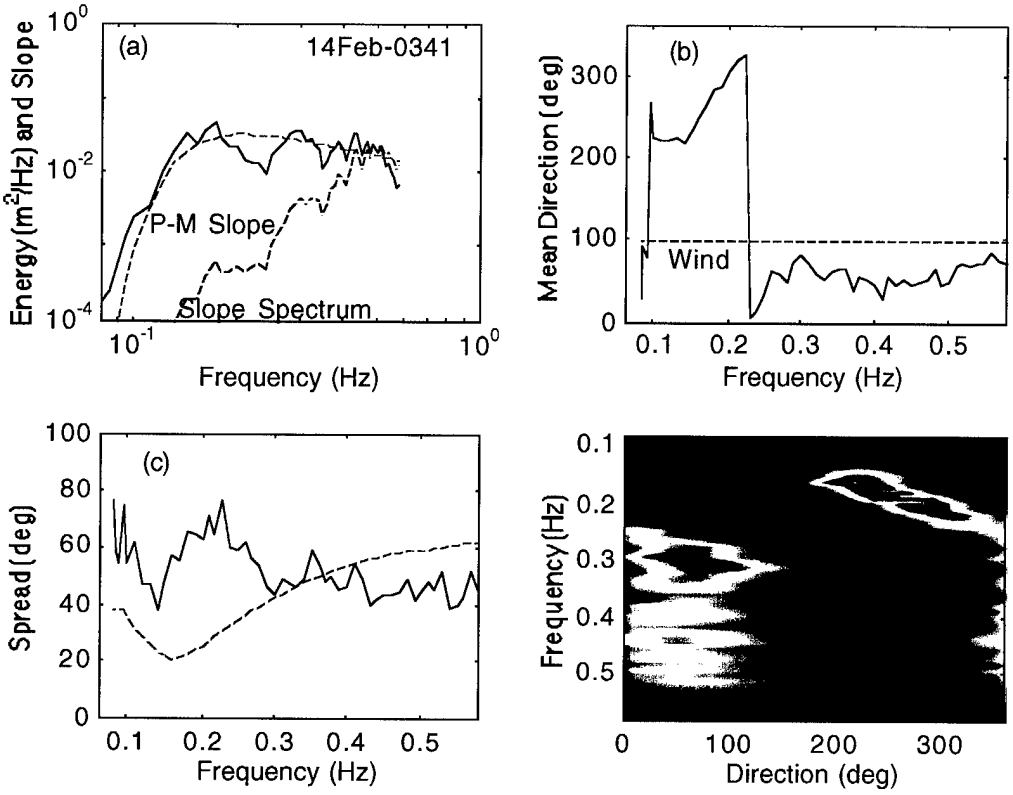

Figure 19. **Event B**--14Feb-0341. (See Figure 16 for legend.)

relative wind and swell directions from 15Feb-2041 to 2341 is difficult because the swell components are directionally dispersed, without one centralized mean direction of propagation. At the beginning of Event D (Figures 31-34), the relative directions of wind and swell are "confused" between opposing and perpendicular directions; from 15Feb-0141 on, the swell components settle into a mean direction perpendicular to the

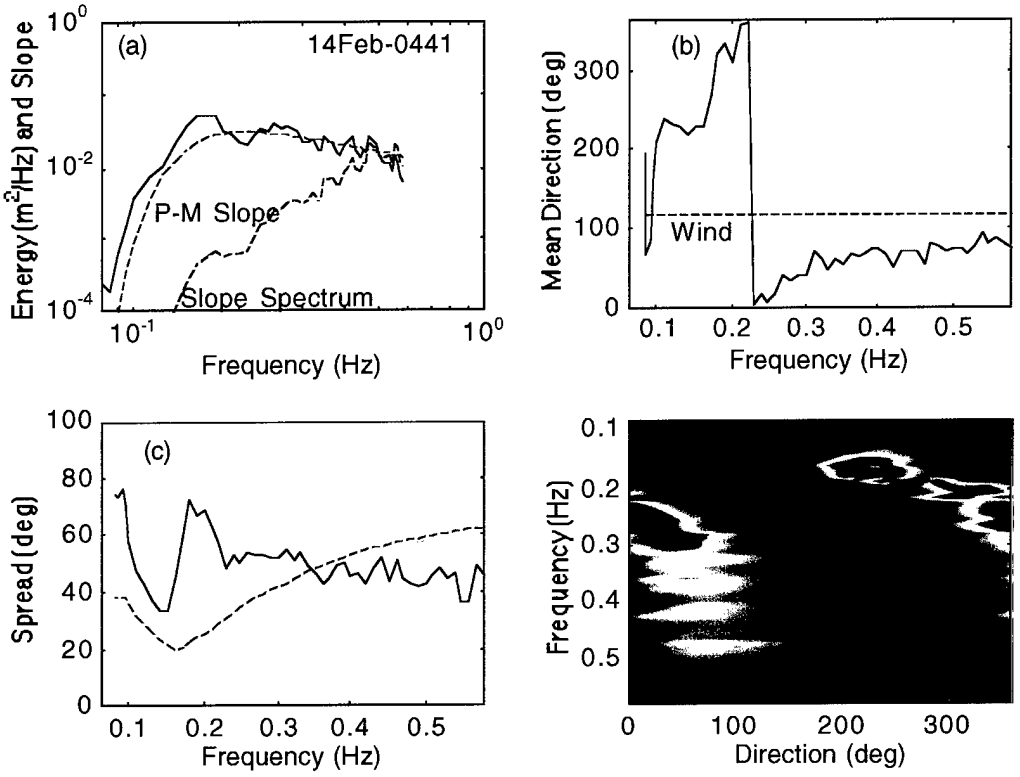

Figure 20. **Event B**--14Feb-0441. (See Figure 16 for legend.)

wind. Again, the offwind wave growth in Event D (Table 4) exhibits similar features encountered in previous events. At 14Feb-2141 (Figure 32), with a 4.5 m/s wind from 95°, the wind-wave system appears at 65°. The wind-wave system slowly develops toward the wind vector until 15Feb-0140 (Figure 36), when the wind-sea develops in an uncharacteristic behavior. At 15Feb-0041 (Figure 35), the directionally "confused" swell system becomes more coherent around its direction of propagation,

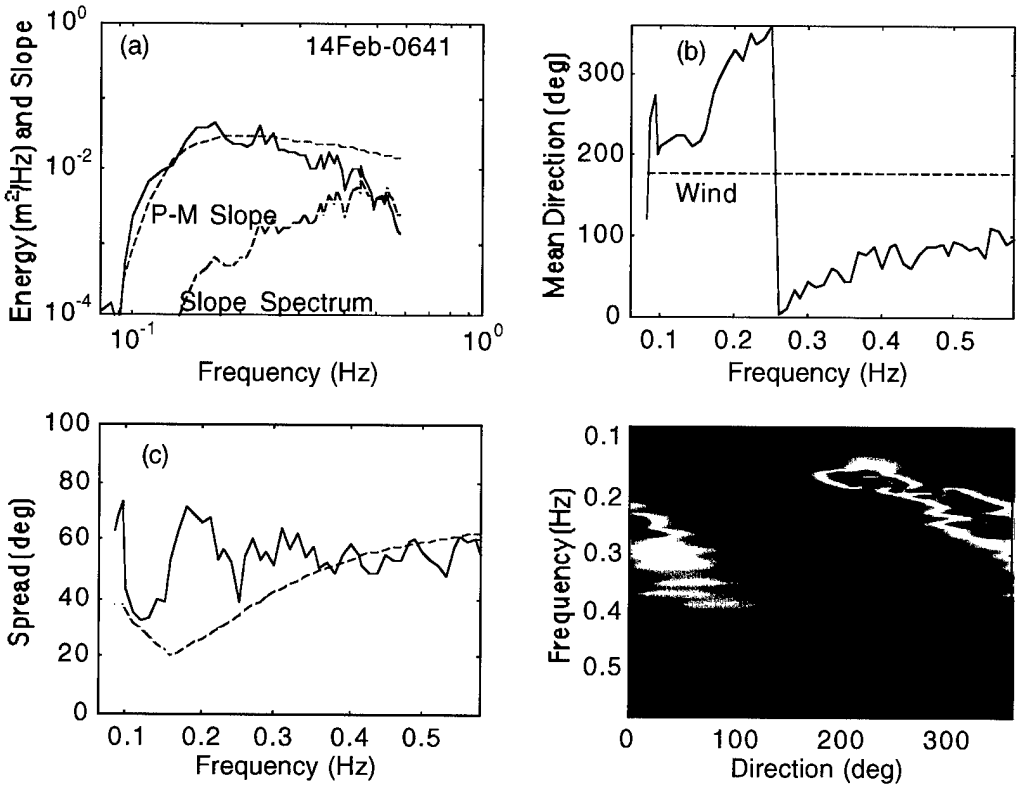

Figure 21. **Event B**--13Feb-0641. (See Figure 16 for legend.)

and the wind-wave system shifts from 76° to 65° at 15Feb-0140. This shift does not appear to be caused by the wind field. There is no significant change in wind speed and the wind has turned only slightly from 116° to 132°. The wind-wave system however turns away from the rather than toward the wind vector. Looking at the directional spectrum of 15Feb-0140, there are now three discernible wave systems:

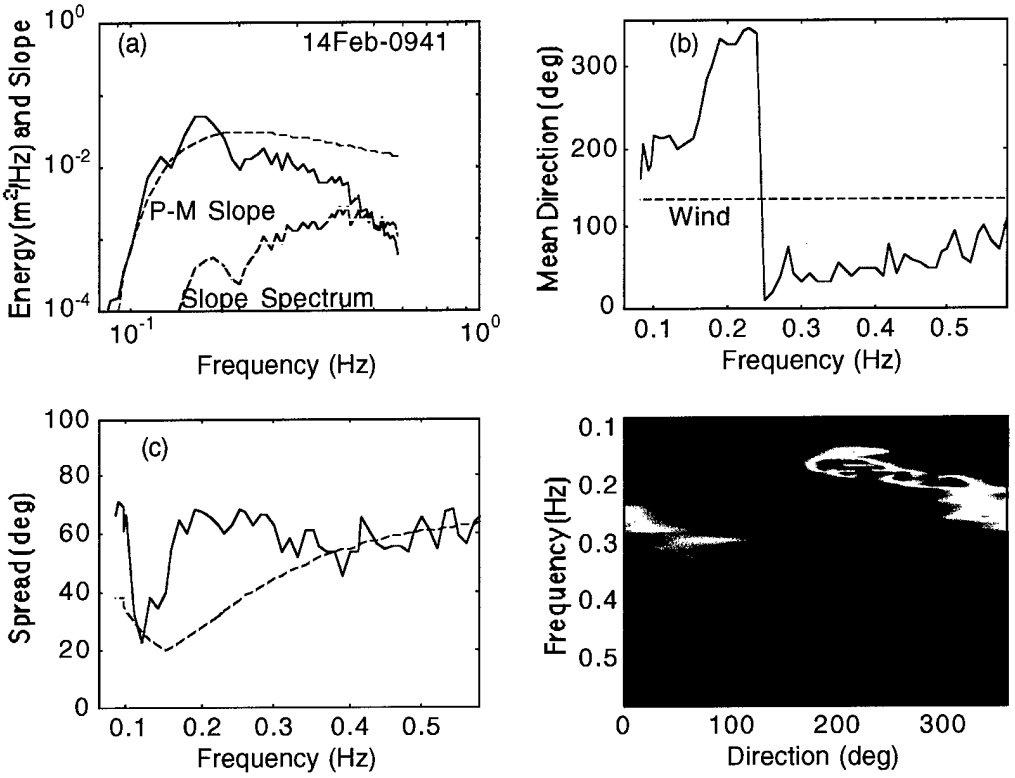

Figure 22. **Event B**--14Feb-0941. (See Figure 16 for legend.)

one swell system from a distance arriving at 233°, one "intermediate" system consisting of older wind-waves traveling at approximately 155°, and one young wind-wave system at 65°. The turning of the young wind-wave system away from the wind vector suggests that the low frequency systems, which are now more focused at 15Feb-0140 than at 15Feb-0041, are responsible for altering the growth pattern of the

Table 3. **Event C**--Wind speed and direction, wave direction for low and high frequencies, and wave energy spread.

Time ddmm-hour	U_7 m/s	∂_w deg	θ_{m1} deg	θ_{m2} deg	σ_{min} deg
14Feb-1141	3.97	129	265	—	—
14Feb-1241*	4.33	145	239	100	40
14Feb-1341*	3.70	138	250	107	30
(14Feb-1441*)	3.07	147	223	109	33
14Feb-1541	1.57	142	226	112	36
14Feb-1641	2.50	124	241	114	39
14Feb-1741	1.77	111	254	126	50
14Feb-1841	2.13	55	250	130	57
14Feb-1941	2.97	88	262	122	55

* classified as Stage I sea
( ) spectrum not included in figures
U_7 wind speed and ∂_w wind direction--same as Table 1
θ_{m1} low-frequency peak direction, θ_{m2} high-frequency peak direction, and σ_{min} average minimum wave spread--same as Table 1

young wind-sea. From 15Feb-0140 to the end of Event D (15Feb-0440), the wind-waves continue to develop away from the wind vector as it veers from 132° to 113°. However, it is interesting to note that the low frequency peak is also turning from 273° to 222°.

Soon after Event D ends, Event E begins. The evolution of the multimodal

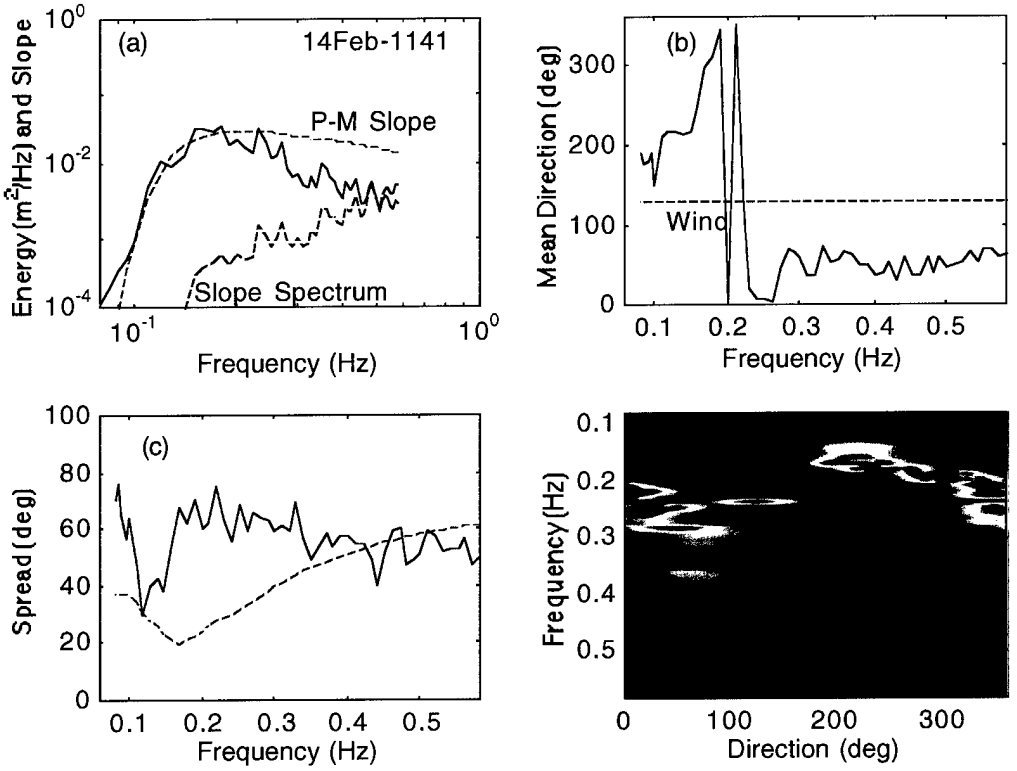

Figure 23. **Event C**--14Feb-1141. (a) Wave energy spectrum (blue solid), wave slope spectrum (red dashed), and P-M slope spectrum for a developed sea with modal frequency of 0.15 Hz (green dashed). (b) Mean wave (blue solid) and wind (red dashed) directions. (c) Wave spread (blue solid) and Donelan et al. (1985) spread model (green dashed). (d) Directional wave energy spectrum.

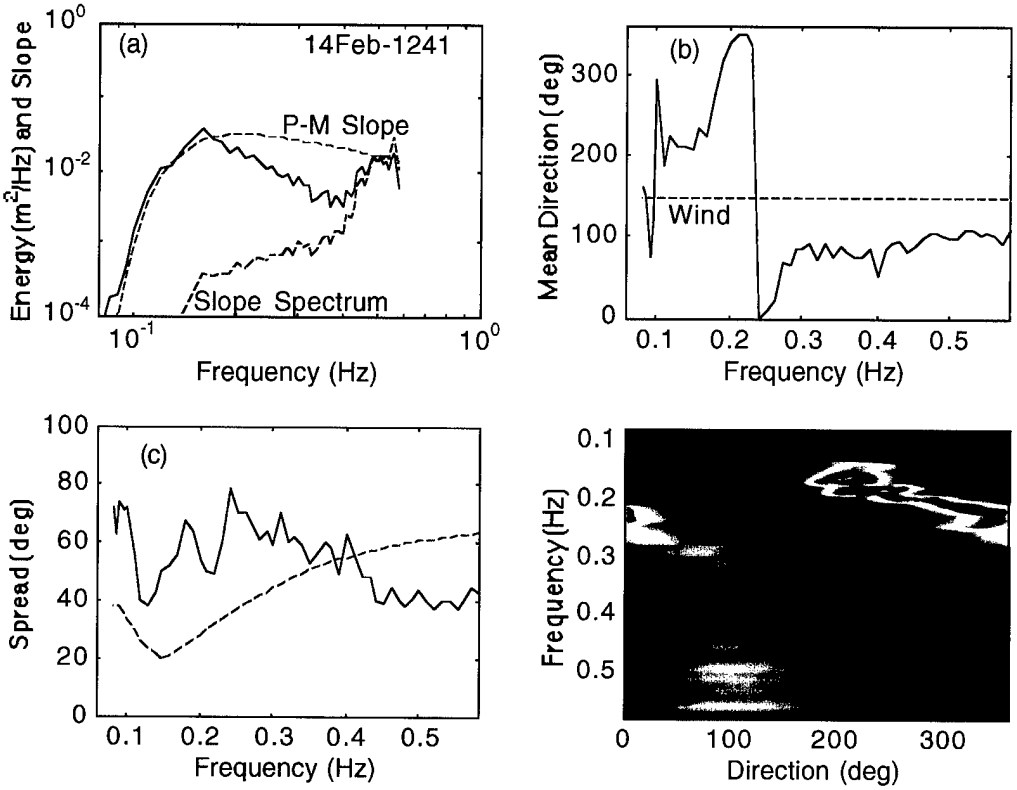

Figure 24. **Event C**--14Feb-1241. (See Figure 23 for legend.)

system during Event E is noteworthy. Typically, a prevailing long wave system dominates the wave field and ultimately absorbs the wind-wave energy, accelerating the decay of the wind-wave system. An example of this situation will be seen at the end of Event E. However, at the beginning of Event E, it is the wind-wave system that prevails, and the swell system that degenerates. At 15Feb-0740 (Figure 41), the

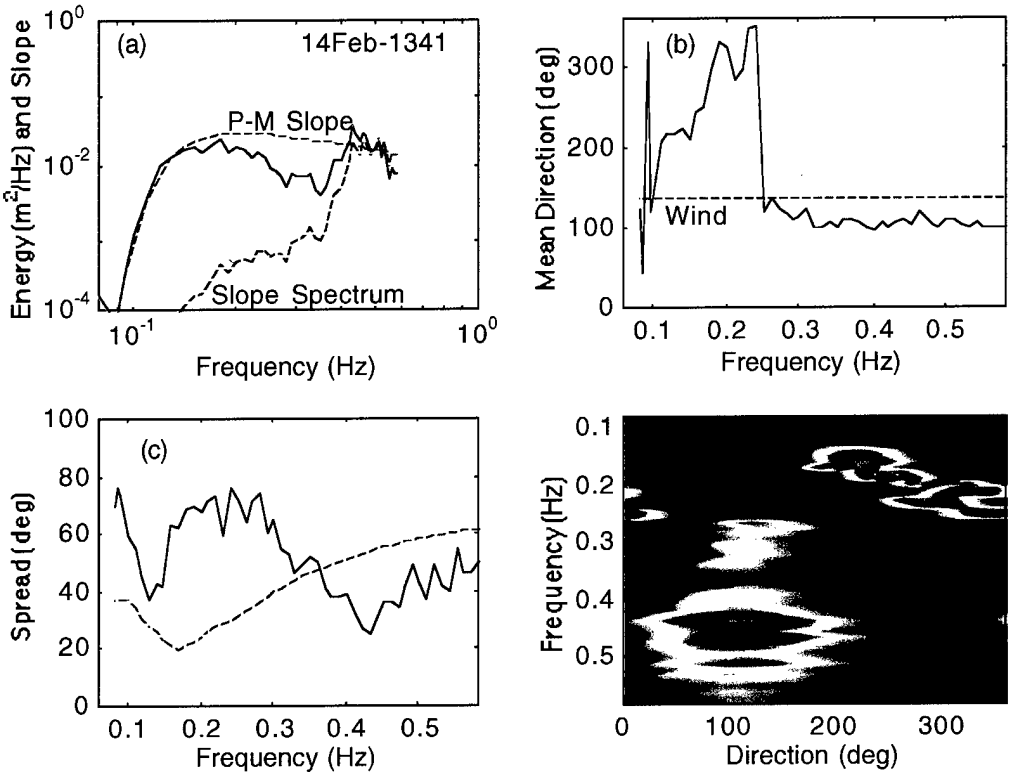

Figure 25. **Event C**--14Feb-1341. (See Figure 23 for legend.)

recently developed wind-wave system at 0.21 Hz, from 134°, dominates the longer waves of a decaying swell system at 0.17 Hz, propagating from roughly 210°. The interaction between the two systems results in the integration of most of the swell energy into the old wind-sea, as seen in 15Feb-0840 and 0940 (Figures 42 and 43). The absorption of the swell energy produces an overshoot in the energy density of the wind-wave peak (Figure 42a). The swell system disappears and the sea state becomes

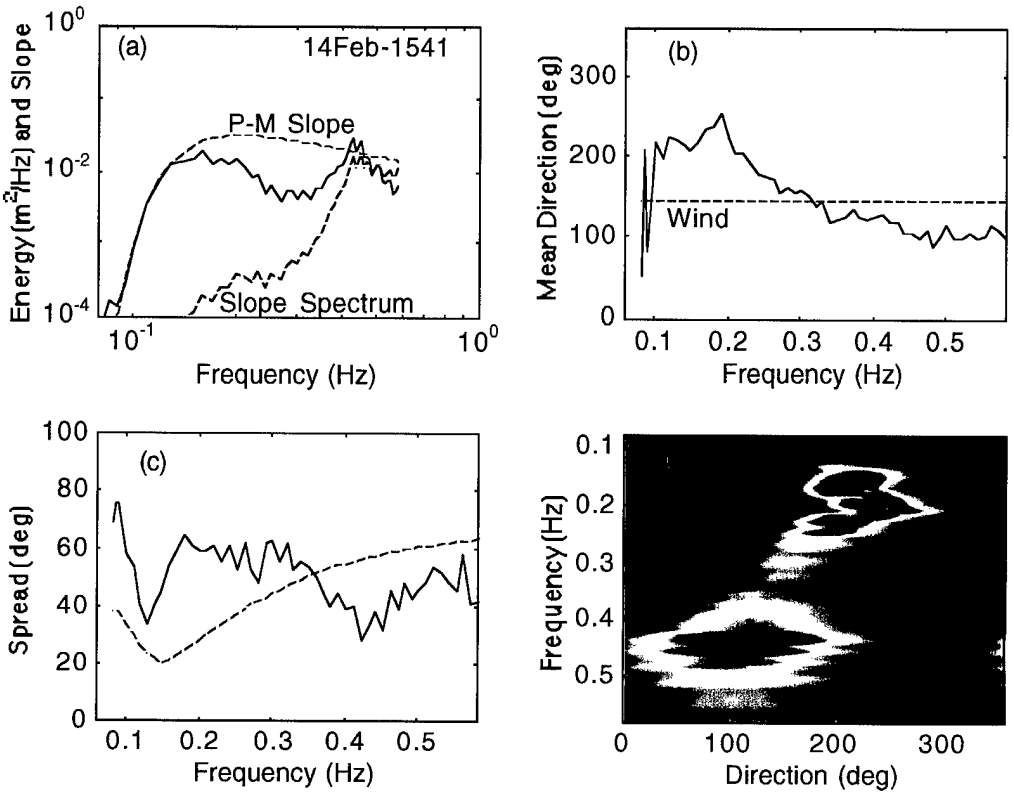

Figure 26. **Event C**--14Feb-1541. (See Figure 23 for legend.)

bimodal, with an overdeveloped wind-wave system traveling at 147° and a wind-wave system at 90°. In the last hours of Event E, the bimodal sea state disappears as the wind-sea interacts with the closely aligned low frequency system (Figures 50-52).

In some studies, such as Reid (1995), there is no evidence to indicate that, when the wind vector and swell direction are aligned, bimodalism in the wave spectrum is observed. For conditions of aligned wind and swell directions, bimodal

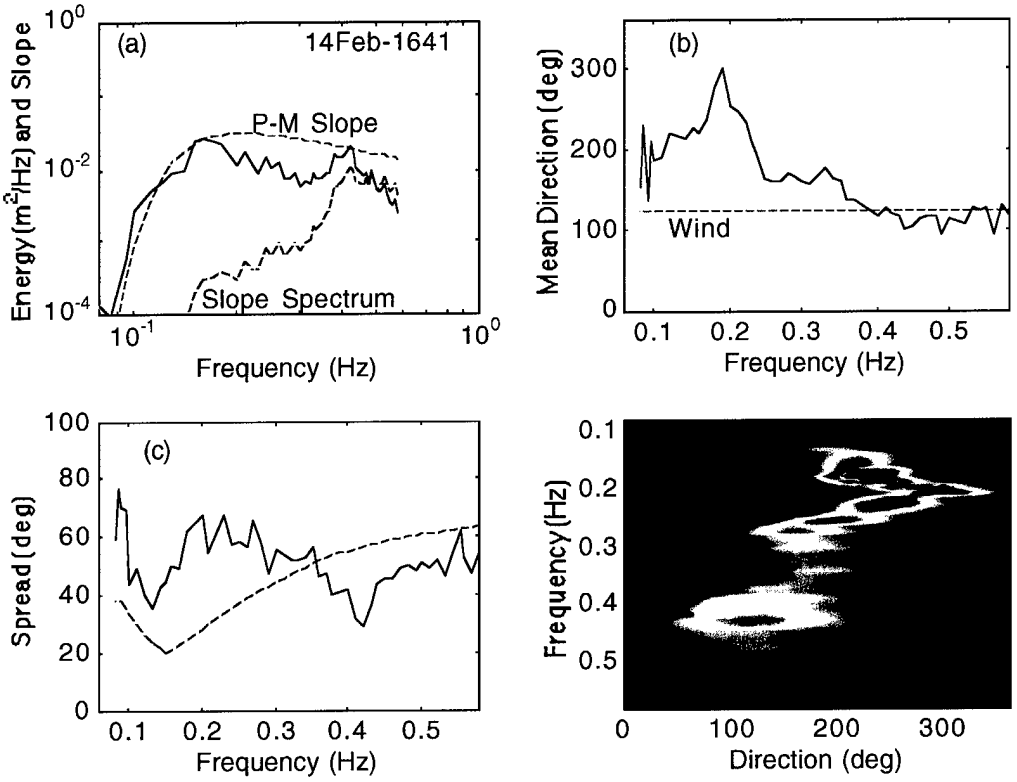

Figure 27. **Event C**--14Feb-1641. (See Figure 23 for legend.)

wave spectra are observed later in Event E. The influence of wind duration, as well as that of swell presence, can be observed in the remainder of Event E. Except for a brief fluctuation down to 3.9 m/s, the wind speed remains relatively steady between 4.4 m/s and 5.2 m/s, from 15Feb-1140 to 1811 (Table 5). During this period, the wind-sea system grows at an angle of 15-45° to the wind vector. As the shorter wind-waves

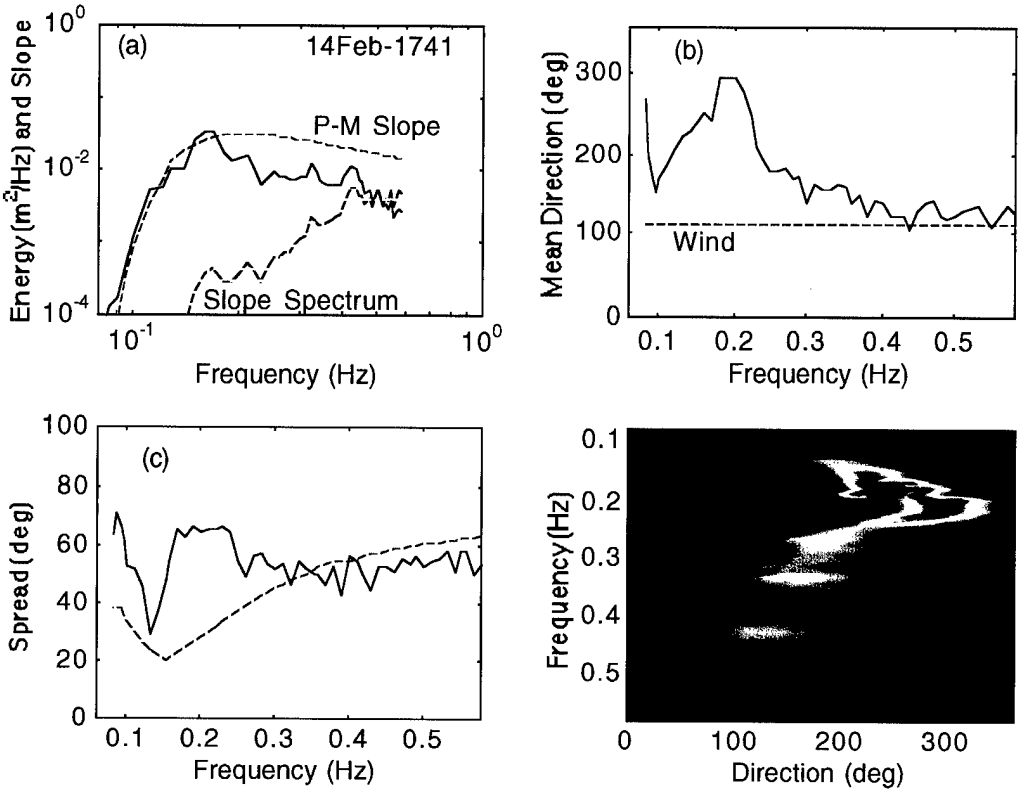

Figure 28. **Event C**--14Feb-1741. (See Figure 23 for legend.)

grow longer in length, they begin to interact with the swell system and become incorporated into the long wave system, as seen from 15Feb-1511 to 1911 (Figures 46-48). The short wind-waves, with a modal frequency of about 0.45 Hz, continue to propagate 20-40° from the long wave components, for this case of closely aligned wind vector and swell direction. Between 15Feb-1911 and 2111, the wind increases

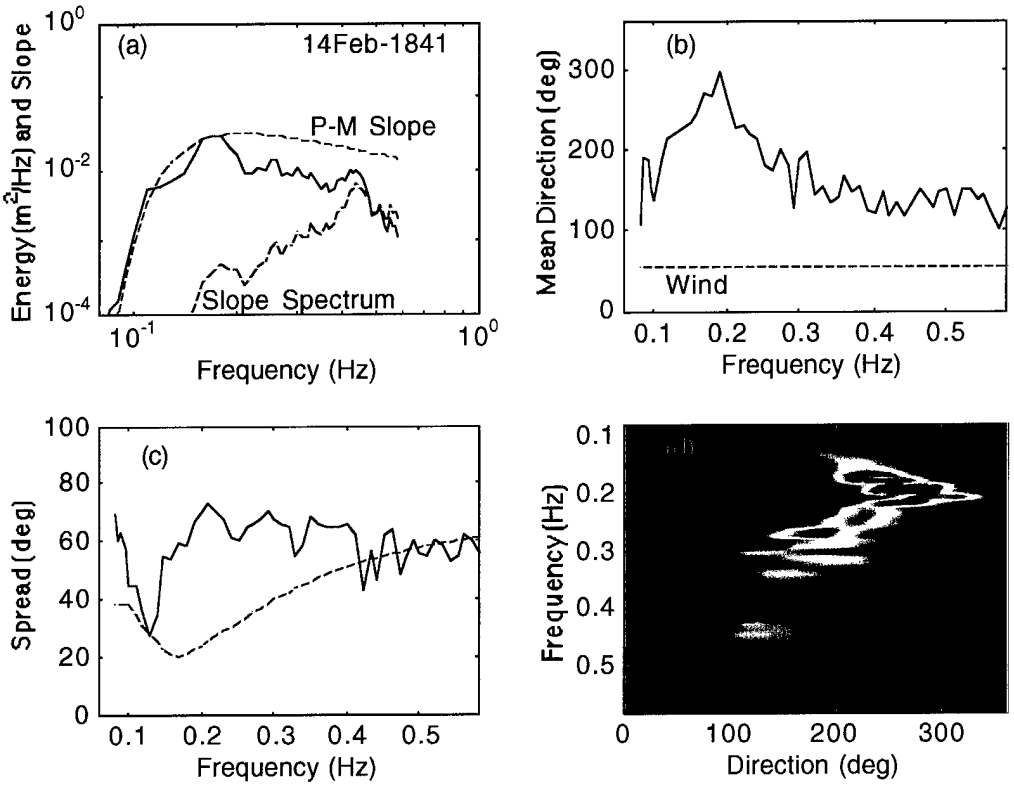

Figure 29. **Event C**--14Feb-1841. (See Figure 23 for legend.)

to over 6 m/s and then reduces gradually to 3.6 m/s at 16Feb-0441. From 15Feb-0940 to 16Feb-0441 (Figures 43d-52d), one can witness the maturing of a wind-sea in the presence of a dominant long wave system. The bimodal spectrum at 15Feb-0940 becomes "lost" in Stage II as the growth of the younger wind-sea progresses under sustained wind forcing. The two systems begin to merge at 15Feb-1140 (Figure 45d).

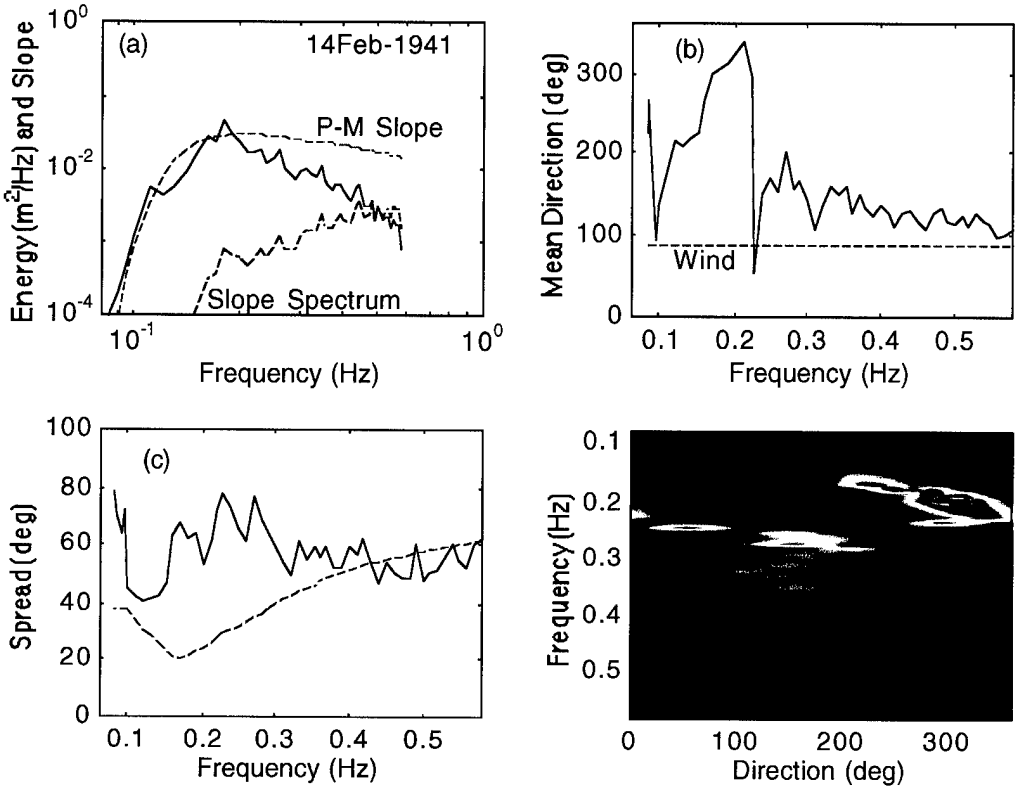

Figure 30. **Event C**--14Feb-1941. (See Figure 23 for legend.)

In this case, the longer waves are not assimilated by the shorter waves, as was seen earlier in this event. At 16Feb-0441, the younger wind-sea has combined with the older wind-sea completely, resuming the unimodal shape of Stage III spectra. All wind-wave components are now aligned with in the direction of the longer waves (Figure 52b).

Table 4. **Event D**--Wind speed and direction, wave direction for low and high frequencies, and wave energy spread.

Time ddmm-hour	U_7 m/s	∂_w deg	θ_{m1} deg	θ_{m2} deg	σ_{min} deg
14Feb-2041	4.53	93	300	104	54
14Feb-2141*	4.53	95	305	65	31
14Feb-2241*	3.47	96	296	77	39
14Feb-2341*	4.23	105	268	69	37
15Feb-0041*	4.40	116	273	76	37
15Feb-0140*	3.87	132	233	65	48
15Feb-0240*	4.00	122	234	50	55
15Feb-0341	3.73	119	229	54	56
15Feb-0440	3.23	113	222	46	56

* classified as Stage I sea
( ) spectrum not included in figures
U_7 wind speed and ∂_w wind direction--same as Table 1
θ_{m1} low-frequency peak direction, θ_{m2} high-frequency peak direction, and σ_{min} average minimum wave spread--same as Table 1

The offwind wave growth observed in Event E and in former events, along with the effects of swell and wind on wind-sea development, will further be discussed in Section 4. In mixed seas, the effect of swell on wind-waves can also be detected in the directional spreading of wind-waves. For these same events, the modulation of the directional spreading of wind-waves by swell is described next.

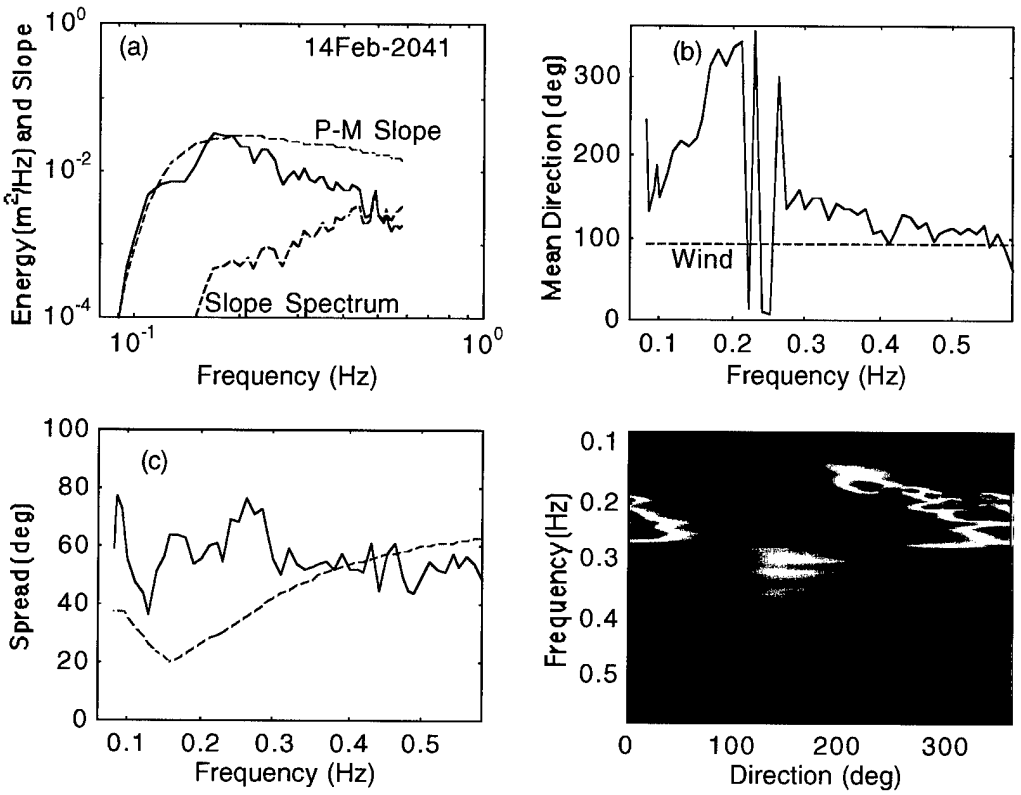

Figure 31. **Event D**--14Feb-2041. (a) Wave energy spectrum (blue solid), wave slope spectrum (red dashed), and P-M slope spectrum for a developed sea with modal frequency of 0.15 Hz (green dashed). (b) Mean wave (blue solid) and wind (red dashed) directions. (c) Wave spread (blue solid) and Donelan et al. (1985) spread model (green dashed). (d) Directional wave energy spectrum.

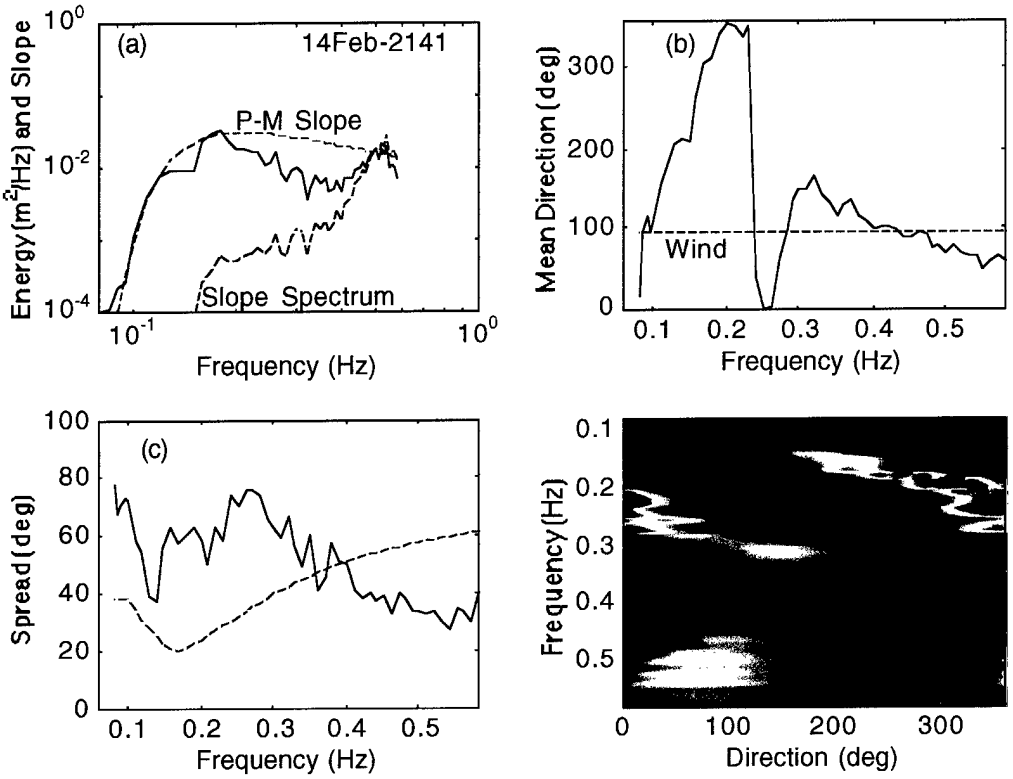

Figure 32. **Event D**--14Feb-2141. (See Figure 31 for legend.)

3.4 Directional Spread of Mixed Seas

As discussed in Section 1.3, the directional spreading of a unimodal wave field is mainly dependent on the wave frequency, relative to the peak frequency. The different conditions of mixed seas found in all events suggest that the relative locations

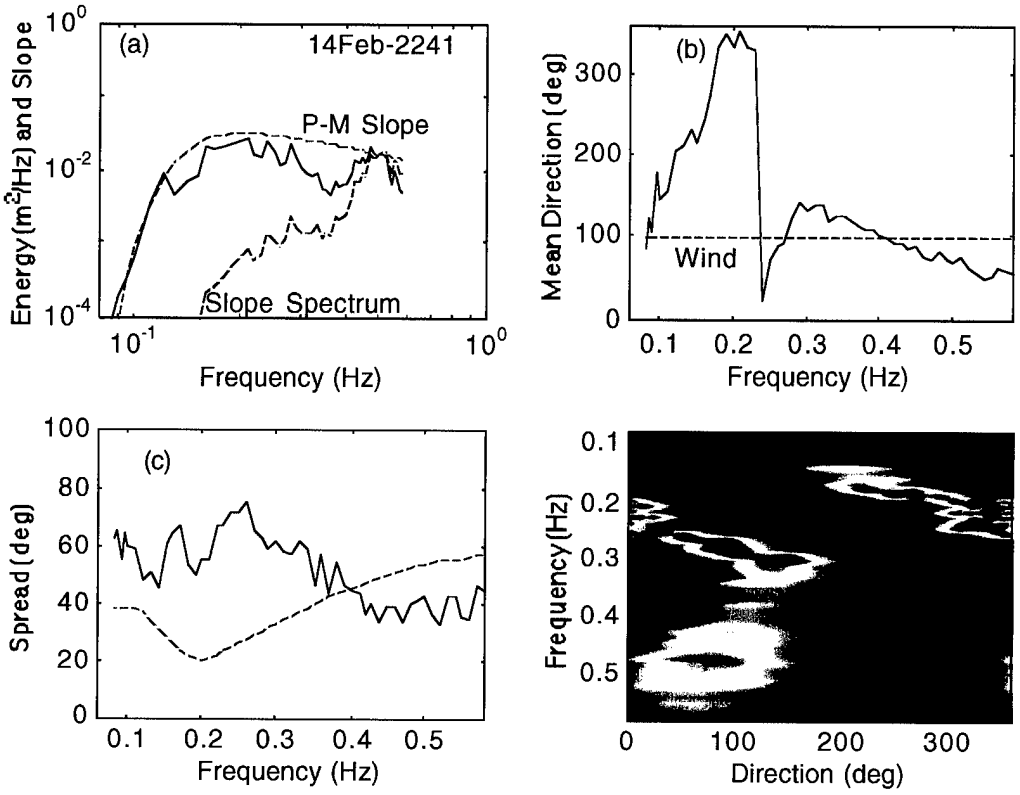

Figure 33. **Event D**--14Feb-2241. (See Figure 31 for legend.)

of the swell and wind-wave systems in the direction space have significant effects on the angular spreading of wind-waves. The directional spread distribution of aligned and opposed seas have different features and the cases of opposing systems are described first.

At the outset of Event A, the directional spread of the unimodal wave field at 12Feb-2341 resembles those obtained by directional models of Section 1.3. (See

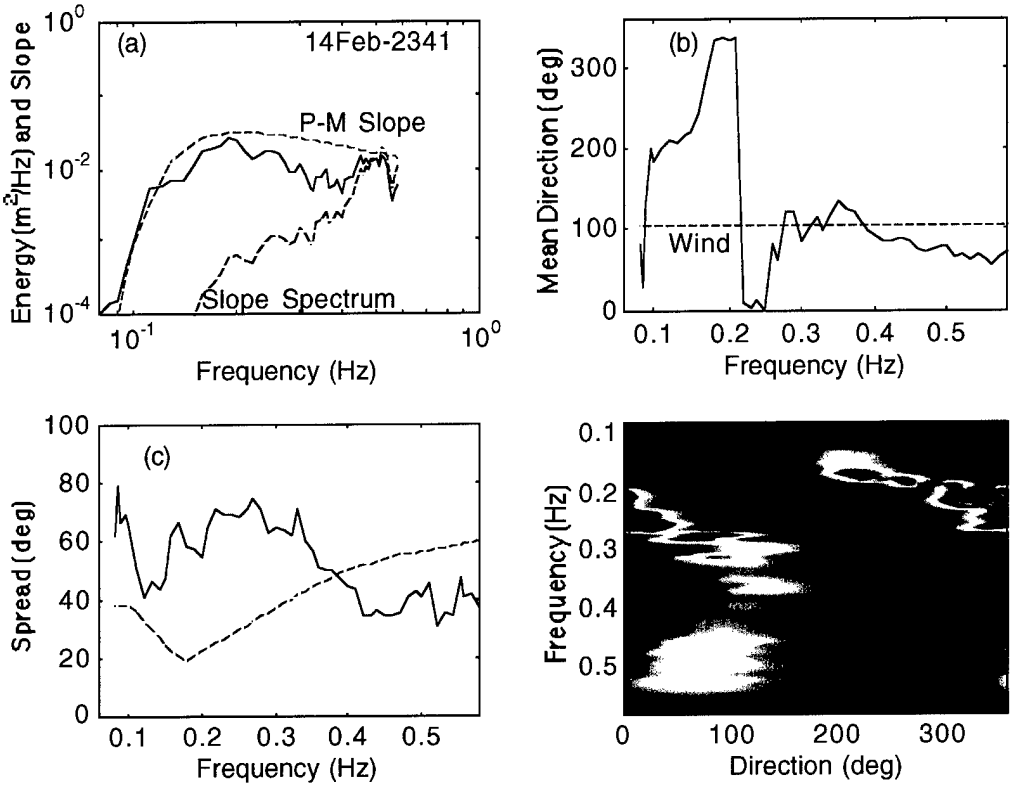

Figure 34. **Event D**--14Feb-2341. (See Figure 31 for legend.)

Figures 4 and 10c). Accompanying the secondary wave peak at 13Feb-0041, a secondary local minimum appears in the spread distribution. The lowest angular spread of 36° is much broader than the 20° minimum of the unimodal spectrum, as predicted by the Donelan et al. (1985) formula (Figure 11c). The spreading of wave frequencies above 0.4 Hz broadens as the development of the wind-sea system

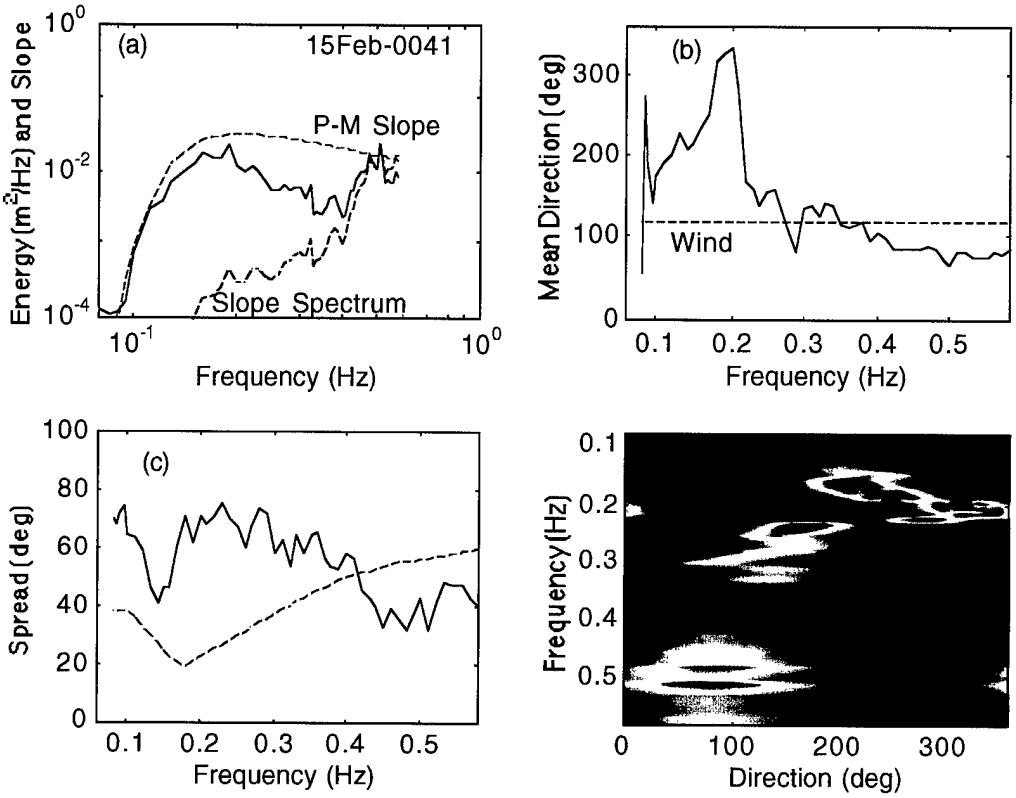

Figure 35. **Event D**--15Feb-0041. (See Figure 31 for legend.)

progresses, indicating an increased angular dispersion of wave energy about its mean direction of propagation. An interesting observation is the existence of a local maximum in the directional spread distribution between the two minima; this peak corresponds with the transition regime between the two wave systems. The shifting of the transition peak from about 0.35 Hz (13Feb-0041) to 0.25 Hz (13Feb-0441) indicates that the presence of an angular spread peak can provide an alternative method

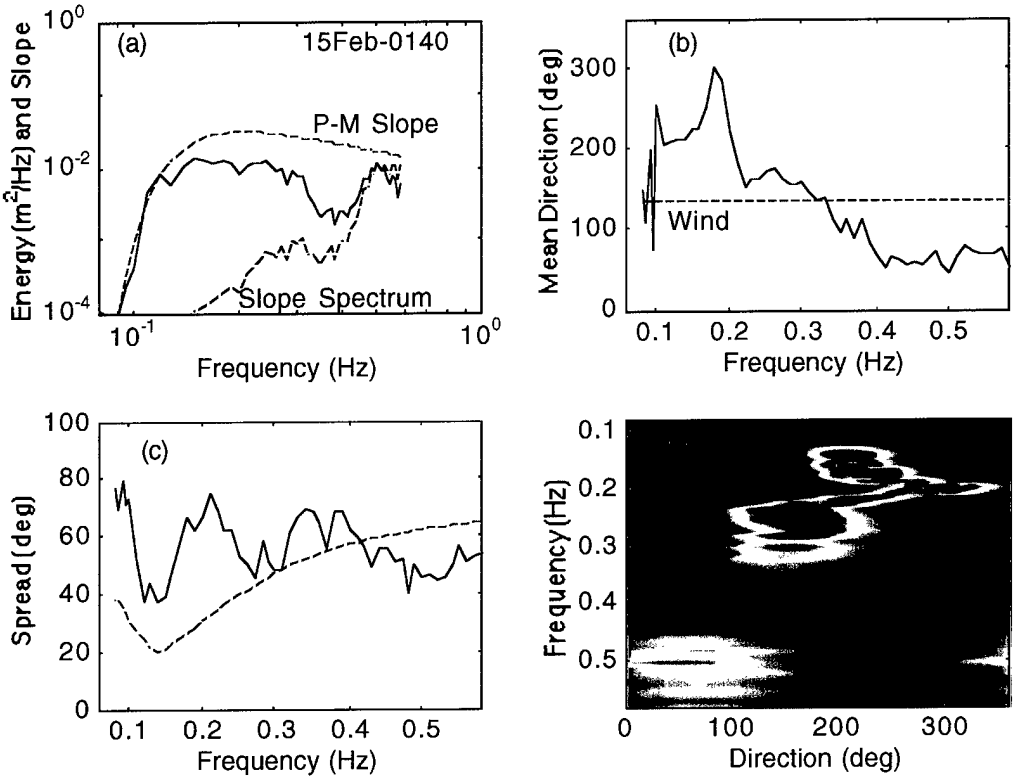

Figure 36. **Event D**--15Feb-0140. (See Figure 31 for legend.)

of tracking the transition regime between wave systems (Figures 11-14). This trait in the energy spread also appears in Event B, where the wind vector relative to swell direction varies from 52° to 161°.

The spread features in Event B are very similar to those in Event A. The bimodal sea at 14Feb-0041 (Figure 16a and 16c) has two corresponding valleys, with

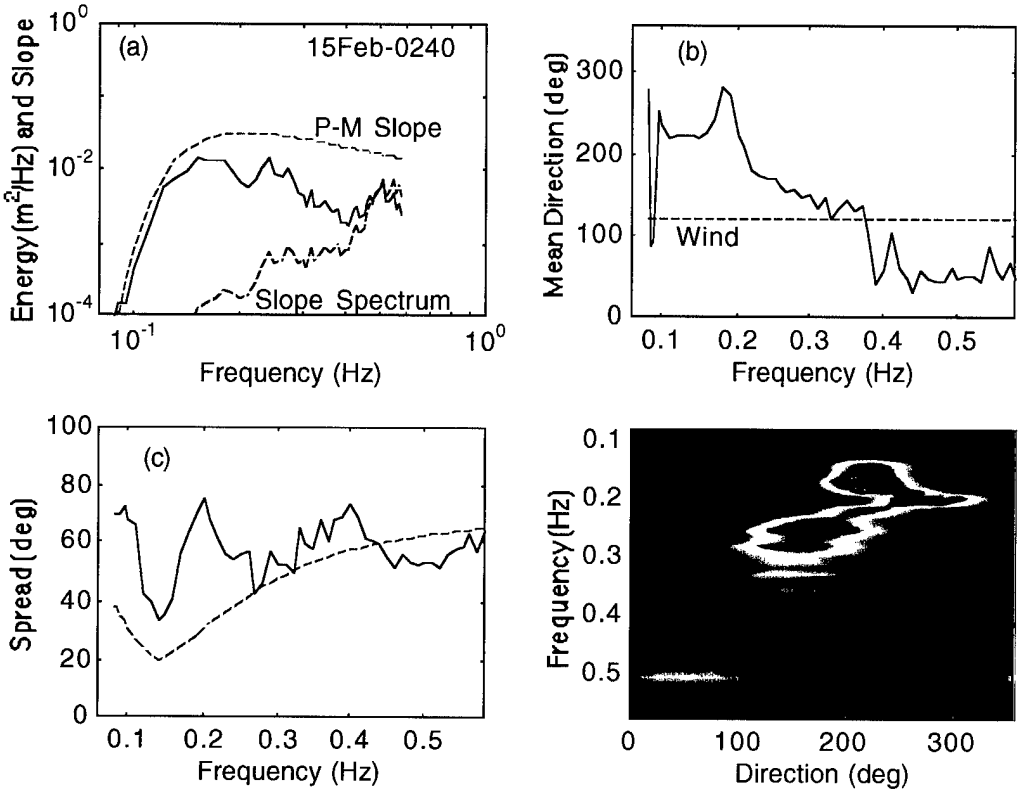

Figure 37. **Event D**--15Feb-0240. (See Figure 31 for legend.)

the minimum spread for the wind-wave system of about 35°. As the wind-waves develop into a Stage II sea, the angular spreading of the wind-waves levels out and broadens to 57°, while the transition peak slowly shifts from 0.26 Hz to 0.17 Hz. Unfortunately, further maturity of the mixed sea is preempted by an increase in wind, which produces Event C.

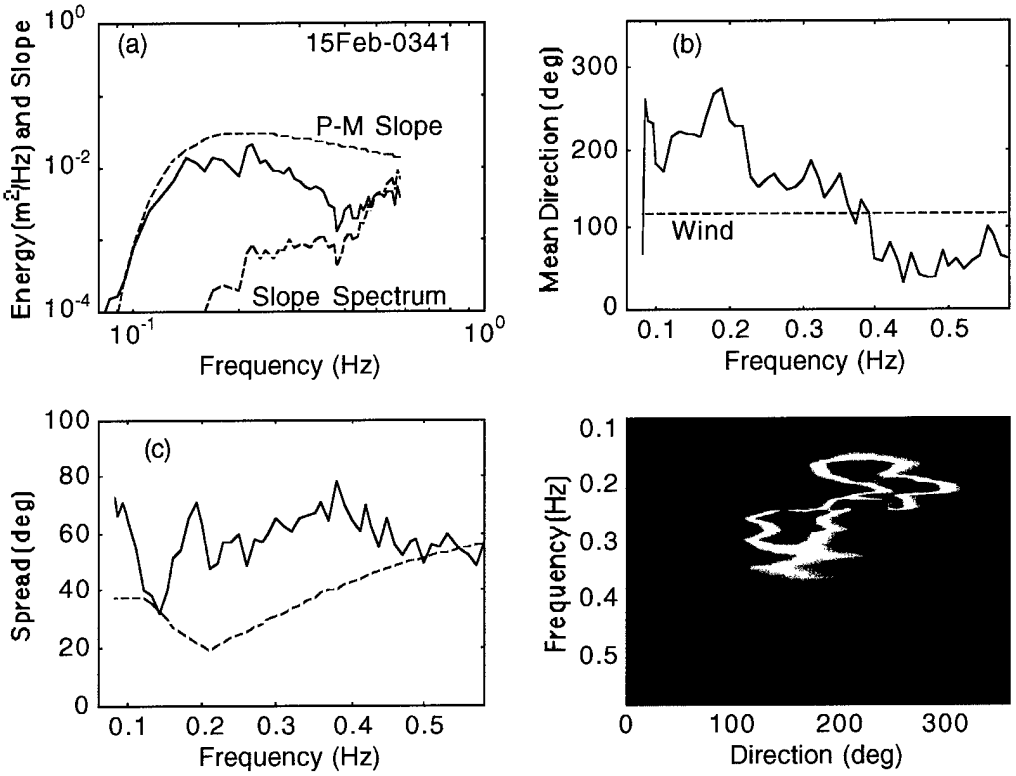

Figure 38. **Event D**--15Feb-0341. (See Figure 31 for legend.)

As in Events A and B, the existence of a wind-wave system in Event C can also be detected in the directional spread distribution. In Event C, at 14Feb-1141, the increasing wind speed forces the small waves into one direction, reducing the angular spread to roughly 50° (Figure 23c). When the sea becomes bimodal at 14Feb-1241 (Figure 24c), the wind-wave spreading reduces to 40° and another valley, associated with the wind-sea peak, forms in the spread distribution. At 14Feb-1341, the wind-

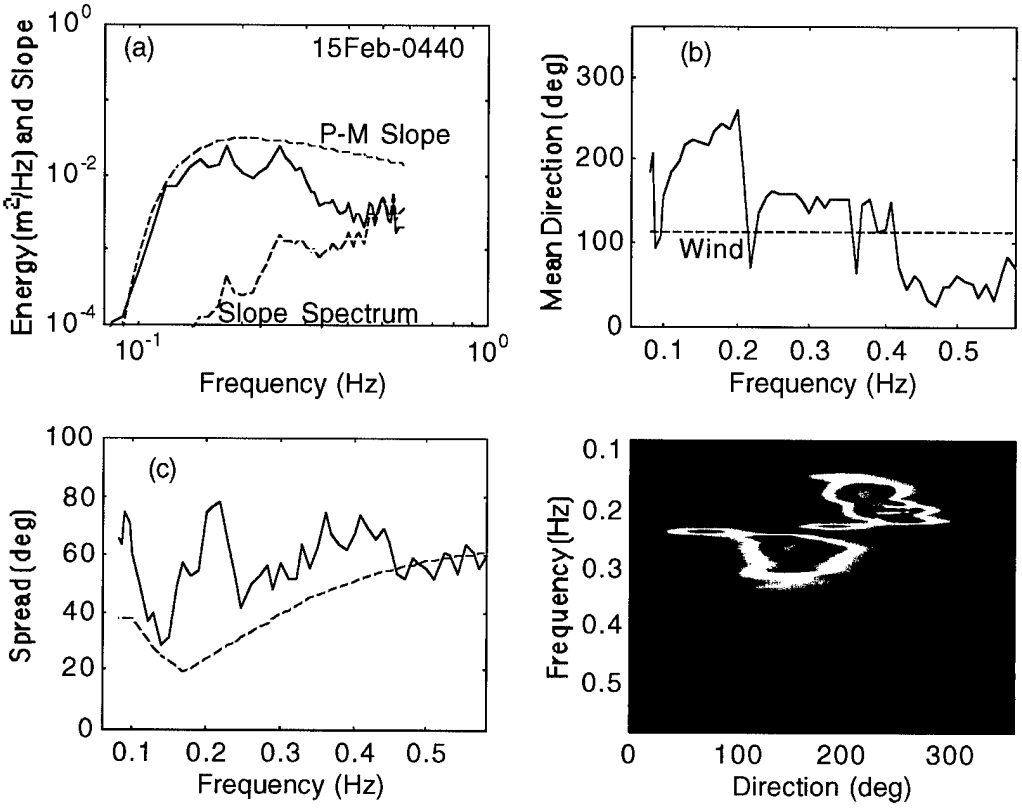

Figure 39. **Event D**--15Feb-0440. (See Figure 31 for legend.)

sea peak is amplified and a distinct minimum appears in the spread distribution (Figure 25c). The minimum spread of the wind-wave system in Event C comes 5° closer to the values predicted by the models than do the minimum values of Events A and B. At this point in Event C, the wind waves are more energetic than the swell, while in Event A the swell system contained most of the wave energy (Figures 25-26 and 11-12).

Table 5. **Event E**--Wind speed and direction, wave direction for low† and high frequencies, and wave energy spread.

Time ddmm-hour	U_7 m/s	∂_w deg	θ_{m1} deg	θ_{m2} deg	σ_{min} deg
15Feb-0640	4.33	123	162	—	—
15Feb-0740*	4.67	115	134	88	44
15Feb-0840*	4.73	125	145	104	40
15Feb-0940*	5.07	125	147	90	44
15Feb-1040*	5.57	123	138	95	41
15Feb-1140	5.23	133	144	101	41
(15Feb-1311)	3.87	145	153	102	46
(15Feb-1411)	4.80	149	156	122	40
15Feb-1511	4.43	146	154	119	36
15Feb-1611	4.60	132	158	123	43
(15Feb-1711)	4.67	141	151	134	54
(15Feb-1811)	4.90	138	152	123	44
15Feb-1911	5.67	136	140	120	42
(15Feb-2011)	6.27	131	136	112	38
15Feb-2111	5.97	128	140	107	38
(15Feb-2211)	4.83	127	138	110	39
(15Feb-2311)	4.67	142	140	112	37
16Feb-0011	5.57	152	142	118	35
(16Feb-0111)	4.20	170	145	122	36
16Feb-0211	4.27	156	147	123	41
(16Feb-0341)	2.93	133	149	142	45
16Feb-0441	3.60	146	151	150	50

* classified as Stage I sea, ( ) spectrum not included in figures

† refers to mature wind-sea at 0.21 Hz

U_7 wind speed and ∂_w wind direction--same as Table 1

θ_{m1} low-frequency peak direction, θ_{m2} high-frequency peak direction, and σ_{min} average minimum wave spread--same as Table 1

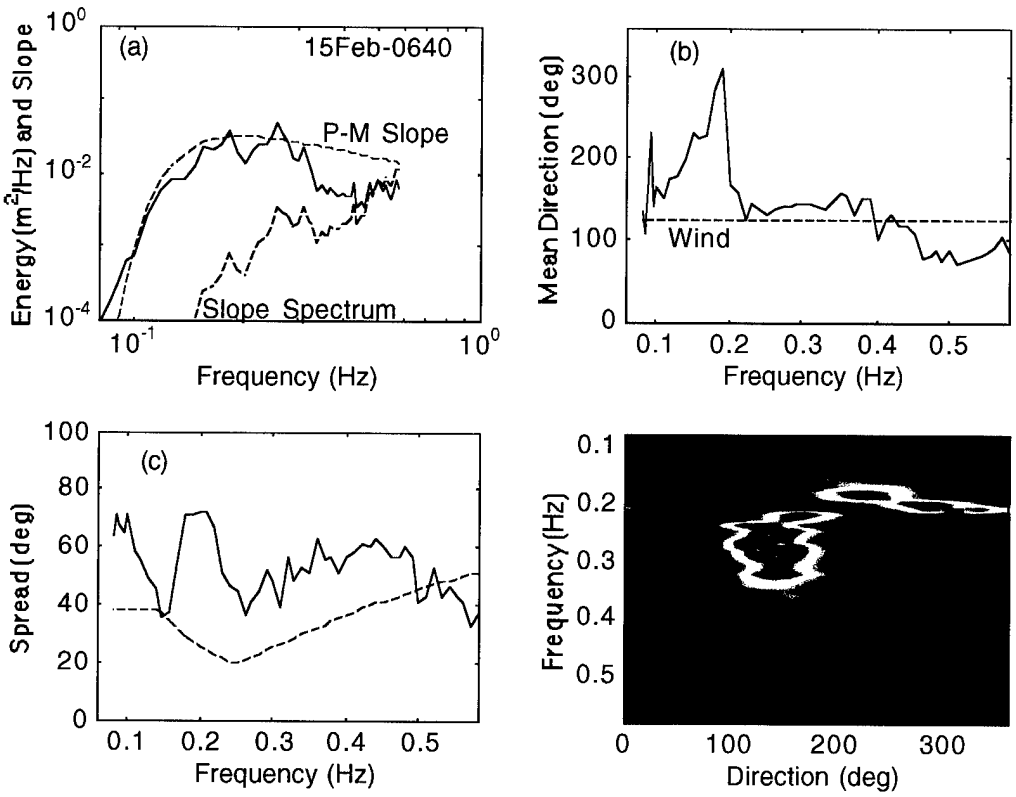

Figure 40. **Event E**--15Feb-0640. (a) Wave energy spectrum (blue solid), wave slope spectrum (red dashed), and P-M slope spectrum for a developed sea with modal frequency of 0.15 Hz (green dashed). (b) Mean wave (blue solid) and wind (red dashed) directions. (c) Wave spread (blue solid) and Donelan et al. (1985) spread model (green dashed). (d) Directional wave energy spectrum.

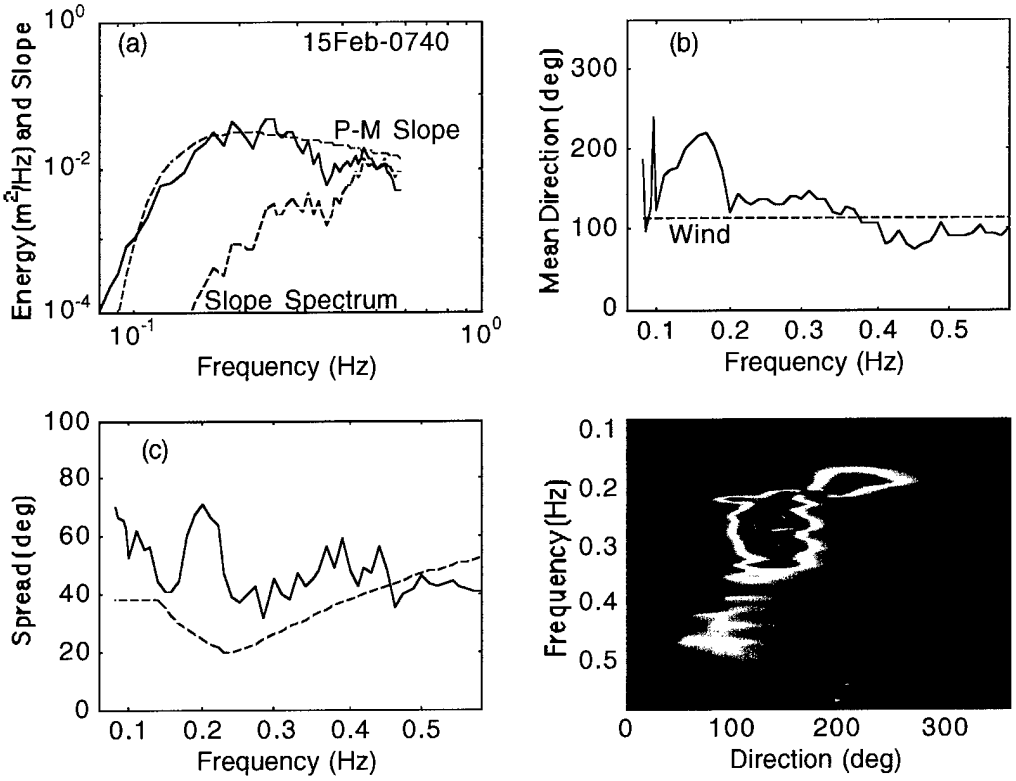

Figure 41. **Event E**--15Feb-0740. (See Figure 40 for legend.)

As the wind-sea grows and interacts with the swell system, the second minimum in the spread distribution disappears and the spreading of the high frequency waves broadens while the transition regime remains a salient feature (Figures 27c-30c). Anticipating that further development of the Stage II sea will result in a unimodal sea, one can expect the transition peak to diminish and the spreading to approach the expected

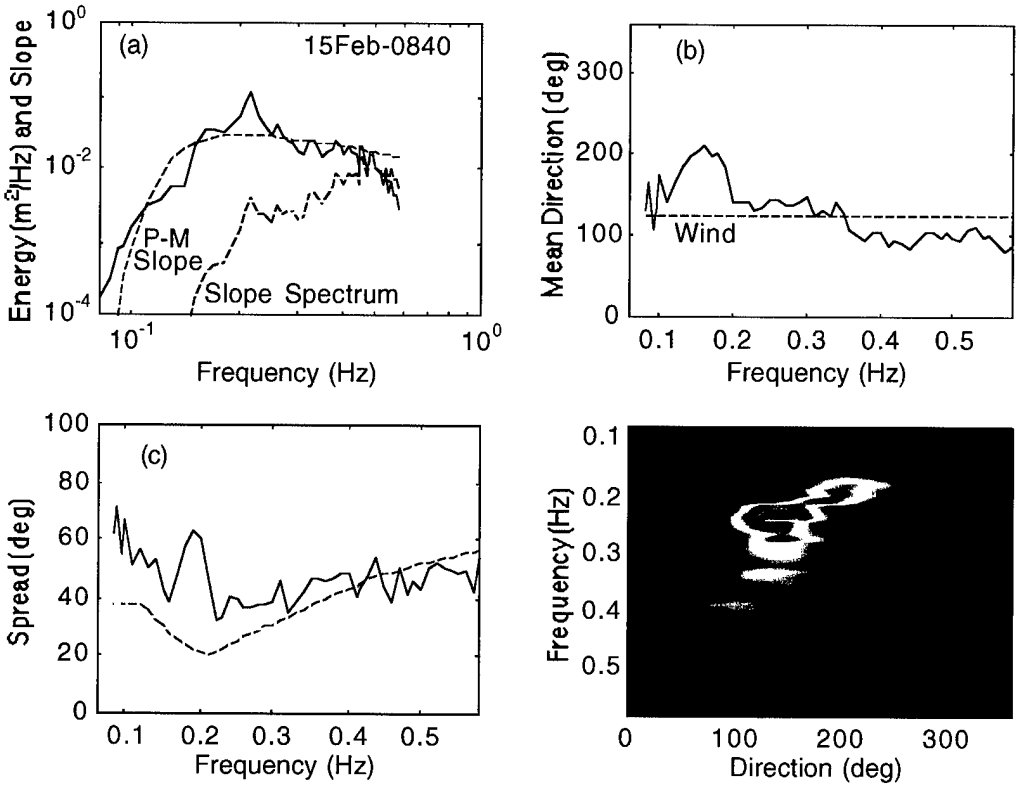

Figure 42. **Event E**--15Feb-0840. (See Figure 40 for legend.)

values given by directional models, as will be seen in Event E. However, in this event, the development of the wind-sea fails to reach Stage III. Thus observed spread distribution fails to resemble the "V" shape characteristic of unimodal seas.

The multimodal seas of Event D produce striking features in the spread distribution. The existence of an "intermediate" wave system between the swell and

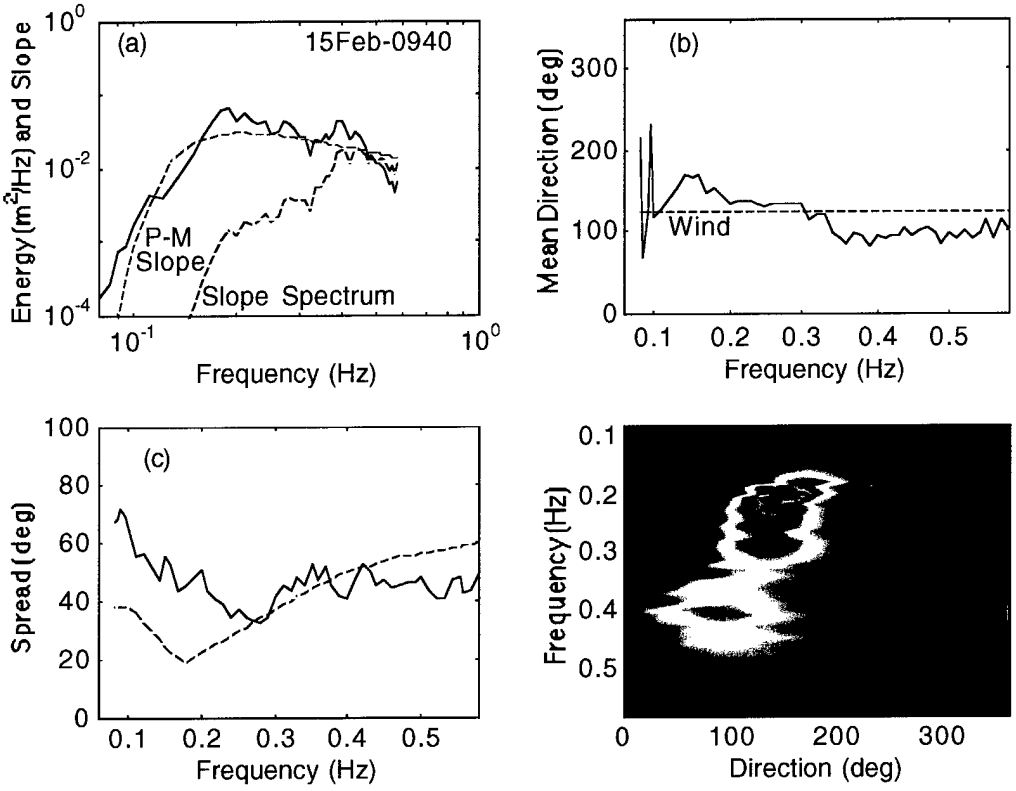

Figure 43. **Event E**--15Feb-0940. (See Figure 40 for legend.)

young wind-sea system is difficult to isolate in the omnidirectional spectrum of 15Feb-0140 (Figure 36). However, the "intermediate" system can be detected in the directional spectrum at about 0.24 Hz, at 160°. Further evidence of this system is identified by the third minimum in the angular spread distribution, in what would have been the transition regime between the original swell and the young wind-sea. At

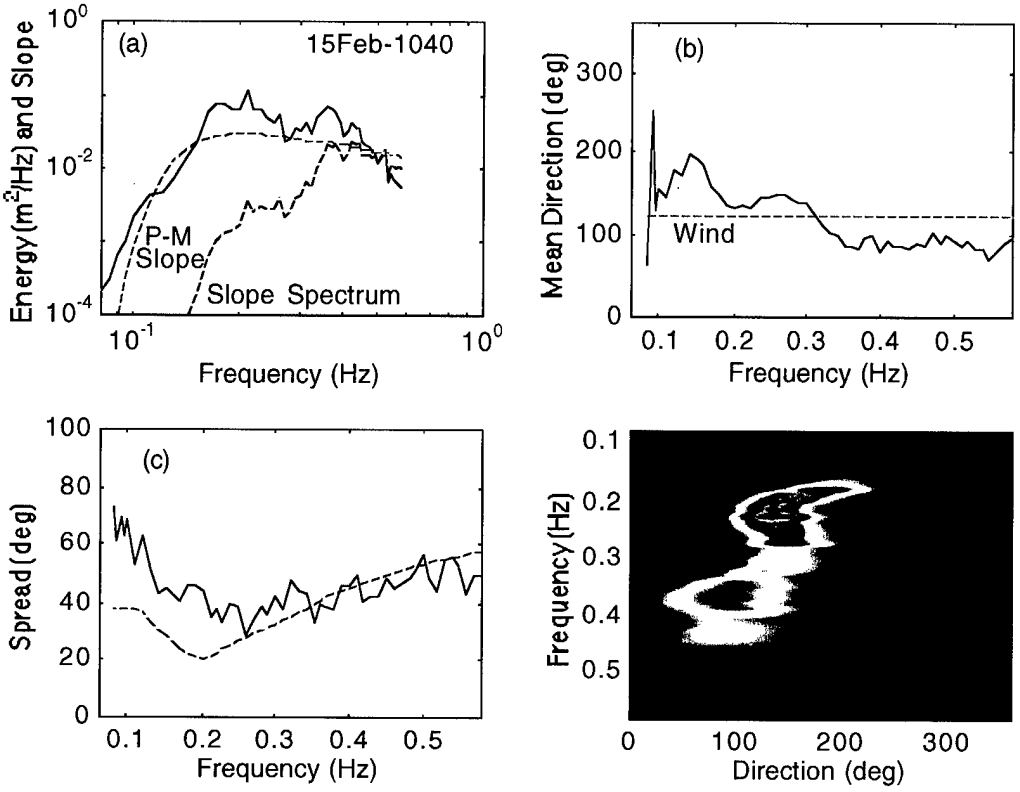

Figure 44. **Event E**--15Feb-1040. (See Figure 40 for legend.)

15Feb-0041, the minimum spreading of the young wind-sea is 37° (Figure 35c). With the emergence of the third wave system, at 15Feb-0140, the minimum value of the high frequency spreading increases to 48°. This increase in the spreading suggests that these long waves of the "intermediate" system are somehow interacting with the short wind-waves to increase the directional dispersion of the wind-wave energy.

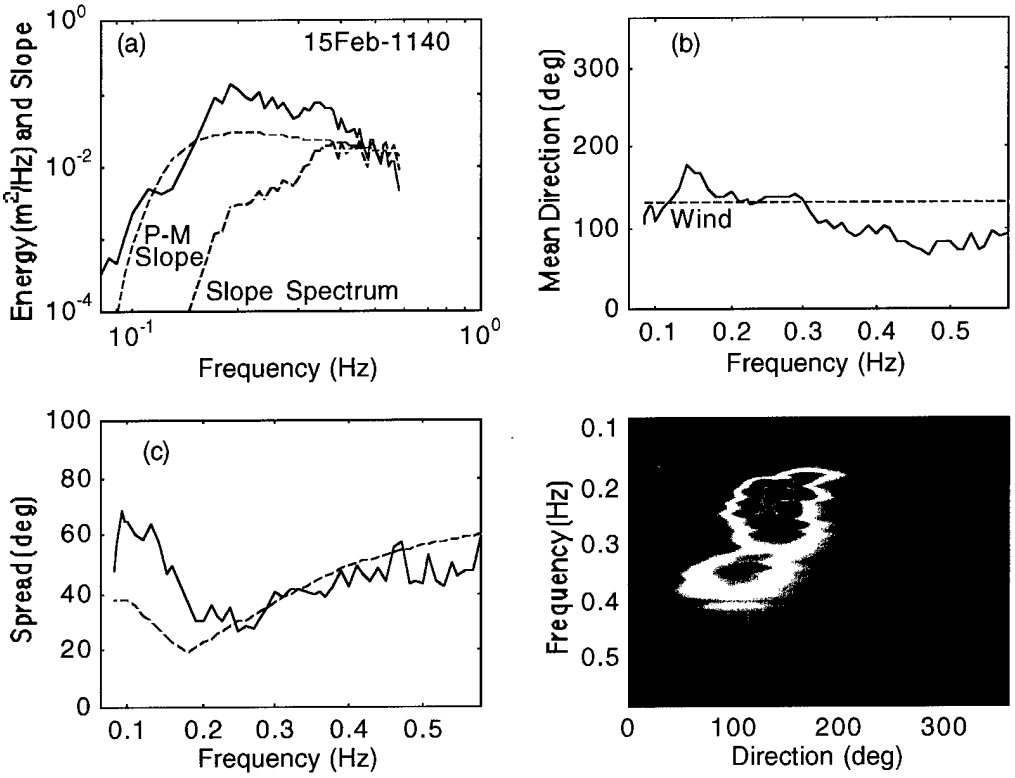

Figure 45. **Event E**--15Feb-1140. (See Figure 40 for legend.)

In the multimodal seas of Event E, the evolution of the directional spreading is marked by the interactions between the three distinct systems. At 15Feb-0740 (Figure 41), the three wave systems begin to interact, and accordingly, the directional spread distribution undergoes significant changes. From 15Feb-0740 to 0840 (Figures 41c and 42c), the transition peak between the mature and young wind-seas has diminished as the two wave systems have begun to merge; meanwhile, the swell

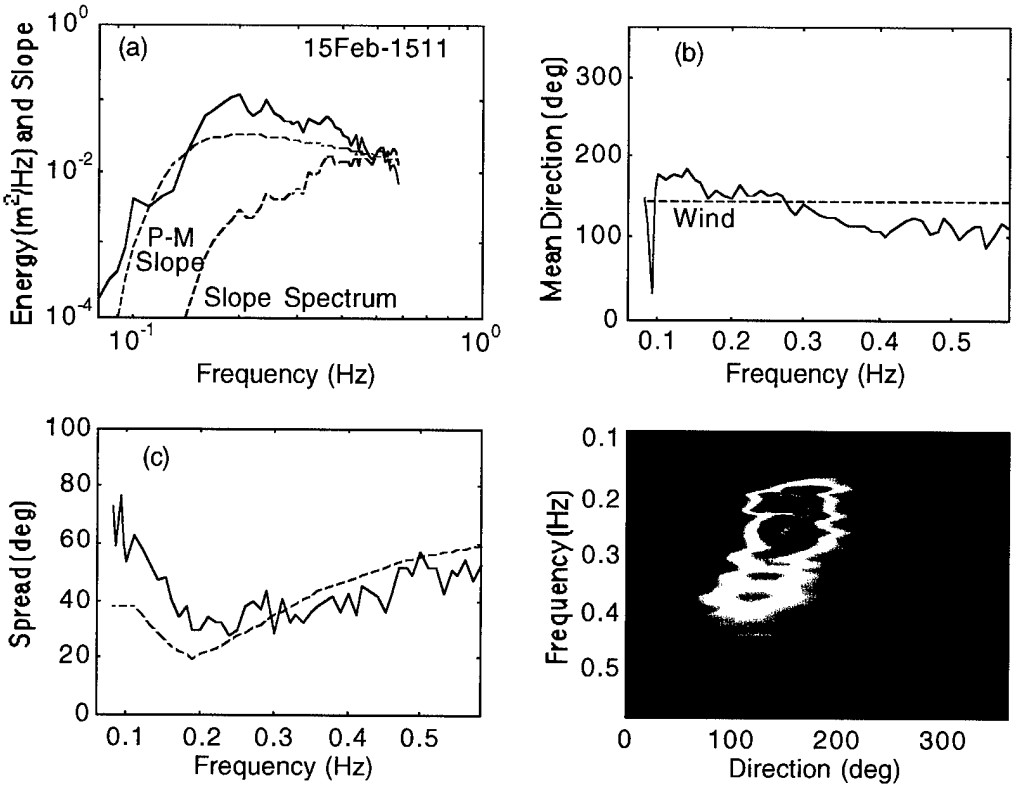

Figure 46. **Event E**--15Feb-1511. (See Figure 40 for legend.)

components have almost been integrated into the mature wind-wave system. At 15Feb-0940, the wave field consists essentially of a mature wind-sea at 0.21 Hz and a younger wind-sea at 0.34 Hz. Atypical to directional models and to most observations, the minimum spread does not lie at or below the peak frequency of 0.21 Hz. The minimum of the entire spread distribution is located above the peak frequency, at approximately 0.26 Hz (Figure 43c). This further supports the claim

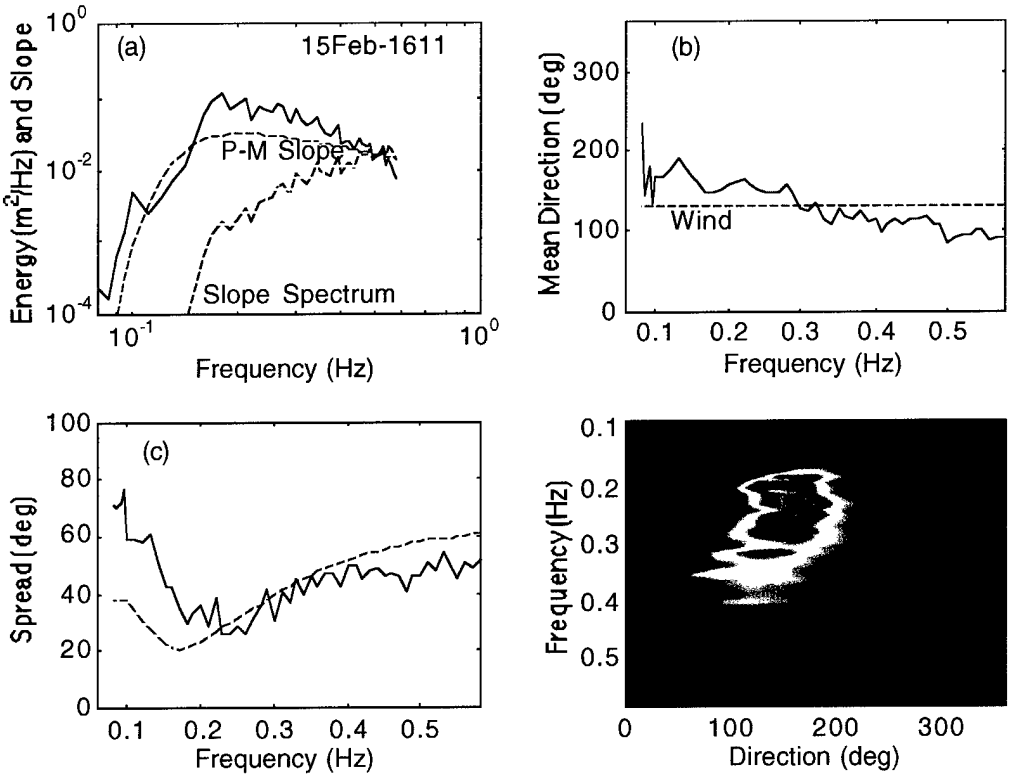

Figure 47. **Event E**--15Feb-1611. (See Figure 40 for legend.)

that the presence of other wave systems can greatly modify the directional distribution of wind-waves. As the older wind-wave system matures, the minimal spread of wave energy decreases and shifts down in frequency space, reaching approximately 20° and 0.13 Hz, respectively, at 16Feb-0441 (Figures 42-52). The conclusion of Event E at 16Feb-0441 is distinguished by the transformation of a multimodal sea state into a unimodal sea and by the widening of the high frequency angular spread to agree with

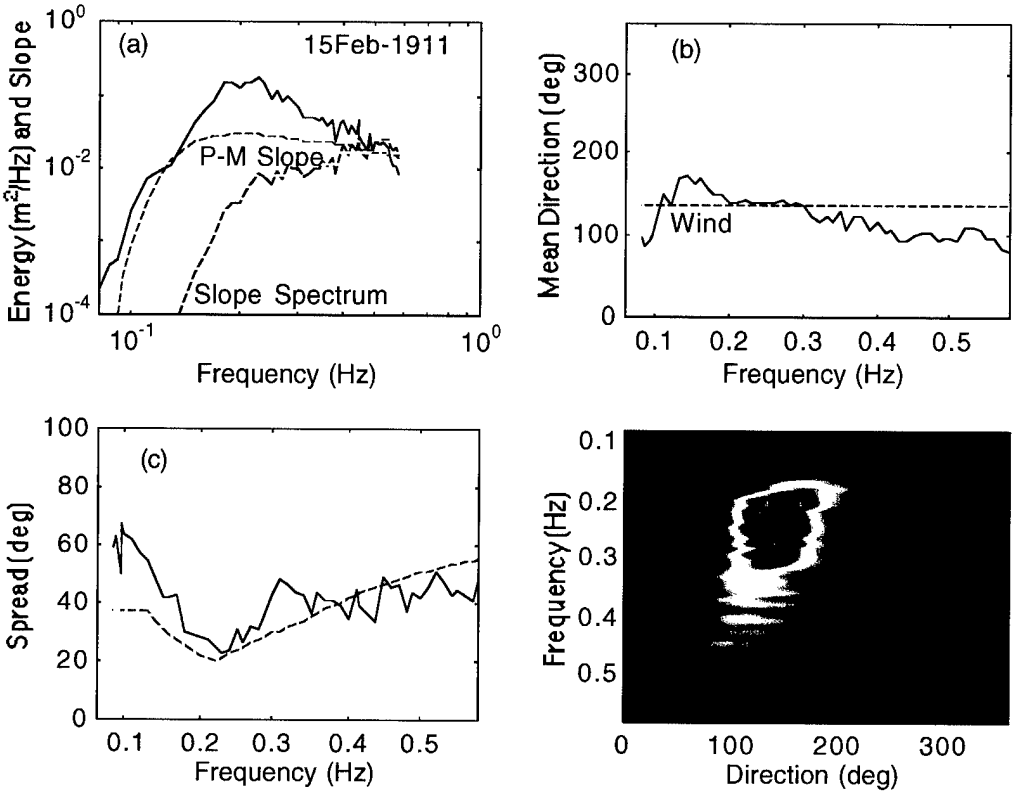

Figure 48. **Event E**--15Feb-1911. (See Figure 40 for legend.)

the "V" shaped distribution of directional models (Figure 52).

From these five events, the directional distribution of a sea state is found to depend on the directionality of the different wave systems. In Stage I, when wave systems propagate at least 60° from one another, the angular spreading resembles a composite of the individual swell and wind-sea systems, where the minimum for each

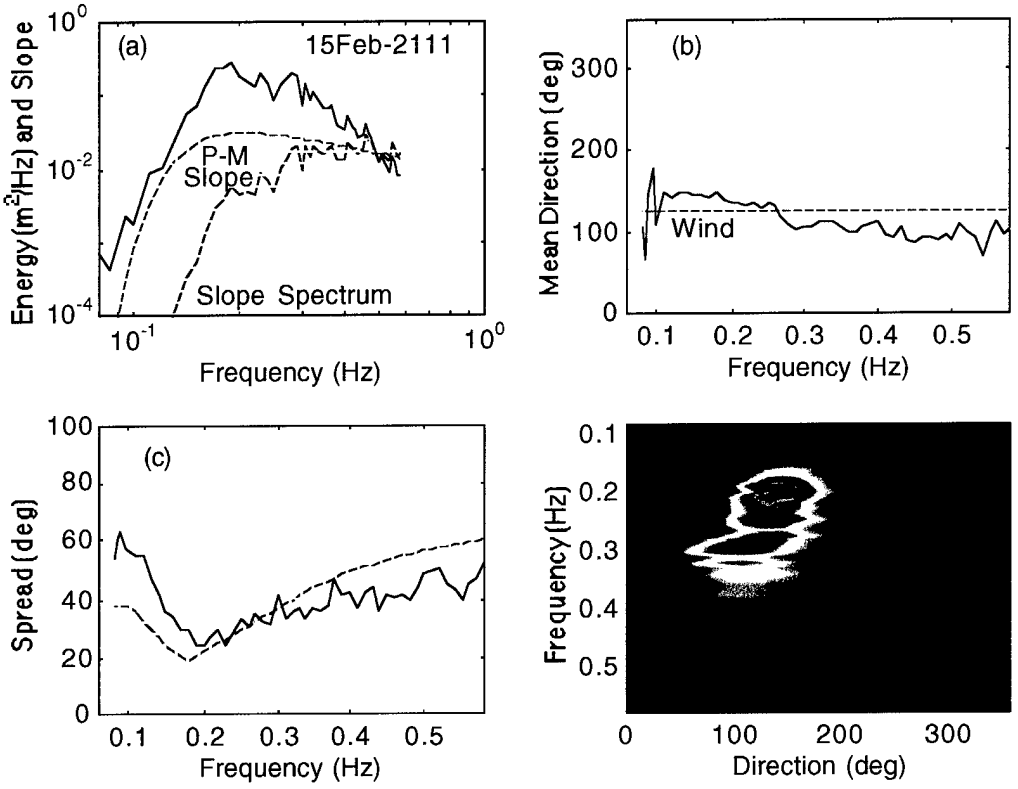

Figure 49. **Event E**--15Feb-2111. (See Figure 40 for legend.)

system remains well defined. For Stage I wave systems propagating in close alignment, the directional distribution for high frequency components is generally greater than that observed for situations of perpendicular and opposed seas.

As mentioned earlier in the description of offwind wave growth (Section 3.3), at the end of Event E, the short wind-waves align along the wind vector. For this

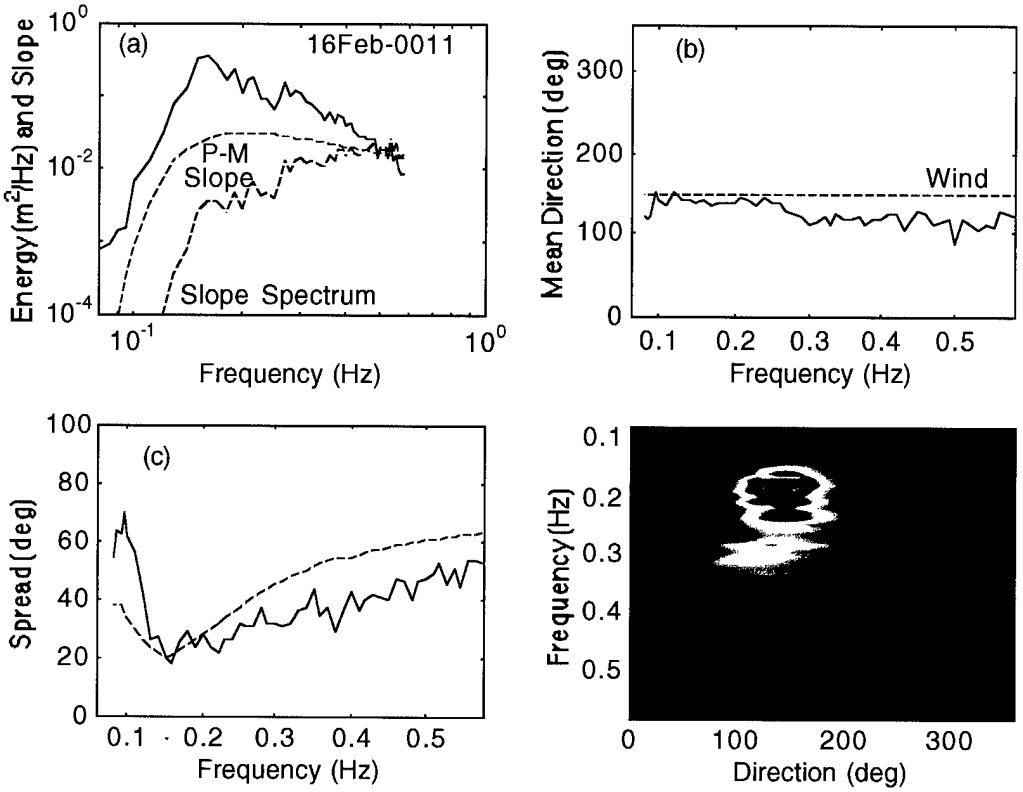

Figure 50. **Event E**--16Feb-0011. (See Figure 40 for legend.)

case, the wind vector is also aligned with the mean direction of the young swell system. In Event E, as well as in other events, this conformity to the wind vector typically occurs in wind-seas with older wave ages or under light wind forcing. For the decaying wind field of Events E and C, the alignment of the wind-waves to the wind vector points to interactions between swell and wind-waves. Under these

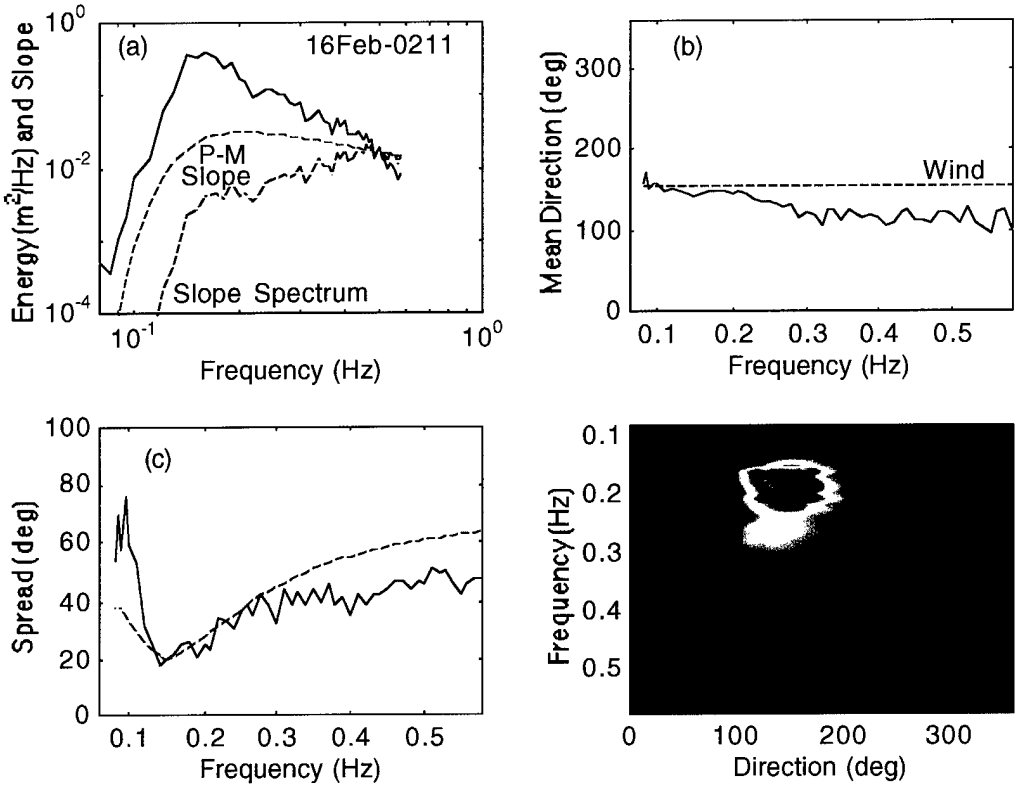

Figure 51. **Event E**--16Feb-0211. (See Figure 40 for legend.)

reduced wind speeds, the high energy waves are basically independent of the wind field. The coupling between systems causes the short waves to align with the long waves, which coincide with the wind vector. These interactions between swell and wind-seas remain to be understood. However, from the five events of this experiment, it can be concluded that *the relative location of the individual wave*

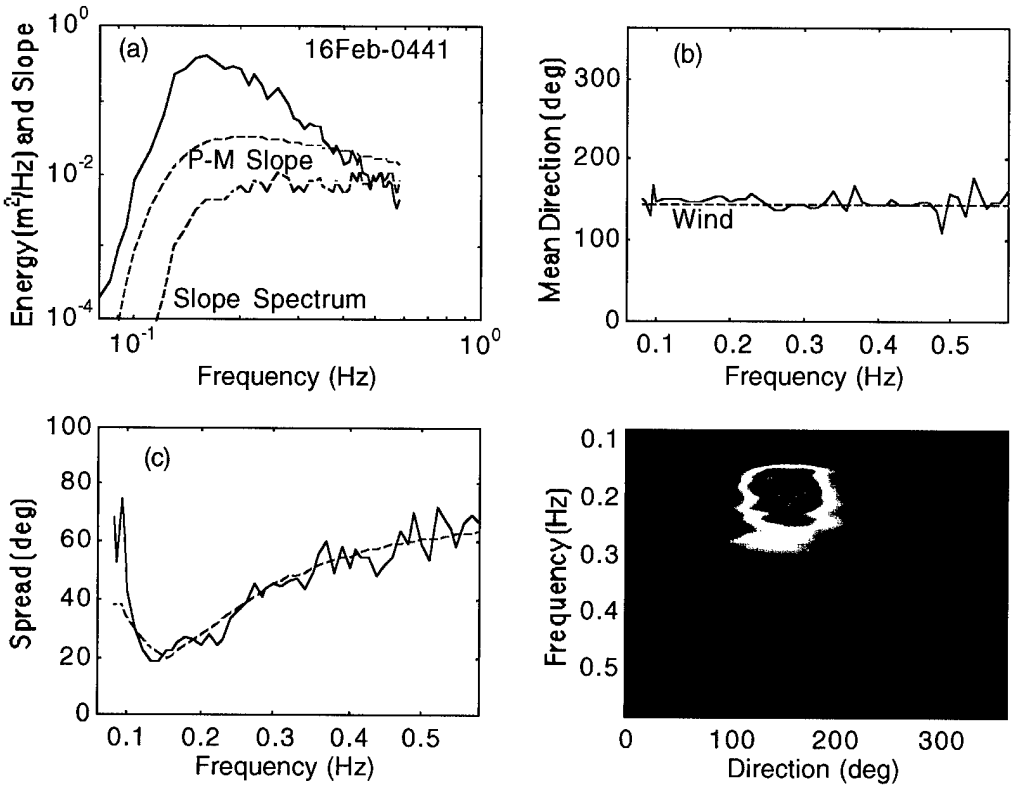

Figure 52. **Event E**--16Feb-0441. (See Figure 40 for legend.)

systems in the direction space, in addition to their relative location in the frequency space, is an important factor in how pre-existing swells modify the growth of wind-driven waves. The directional development of multimodal seas and the interactions between swells and wind-waves are the subjects of the next section.

4. Discussion

According to our current understanding, the development of pure wind-driven waves is controlled by three basic processes: energy input from wind to surface waves, nonlinear wave-wave energy transfer, and energy dissipation due to wave breaking. Previous investigations have shown that the presence of coexisting swell modifies these processes, thereby modifying wind-wave growth. While results from some of these studies disagree with the field data of this experiment, results from other studies support the wave development observed in the events described in Section 3.

4.1 Wave Growth Comparison

The field observations of mixed seas wave growth from this experiment support the results of previous laboratory studies (Donelan, 1987; Mitsuyasu, 1966; Cheng and Mitsuyasu, 1992). The growth of wind-waves generated in close alignment to the direction of a long wave system is found to be reduced by the swell presence. Wind-seas formed in opposing directions to the swell system experience enhanced growth. This result is shown in Figures 53 and 54. The database was selected for wind-waves of Stage I seas only. Equation 15 was used to compute the energy of the wind-wave systems, where the low frequency cutoff between the swell and wind-sea systems was taken to be the component with minimum energy in the transition frequency regime. Only Stage I seas were selected for two reasons: (1) the feasibility of separating the individual wave systems and (2) these wind-wave systems

were under relatively high wind action. The result obtained by Donelan et al. (1992), in a Lake St. Clair experiment,

$$e_{ws} = 2.2 \times 10^{-3} \left(\frac{U}{C_p} \right)^{-3.3} \qquad \text{Eq. 18}$$

serves as a comparison for the growth of pure wind-waves (shown in solid in Figures 53a and 54a). Here, the nondimensional wind-sea energy $e_{ws} = E_{ws} g^2 / U^4$, where E_{ws} is the energy of the wind-sea. In the Donelan et al. (1992) study of offshore waves, the effective wind U in Eq. 18 was taken to be the component in the mean direction of the wind-sea, $U\partial = U \cos\partial$ where ∂ is the angle between the wind vector and the wind-sea direction. For the date set in his study, Hanson (1996) found that U, rather than $U\partial$, produced a better correlation with the nondimensional wave energy. For this reason, the results for both U and $U\partial$ are presented. Also, the conversion of wind measurements at 7 m to the standard 10-m height produced no significant difference in the results; thus the original 7 m wind measurements were used.

Shown in Figures 53a and 54a as a function of inverse wave age, wind-waves of opposing bimodal seas (designated as asterisks) have higher nondimensional energies than those of wind-wave systems in aligned or directionally mixed, multimodal seas (circles and pluses). The use of $U\partial$ offers clear evidence that opposed swell magnifies wind-wave growth; confirmation of this effect appears less definite with the use of U. The cases which fall on the Donelan et al. (1992) curve indicate that the effects of background swell on wind-wave growth are slight. This is likely due to the small slopes of the low frequency waves. Mitsuyasu (1966) and Cheng and Mitsuyasu (1992) reported that long waves of greater steepness had a larger effect on the growth of short waves. The wave slope spectra of Figures 10a-52a show that the slopes of the longer waves encountered in this experiment are much

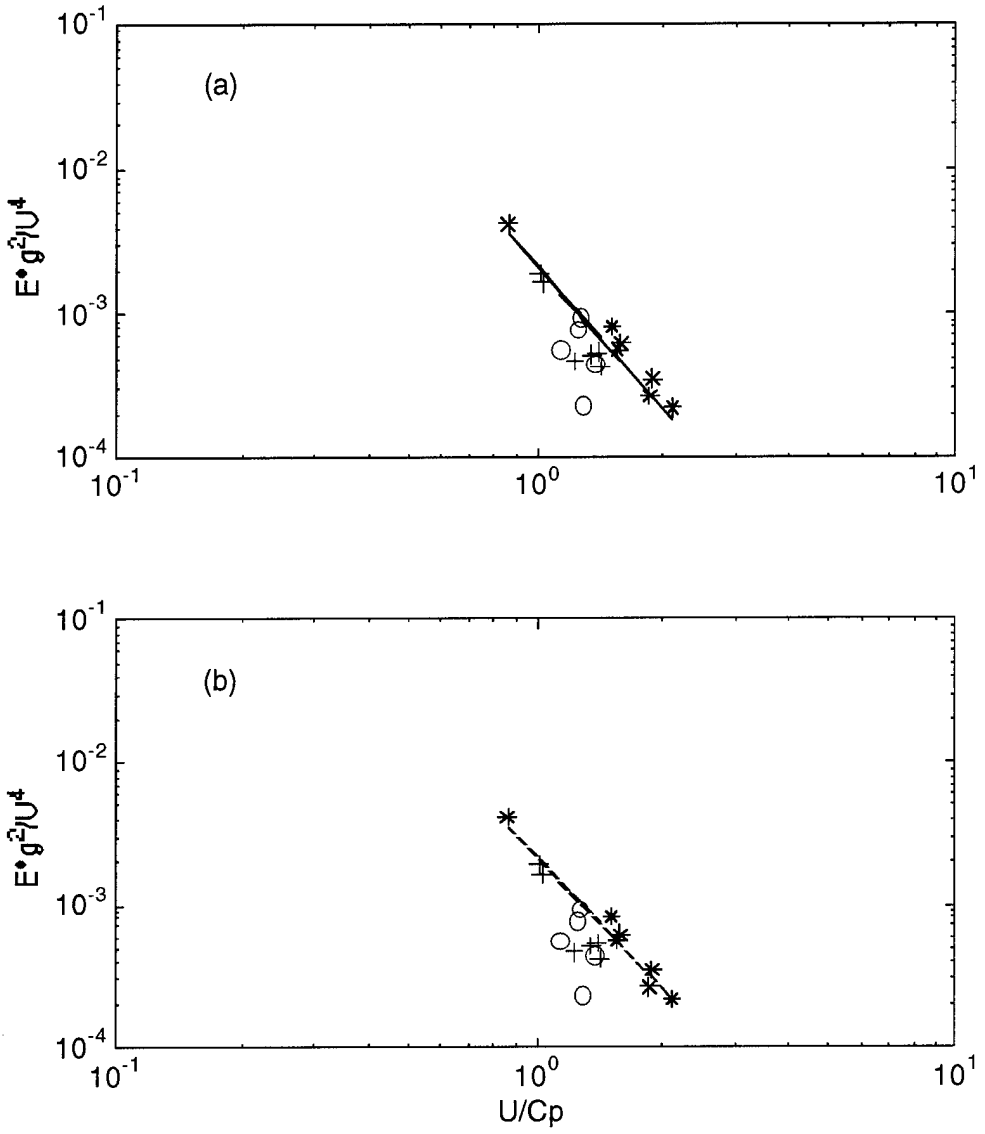

Figure 53. Comparison of wind-wave growth and inverse wave age for Stage I seas, using U. (a) Donelan et al. (1992) for pure wind-waves (–), opposed seas (*), confused seas (+), aligned seas (o). (b) Same as (a) above but with Hanson (1996) curve (--).

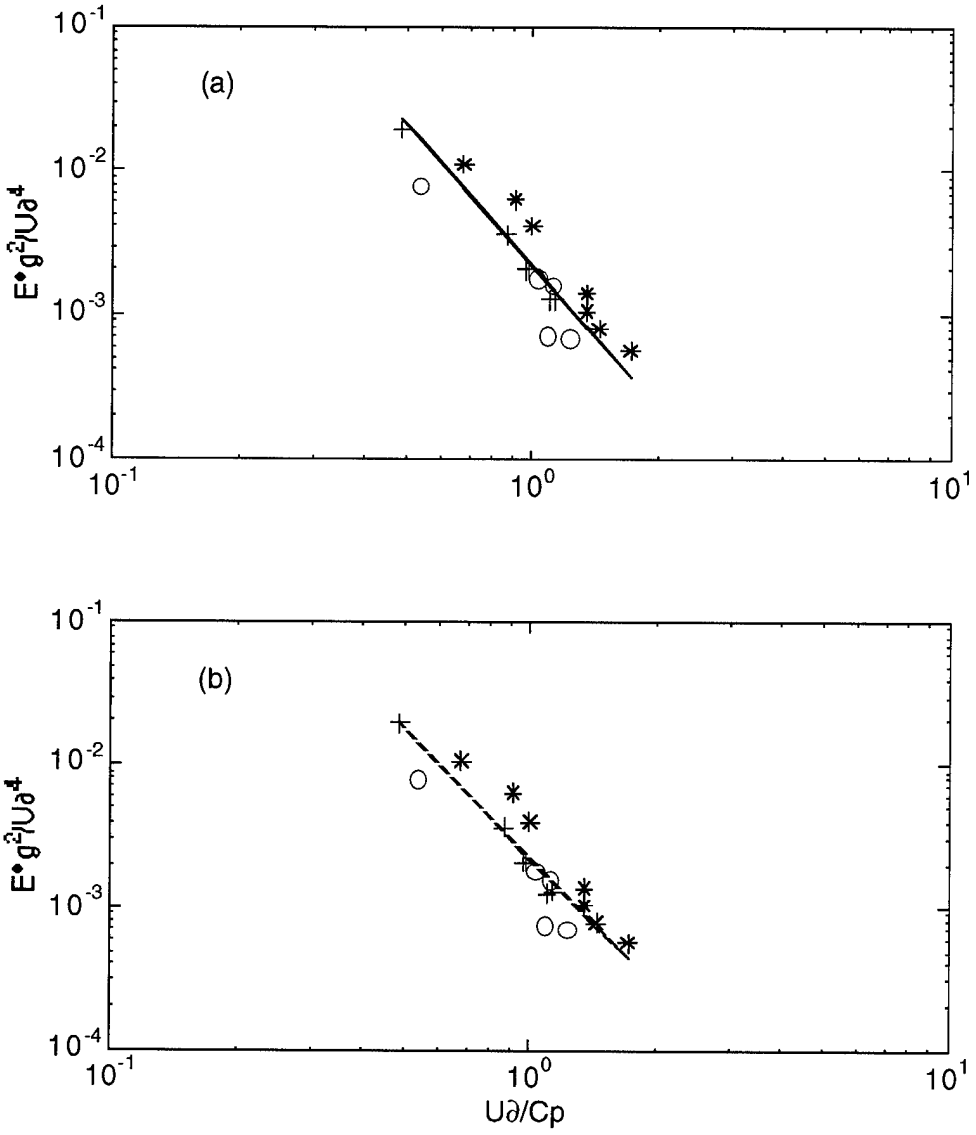

Figure 54. Same as Figure 53, but with wind component in direction of wind-seas, $U\partial$. (a) Donelan et al. (1992) for pure wind-waves (–), opposed seas (*), confused seas (+), aligned seas (o). (b) Same as (a) above but with Hanson (1996) curve (--).

smaller than those of the shorter waves, and those of a developed wind-sea with a peak at 0.15 Hz (P-M slope spectrum). Examining mixed seas in the Gulf of Alaska, Hanson (1996) found that coexisting swells had no apparent effect on local wind-wave growth. The author analyzed wave growth with no swell presence, in addition to wave growth in mixed seas. For unimodal wind-seas, Hanson (1996) obtained a wave growth regression comparable to Eq. 18,

$$e_{ws} = 2.2 \times 10^{-3} \left(\frac{U}{C_p} \right)^{-3.02} . \qquad \text{Eq. 19}$$

The comparison of Eq. 19 (dashed line) and the wind-seas of Figure 53a is shown in Figures 53b and 54b. Equation 19 yields ambiguous results regarding the effects of the swell and wind-sea directionality on the wave growth. The comparison of Eq. 19 with data in Figure 53b shows that swell in opposing and directionally confused seas both enhances and diminishes short wave growth. Equation 18 gives better corroboration with findings of the laboratory studies cited previously. The wave growth cases in Figures 53a and 54a support the hypothesis that *opposed swell intensifies wind-wave growth and aligned swell attenuates wave growth.*

4.2 Directional Development of Wind-Seas

The formation of wind-waves at an angle to the wind vector has been reported by such investigators as Donelan et al. (1985) and Huang (1996). In cases of coexisting swell and wind-sea, studies by Geernaert et al. (1993) and Rieder et al. (1994) suggested that long waves, propagating at an angle to the local wind direction, modified the wind stress vector. The authors found that the wind stress vector, and

consequently the wind-waves, were generally located between the wind and the swell directions. However the results of this experiment do not agree with this hypothesis. In most events described in Section 3, young wind-seas do not form between the wind and swell vectors. In reference to the wind vector, wind-seas are found not on the side of existing long waves, but rather on the side absent of the swell system. (See Figure 55a.) What factors contribute to this phenomenon of offwind wave growth?

Observational studies by Hasselmann et al. (1980) and Allender et al. (1983) and the numerical study by Young et al. (1987) showed that in conditions of veering winds, mean wave directions lagged behind wind directions; this delayed directional relaxation can be seen in higher frequencies of the wave field (Figure 7c). Veering of the wind can contribute to the offwind wave growth observed in the initial stages of Event A and Event B. In Event A, a light wind precursor to the event turns from a steady direction of 225° to roughly 270°, then suddenly to 61° at 12Feb-2341 (Figure 9b). The very small waves generated by the light wind would experience a directional lag relative to the turning wind. When the wind speed jumps to 7.1 m/s, the increased wind energy would be fed into the pre-existing short waves rather than generating a new wind-wave system between the wind vector and the swell system. This is one explanation of why the wind-sea appears at about 25° instead of appearing somewhere between 65° and 225°, as Geernaert et al. (1993) suggested.

The history of the local wind field can play an important role in wave observations. In the study by Rieder et al. (1994), the wind field recorded was quite unsteady, in that the wind direction was generally in a state of change. In a situation where the wind vector is turning away from the swell direction, the lagging wind-waves would be found to lie between the wind and the swell directions. In a contrasting situation where the wind turns quickly toward the swell direction, the wind-waves would follow, not lead, the wind vector. Since wind-waves trail a

turning wind, they would not appear between the wind vector and the swell direction; they would appear on the side of the wind vector absent of the long waves. Although such conditions can be found in Rieder et al. (1994), in their Figure 5 (March 7-8, 1990), this situation was not addressed. These cases would differ from the results of Geernaert et al. (1993) and Rieder et al. (1994). This wind condition can contribute to the offwind growth observed in Events A and B. (See Feb. 13-14 of Figure 7c.)

The directional history of the wind field can also be responsible for the initial wind-sea development of Event D. At the beginning of Event D (14Feb-1941), a rising wind veers from 50° to nearly 100°. Then at 14Feb-2141, a wind-sea forms at approximately 65°, which follows the direction of the turning wind. However at an hour earlier (14Feb-2041), the existing high frequency waves (above 0.50 Hz) do propagate between the wind vector and the swell direction, at 104°. Even though the wind turns slightly, the question remains: why does the wind not act on these pre-existing short waves which already lie between wind and swell directions, as the Geernaert et al. (1993) and Rieder et at. (1994) studies would predict? One explanation suggests that the development of wind-seas is dependent on the relative direction of the swell system and the resulting wind-waves, and not just on the relative location of the wind vector and the mean direction of the long waves.

As discussed in Section 4.1, wind-waves propagating in the same direction as swells are attenuated by the longer waves, whereas opposing swells enhance the growth of wind-waves. Experiments investigating perpendicular seas and other directionally mixed seas are lacking; one is left to speculate on what effects background swells in different directional conditions have on wind-wave evolution. Because the growth of wind-waves is reduced in the presence of aligned swells, it implies that wind-waves in the open ocean, not constrained by the boundary conditions of a wave tank, would tend to develop at an angle away from the swell

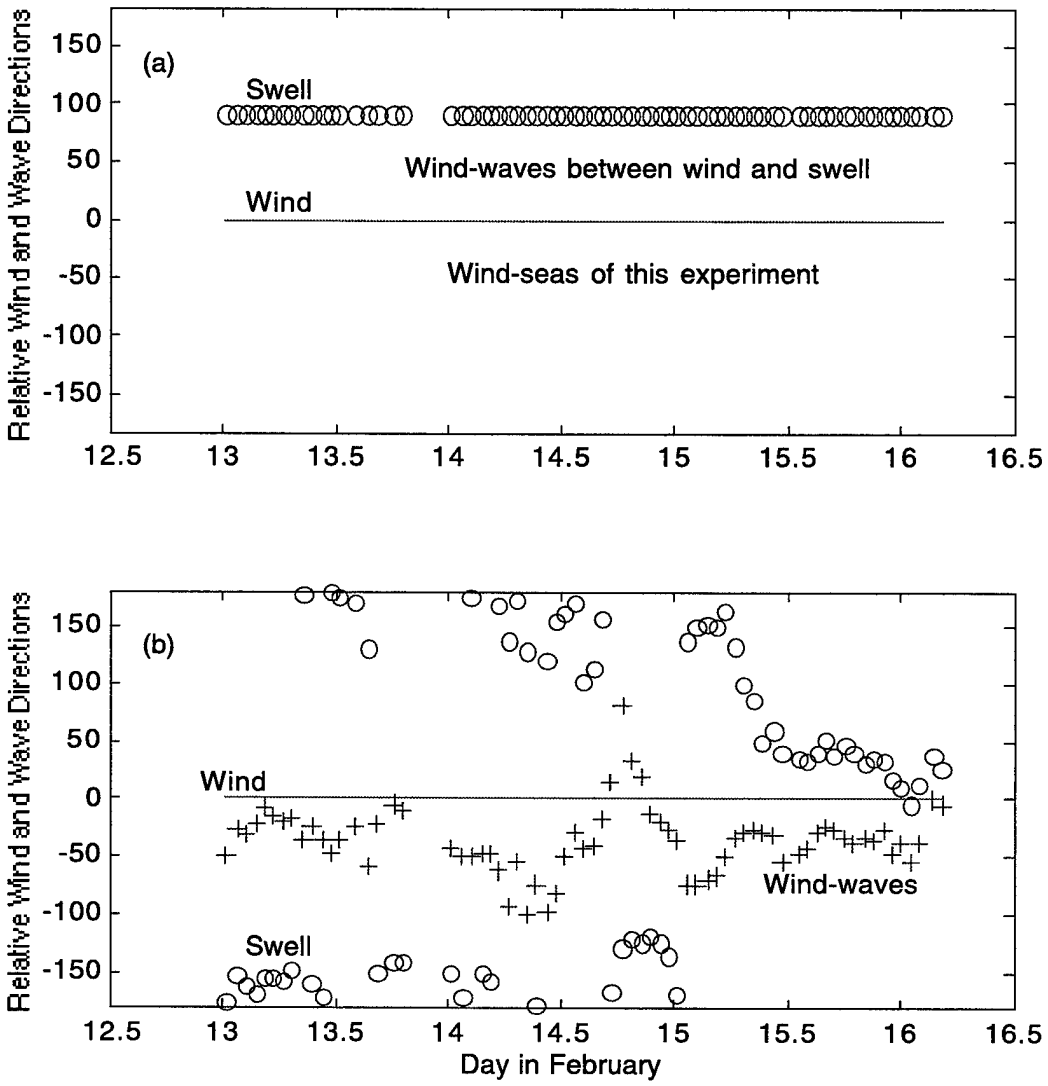

Figure 55. Swell and wind-wave directions relative to wind vector. (a) Illustration of result from Geernaert et al. (1993) and Rieder et al. (1994), swell (o) and wind (–). (b) Experiment data, with wind-wave directions taken at 0.45-0.50 Hz and swell directions at 0.15-0.20 Hz; swell (o), wind-waves (+), and wind (–).

direction. This is not discernible from Figure 55b. The directions plotted were averaged over wave frequencies of 0.45-0.50 Hz for wind-waves, and over frequencies of 0.15-0.20 Hz for swell. Figure 55b seems to support the results of Geernaert et al. (1993) and Rieder et al. (1994). However, this agreement is presumably spurious, because (1) the wave frequencies were selected arbitrarily and (2) in a decaying or a decayed wind field, the short waves are more influenced by interactions with swell than by wind forcing. (This point will be discussed in Section 4.3.) To eliminate the influence of these factors, the wave data is restricted to cases of Stage I seas only, as in Section 4.1 The wind-wave directions correspond to the direction of the modal frequencies. The result in Figure 56 shows that wind-waves typically do not lie between the wind vector and the swell direction.

In Event B, at 14Feb-0041, the wind-sea develops in the north-northwest direction of 24° under an increasing wind that, for several previous hours, came from roughly 65°, and the low frequency waves are propagating from approximately 225°. If the wind-sea had formed between the wind vector and the long wave system, the relative angle between the swell and wind-wave systems would be 130°. For the case of opposed wind and swell at 14Feb-0041, the current wave systems are in closely opposing directions (about 160°). Recall that for the case of opposing systems, Mitsuyasu (1992) and Cheng and Mitsuyasu (1992) found that swell presence intensifies wind-wave growth, as supported by results in Figures 53a and 54a. In Event C, at 14Feb-1241, the wind-waves are found to be roughly 139° from the swell system. If the wind-sea had formed between the wind and swell directions, at about 180°, it would have been only 60° from aligning with the long wave system. This propensity for wind-waves to develop away from the long wave systems can also be the reason for the sudden shift of a wind-sea away from the wind and the long wave directions, as observed in 15Feb-0140 of Event D.

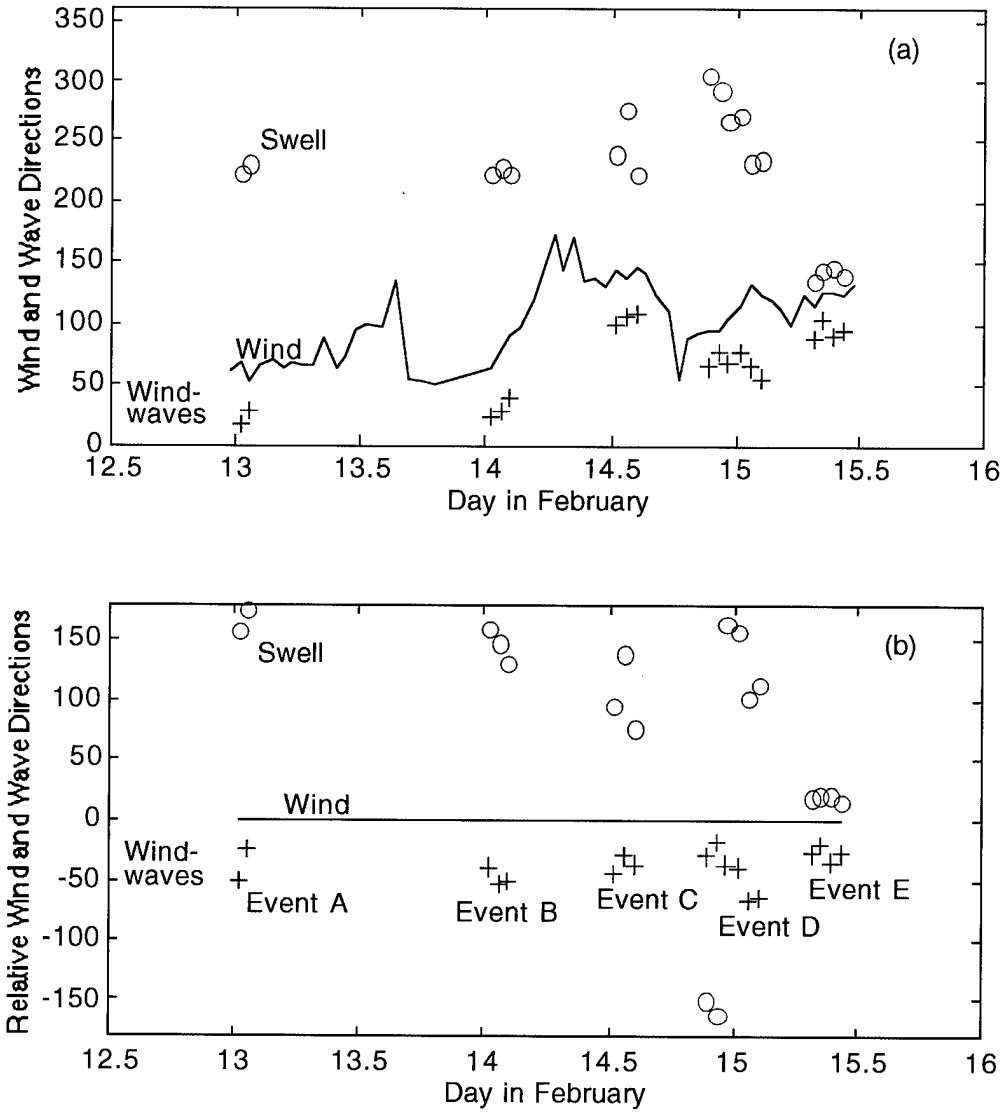

Figure 56. Relative wind-to-wave directions for Stage I seas only: reference wind vector set at zero (red –), wind-wave direction relative to wind (blue +), and swell direction relative to wind (blue o); 14Feb-2141 to 15Feb-0041 of Event D (green +, o) and 15Feb-0140 (red +, o).

At 15Feb-0041 (Figure 35), the wind-waves are at approximately 80^0 and the longer waves arrive from scattered directions. In the next hour, at 15Feb-0140, the old wind-wave system and the swell system have become more focused and the young wind-wave system has shifted away from the wind vector. The wind-sea is now found at 65°. This sudden shift is not suspected to be caused by the wind field, because the local wind is relatively steady, particularly in direction. This phenomenon is concisely depicted in Figure 56. Again, at the start of Event D, the wind-waves do lie between the swell and wind directions (denoted by green marks). Then at 15Feb-0140 (red marks), the mean swell direction "turns" toward the reference wind vector while the wind-waves "turn" away from the wind vector. Since it is the wind vector that is actually turning toward the swell direction, the word "turn" is applied loosely to surface waves to illustrate the effect of coexisting long waves on short waves. The surface field now is composed of three seas, of which the long wave systems consist of a swell system and an old wind-sea. The old wind-sea propagates at 155°; the swell, at 233°. The young wind-sea propagates at angles of 95° and 150° relative to the respective long wave systems. Since the young wind-sea lies closer to the old wind-sea in frequency and in direction, it is believed that the young wind-sea interacts with both the old wind-sea and the longer swells, and that this directional shift in the young wind-sea is influenced more by the old wind-sea than by the swell system.
A discussion of this interaction between wave systems can be found in Section 4.3.

In situations where the wind vector is aligned in the direction of swell, wind-waves develop at a smaller angle, generally 20-30°, to the wind vector. This is found in Event E of Figure 56b, where the wind and swell are approximately 15-30° apart. This wave growth behavior is also observed in several events after Event E. One such event on February 17 is briefly mentioned to provide additional evidence for the case of aligned wind and swell (Figure 57). The wind was steady around 3 m/s and

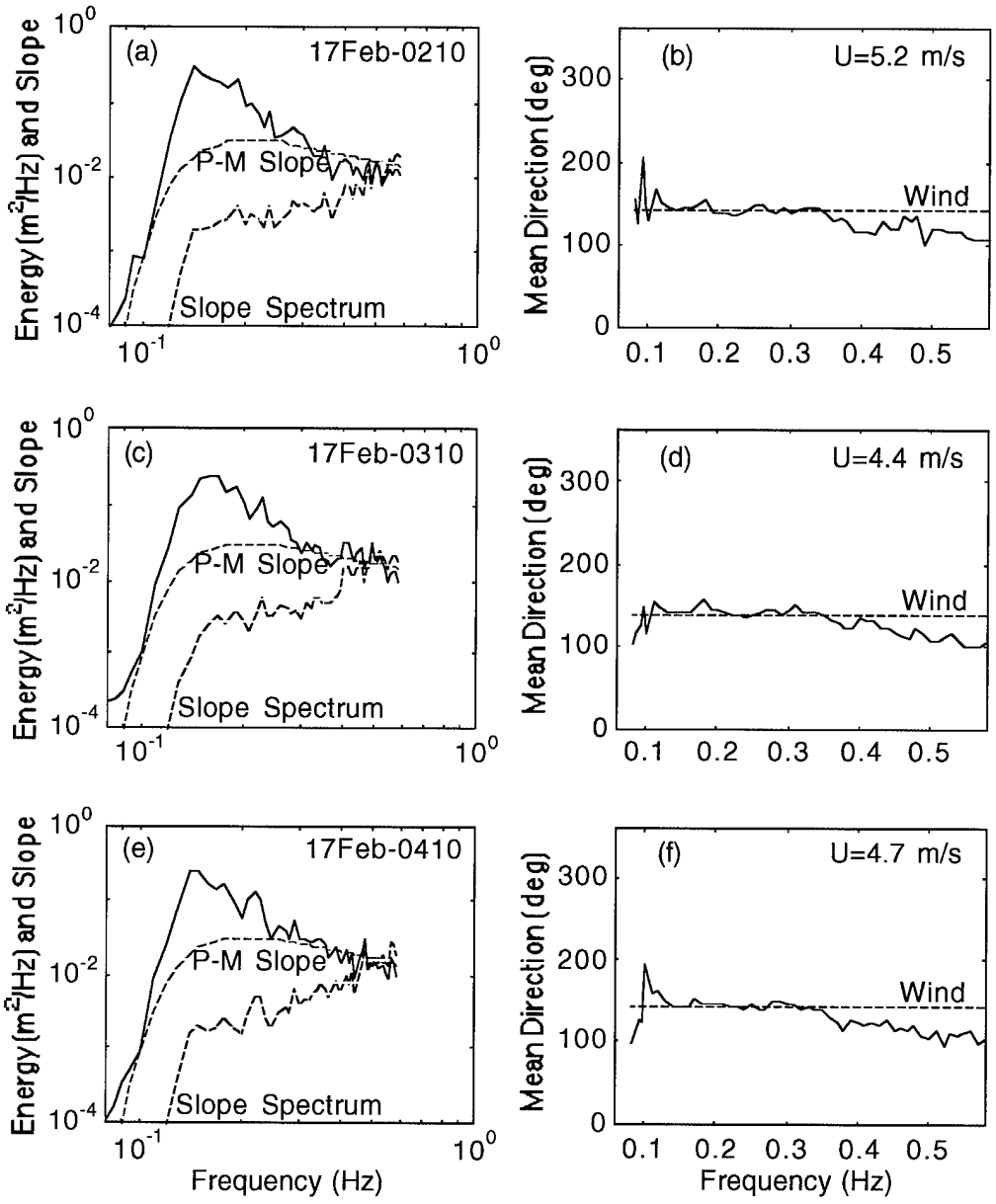

Figure 57. Wave growth in aligned wind and swell. On the left: three onmidirectional spectra (f), slope spectra (red --), and P-M slope spectrum for wave system with peak at 0.15 Hz. On the right: mean wave directions (f), wind speed U, and wind direction (--).

increased to 5.2 m/s at 17Feb-0210. As in Event E, the wind-waves in the high frequencies are approximately 20-30° off of the wind vector.

The directional locations of coexisting wave systems appear to influence the directional spreading of wind-seas. Wind-waves in multimodal seas have larger minimum spreads than pure wind-waves. Directional models for pure wind-waves predict the smallest angular spread to be roughly 20°. Observed wind-waves in mixed seas have minimum angular spreads typically between 30° and 45°. (See Figure 58.)

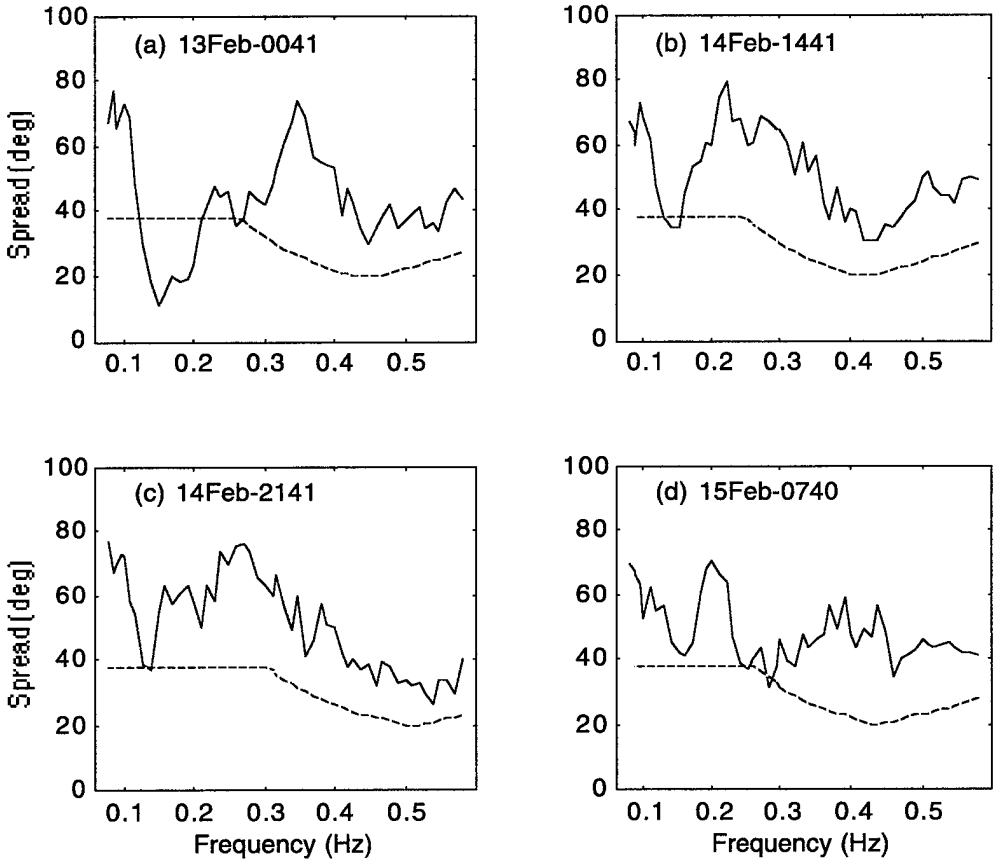

Figure 58. Directional spread of four Stage I wind-seas (f) compared with the Donelan et al. (1985) model (--).

This scatter in the minimum spread can be partially attributed to the effects of the directionality of wave systems. Another observation on the effect of swell on the directional spread of wind-seas is that the minimum spread lies around the wind-wave peak. In agreement with the results of the directional models, the minimum angular spread for the long wave systems in the first four events generally lies at or below the

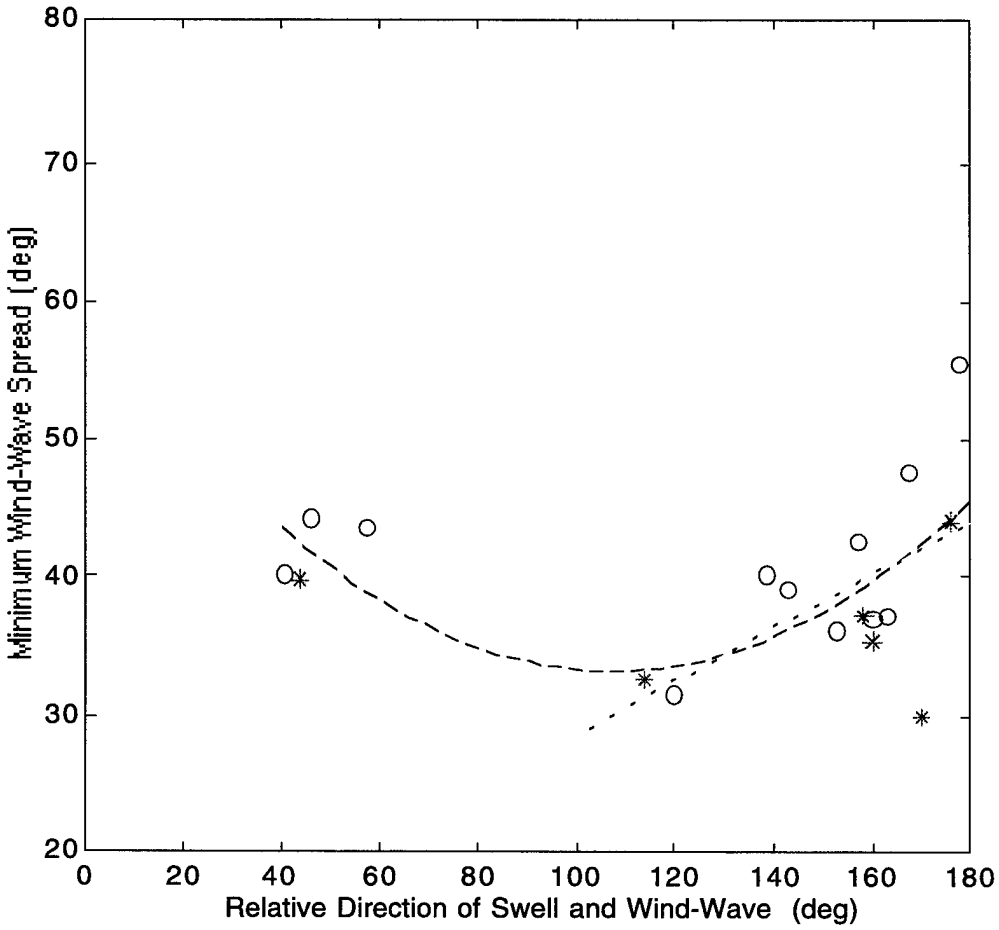

Figure 59. Minimum angular spread for wind-waves of Stage I seas versus direction of wind-waves relative to swell: swell energy density greater than wind-wave energy density (o), wind-wave energy greater than swell energy (*), and curve fit for all data points (--) and for cluster of perpendicular to opposing seas (..).

peak frequency. However, the minimum spread for wind-waves does not consistently exhibit this property. In Figure 59, the minimum angular spreading of the Stage I wind-seas (same as those of Figure 56) shows that closely aligned and perpendicular systems have slightly higher minimum spreads. The dotted line in the figure is a curve fit for the perpendicular-opposing seas cluster only, while the dashed line includes the data points of seas in close alignment. Due to the lack of data in the aligned to perpendicular region, these curve fits are inconclusive, but provide hints of spread characteristics dependent on the directionality of wave systems. Some of the scatter in spread data can be attributed to the effects of relative energies of the wave systems and to the effects of wave age (Mitsuyasu, 1966). In Figure 59, the cases in which the wind-sea is more energetic than the swell (shown as asterisks) tend to have lower minimum spread values, although some less energetic wind-seas (circles) also produce small spread widths. An attempt to reconcile the low spread values of these less energetic wind-seas was unsuccessful.

4.3 Comments on Source Terms

In these five events, the observed wave evolution suggests that the development of wind-waves in the presence of background swells is dictated by forcing of the wind field and by competing nonlinear processes. For aligned seas, Phillips and Banner (1974) proposed the nonlinear process to be augmented wind-wave breaking due to enhanced surface drift. Hatori et al. (1981) and Toba et al. (1983) proposed the nonlinear process to be "strong" interactions between wave systems, which act to transfer energy from the short waves to the long waves. The mechanism of these "strong" nonlinear wave interactions remains to be determined.

As mentioned in Section 1.4, the three governing processes of wave development are: energy gained from the wind, energy dissipation due to wave breaking, and nonlinear wave-wave energy transfer. This collection of field data suggests that the wind input and nonlinear interactions dominate wind-wave evolution in mixed seas. For the light wind conditions encountered in this experiment, energy dissipation by wave breaking does not substantially influence the evolution of the wave fields. In the open ocean, swells typically are not steep enough to incur wave breaking; this is evident by the low wave slopes. The wave slope spectra (Figures 10a-52a) show that most low frequency waves have slopes below the P-M values of a developed sea. Wave breaking occurs predominantly in the higher frequency range, as seen at 13Feb-0041 and 14Feb-0041 (Figures 11a and 16a), where the steepness of short wind-waves exceeds the P-M limit. In these instances of rising wind-seas, energy dissipation by wave breaking is significant in limiting the wave energy level. Aside from forcing the spectral energy density of the wave field to a fully developed form, the dissipation function has little other effect on the evolution of mixed-sea spectra.

The development of mixed-sea spectra is controlled by wind input and wave-wave interactions. The initial wave growth stage is dominated by the wind field and air-sea surface interactions. At the beginning of all five events, high wind forcing produces wind-seas that indicate little evidence of coupling with the long wave systems. As long as the wind-sea experiences high wind forcing, its growth continues unhampered by swells. The interaction between systems arises when wind-waves approach swell components in wavelength or when the wind speed is low or decaying. It is observed that, generally, wind waves are forced in some direction associated with the wind and pulled in another by coexisting long waves. At 14Feb-0041 of Event B and at 14Feb-1241 of Event C (Figures 16 and 24), high frequency wave systems are

under strong wind action and exhibit insignificant coupling with low frequency waves. Nonlinear coupling between systems appears to be intensified when wind action decays, at 14Feb-0641 of Event B and 14Feb-1641 of Event C (Figures 21 and 27). This shows that high wind forcing dominates the development of wind-waves. But this statement requires a qualification, contingent on the proximity of wind-wave frequencies and background swell frequencies. At 14Feb-0341 of Event B and 15Feb-1140 of Event E (Figures 19 and 45), relatively high wind continues to act on the shorter wind-waves, yet there is interaction between the longer wind-waves and the swell system. The activity of wave frequencies between the swell peak and the wind-sea peak demonstrates the local nonlinear coupling of wave systems as examined by Masson (1993).

4.4 Wave Interactions

In a numerical study analyzing the contributions of weakly nonlinear wave-wave interactions (see S_{nl} of Section 1.4) to the evolution of aligned bimodal seas, Masson (1993) examined the development of a bimodal sea subjected to the influence of S_{nl} only. The author determined that, under no wind energy input or wave energy dissipation, wave-wave interactions act to couple the wave systems in such a manner as to stabilize the initial bimodal wave spectrum into a self-similar unimodal spectrum. The study shows that wind-wave energy is transferred to swell components, producing a broader unimodal spectrum. Masson (1993) also found that for wind-seas with peak frequencies f_{p2} higher than $1.7\,f_{p1}$, where f_{p1} is the peak frequency of the swell system, there is no significant coupling between the wave systems. It is only

when the peak frequencies of the wave systems are in close proximity that the local wave-wave interactions become active. Masson (1993) determined that for bimodal seas with peak frequency ratios $f_{p1}/f_{p2} < 0.6$, the wave systems are too distant in frequency space for substantial nonlinear coupling to result. The study examined a test case of aligned bimodal seas with $f_{p1} = 0.2$ Hz and $f_{p2} = 0.3$ Hz; it was found that nonlinear wave interactions drove the initial bimodal spectrum into a broad unimodal spectrum within a period of 6 hours. Under light wind forcing, this transformation of the wave spectrum was also observed in this experiment. Under moderate or high wind forcing, coupling between systems generally occurred amongst wave components of comparable length.

An example of local wave interactions between swell and wind-sea under moderate wind action is well illustrated in Event B. In the first hours of this event, the wind-sea appears to develop independently of the swell. At 14Feb-0141, the peak frequencies of the wind-sea and swell systems are located, respectively, at 0.15 Hz and at 0.40 Hz (Figure 17). As the wind-sea develops under the 5.5 m/s wind, the longer wind-waves begin to interact with the swell components. A second example of local interactions between wave systems under relatively high wind forcing can be seen in Event E. The wave field from 15Feb-0940 to 1140 of Event E is subjected to wind speeds slightly higher than 5 m/s. The spectra of these hours (Figures 43-45) show that wave interactions occur locally among the frequency components in the transition regime of 0.25-0.40 Hz; this coupling between systems can be tracked by the migration of the longer wind-waves toward the older wind-sea at 0.20 Hz. At 15Feb-1040, the young wind-sea and old wind-sea peaks are at 0.35 Hz and 0.22 Hz, giving a frequency ratio of 0.63. This coupling between wave systems continues to divert the mean direction of the shorter waves toward the longer wave system, as seen

from 15Feb-1040 to 1911 (Figures 44-48). An interesting phenomenon occurs earlier in Event E. At 15Feb-0740 (Figure 41) the modal frequencies of the old wind-sea and swell system are estimated to be 0.24 Hz and 0.17 Hz, respectively. The frequency ratio, $f_{p1}/f_{p2} = 0.71$, is within the coupling limit as determined by Masson (1993). The spectra from 15Feb-0740 to 0940 suggest that interactions between the old wind-sea and the swell system are responsible for the sudden disappearance of the swell components and the ensuing energy overshoot in the omnidirectional spectrum (Figure 42a). This example illustrates the absorption of a decaying long wave system by a younger wind-sea under sustained wind forcing. In situations of decaying or decayed winds, it is the prevailing long wave system that dominates the development of the wind-sea. In these cases, interactions between wave systems in mixed seas are less localized than predicted by the weakly nonlinear transfer function.

In the second half of Event B, the wind is on the decrease and wave interactions between the two systems begin to dominate the evolution of the wind-sea. At 14Feb-0441, the frequency ratio, f_{p1}/f_{p2}, is approximately 0.63, which is within the limit of 0.6 determined by Masson (1993). In about five hours, the Stage II spectrum at 14Feb-0441 evolves into more unimodal spectrum at 14Feb-0941 (Figures 20-22). This agrees with the predictions of the nonlinear transfer function as computed by Masson. This transformation of a bimodal spectrum into a broad unimodal spectrum is also observed during a period of light wind action in Event C. At 14Feb-1541, the respective wave systems are located at 0.15 Hz and 0.43 Hz, giving a frequency ratio of 0.35. This frequency ratio is beyond the limit of 0.6; for this case, the weakly nonlinear interactions function predicts the wave systems to remain uncoupled. However, the wave spectra from 14Feb-1541 to 1741 (Figures 26-28) show how quickly the long waves extract energy away from the short waves,

suggesting that the wave interactions observed here are stronger than those predicted by the weakly nonlinear interaction theory.

An anomalous interaction phenomenon occurs at the end of Event D. At 15Feb-0140, the directional spectrum shows three modal frequencies, approximately at 0.16 Hz, 0.24 Hz and 0.50 Hz (Figure 36). The ratio of the "intermediate" peak frequency to the young wind-sea peak is 0.48, which again is less than 0.6. Despite continual energy input by 4.0 m/s wind, the wind-sea appears to diminish without migrating toward the old wind-sea. The interaction between the young sea and the older seas does not produce a "bridging" of the short and long waves, where the young wind-sea is broadened in the frequency and directional space by the longer wave system, as observed in Events B and C.

Portions of these mixed seas observations substantiate the theory that local nonlinear wave interactions are responsible for driving a bimodal sea to a unimodal sea. Yet other observations of wave systems interacting over a wide frequency distance suggests that more than weakly nonlinear wave interactions are at work to produce the strong coupling between the wave systems, lending support to the idea of "strong" wave interactions proposed by Hatori et al. (1981) and Imai et al. (1981). Although these wave interactions were detected in their experiments, the dynamics of this physical process remain to be explained.

The study by Masson (1993) did not explore different directional conditions of mixed seas. Thus further research is required to determine what effects the relative directions of coexisting seas have on the interactions between wave systems. As discussed in Sections 4.1 and 4.2, the directionality of wave systems can induce significant effects on the development of wind-seas. In opposing seas, wave growth was enhanced by swell presence. In cases of perpendicular and opposing seas, wind-wave components are modulated from their original direction of travel. As seen

in Event E, these transition peaks in the angular spread disappeared and the spread distribution evolved into the canonical shape of unimodal seas as the wave field stabilized toward a Stage I sea. Whether the transition peaks act to decrease or increase the rate of wave interactions in multimodal seas cannot be determined from this modest collection of data.

5. Conclusions

Multimodal wave spectra observed in open waters indicate that the evolution of wind-seas in the presence of a coexisting swell is dictated by competing processes of wind energy input and nonlinear wave-wave energy transfer. In the initial stages of wind-wave development under moderate or high wind forcing, the wind source term appears to dominate the development of wind-waves. At this stage there is little interaction between the wave systems and the wind-sea evolves in a manner similar to that of pure wind-seas. While wind forcing remains sufficiently high, wind-waves grow at an angle to the wind vector and to the swell direction. This feature of wave growth can be attributed to unsteady wind directions or to the effects of the directionality of coexisting wave systems. A veering wind can result in waves forming at an angle to the wind, due to the lag in wave response. Of the five events examined in this study, veering winds in two cases were determined to contribute to the phenomenon of offwind wave growth. The fact that wind-waves form offwind and away from, not toward, the swell components suggested that long waves have significant effects on the development of short waves. Laboratory experiments have found that a swell system aligned with the wind-wave direction suppresses the growth of wind-waves, and that swell in an opposing direction intensifies the growth of wind-waves. These laboratory findings were confirmed by this set of field data. These effects of coexisting swell may offer an explanation of why, in open ocean conditions, wind-waves tend to develop about $20\text{-}50^0$ offwind, away from the mean direction of the long wave system.

The development of wind-waves in mixed seas produced interesting features in the directional spread distribution of the wave field. For wave systems that were far apart in the direction space, such as perpendicular and opposing seas, the angular

spreading in the transition regime between the wave systems increased to form a local spread maximum. This transition spread peak did not appear to act as a barrier to the interaction between the two wave systems because nonlinear interactions between wave systems are found to be significant in all directional conditions of mixed seas, but additional investigation is required to determine the role of these directional characteristics in the evolution of mixed seas.

It was also observed that nonlinear coupling occurred between wave systems with local peak and distant peak frequencies. The weakly nonlinear interaction function predicted wave-wave interactions to be localized in frequency, for ratios of wind-wave to swell peak frequencies greater than 0.6; however, wave interactions were found to exist in seas with frequency ratios less than this limit. This stronger interaction between systems suggests that the mechanism of nonlinear coupling be further examined, and that more than the weakly nonlinear transfer function may be responsible for the observed evolution of mixed seas.

The results of this mixed seas study are summarized as the following:

(1) Opposed swell enhanced wind-wave growth, while aligned swell attenuated wave growth.

(2) Coexisting swell influenced the directional development of wind-seas. Cases of young wind-seas developing away from the wind vector and the mean direction of the swell system were observed.

(3) The directional spreading of wind-waves had broader minimum values than those of pure wind-waves as predicted by directional models. The minimum spread of wind-seas was found to generally lie at or above the peak frequency.

(4) The spread distribution showed some dependence on the directionality of the wave systems. Aligned seas resulted in broader spreading of wind-waves than opposed seas did. Data suggested that the lowest spread minimum of wind-seas is found in perpendicular seas and for wind-seas more energetic than the swell system.

(5) Under sufficient wind action, the wind input dominated wind-wave development. Wave interactions between systems occurred in the transition regime where wind-wave lengths were comparable to those of swell components.

(6) Under light wind forcing, some cases of nonlinear coupling between wave systems were found to be stronger than predicted by the weakly nonlinear energy transfer function.

Although this study offers some interesting situations of wind-wave evolution in the presence of coexisting background swells, further investigations on this subject are necessary if the complexities of ocean wave evolution are to be understood. Studies from previous generations, such as the P-M investigation and the JONSWAP experiment, have considerably advanced our knowledge of pure wind-seas. To progress to the next level of understanding, extensive studies on the directional development of mixed seas need to be launched, employing the new generation of remote sensing instrumentation.

List of References

Allender, J. H., J. Albrecht and G. Hamilton (1983): Observations of directional relaxation of wind sea spectra. *J. Phys. Oceanogr.*, **13**, 1519-1525.

Banner, M. L. (1990): Equilibrium spectra of wind waves. *J. Phys. Oceanogr.*, **20**, 1264-1277.

Barnett, T. P. and A. J. Sutherland (1968): A note on an overshoot effect in wind-generated waves. *J. Geophys. Res.*, **73**, 6879-6885.

Chu, J. S., S. R. Long, and O. M. Phillips (1992): Measurements of the interaction of wave groups with shorter wind-generated waves. *J. Fluid Mech.*, **245**, 191-210.

Cheng, Z. and H. Mitsuyasu (1992): Laboratory studies on the surface drift current induced by wind and swell. *J. Fluid Mech.*, **243**, 247-259.

Dahl, P. H., D. R. Jackson, and K. L. Williams (1995): The TEVA experiment cruise report. *Applied Physics Laboratory University of Washington Technical Memorandum APL-UW TM 1-95*, March 1995.

Datawell: *Directional Waverider Manual.*

Donelan, M. A. (1987): The effect of swell on the growth of wind waves. *Johns Hopkins APL Technical Digest*, **8**, 18-23.

Donelan, M. A., J. Hamilton and W. H. Hui (1985): Directional spectra of wind-generated waves. *Phil. Trans. R. Soc. Lond.*, **A 315**, 509-562.

Donelan, M. A., M. Skafel, H. Graber, P. Liu, D. Schwab, and S. Venkatesh (1992): On the growth rate of wind-generated waves. *Atmosphere-Ocean*, **30**, no. 3, 457-478.

Geernaert, G. L., F. Hansen, M. Courtney, and T. Herbers (1993): Directional attributes of the ocean surface wind stress vector. *J. Phys. Oceanogr.*, **98**, 16571-16582.

Hanson, J. L. (1996): *Wind Sea Growth and Swell Evolution in the Gulf of Alaska.* Dissertation, Johns Hopkins University, 145 pp.

Hasselmann, K. (1963): On the nonlinear energy transfer in a gravity-wave spectrum, part 2: conservation theorems; wave-particle analogy; irreversibility. *J. Fluid Mech.*, **15**, 273-281.

Hasselmann, K., T. P. Barnett, E. Bouws, H. Carlson, D. E. Cartwright, K. Enke, J. A. Ewing, H. Gienapp, D. E. Hasselmann, P. Kruseman, A. Meerburg, P. Muller, D. J. Olbers, K. Richter, W. Sell, and H. Walden (1973): Measurements of wind-wave growth and swell decay during the Joint North Sea Wave Project (JONSWAP). *Dtsch. Hydrogr. Z.*, **A8**(12), 95 pp.

Hasselmann, K., D. B. Ross, P. Muller, W. Sell (1976): A parametric wave prediction model. *J. Phys. Oceanogr.*, **6**, 200-228.

Hasselmann, D. E., M. Dunckel and J. A. Ewing (1980): Directional wave spectra observed during JONSWAP 1973. *J. Phys. Oceanogr.*, **10**, 718-728.

Hatori, M., M. Tokuda, and Y. Toba (1981): Experimental study on strong interaction between regular waves and wind waves (I). *J. Oceanograph. Soc. Jpn.*, **37**, 111-119.

Huang, N.E. (1996): The development of directional spectrum of coastal wind waves under off shore wind. *Proceedings, 76th AMS Annual Meeting*, American Meteorological Society.

Imai, Y., H. Mitsuhiko, T. Masayuki, and Y. Toba (1981): Experimental study on strong interaction between regular waves and wind waves (II). *Tohoku Geophys. Journ.*, **28**, no. 2, 87-103.

Long, S. R., N. E. Huang, E. Mollo-Christensen, F. Jackson, and G. L. Geernaert (1994): Directional wind wave development. *Geophysical Research Letters*, **21**, no. 23., 2503-2506.

Longuet-Higgins, M. S., D. E. Cartwright, and N. D. Smith (1963): Observations of the directional spectrum of sea waves using the motions of a floating buoy. *Ocean Wave Spectra,* Proceedings of a Conference, 1961, Prentice Hall.

Masson, Diane (1993): On the nonlinear coupling between swell and wind waves. *J. Phys. Oceanogr.*, **23**, 1249-1258.

Mitsuyasu, H. (1966): Interactions between water waves and winds. *Rep. Res. Inst. Appl. Mech., Kyushu University,* **14**, 67-89.

Mitsuyasu, H. (1992): Wave breaking in the presence of Wind Drift and Opposed Swell. *Breaking Waves,* Springer-Verlag Berlin Heidelberg (Pub.), 145-153.

Mitsuyasu, H., F. Tasai, T. Suhara, S. Mizuno, M. Ohkuso, T. Honda, and K. Rikiishi (1975): Observations of the directional spectrum of ocean waves using a cloverleaf buoy. *J. Phys. Oceanogr.*, **5**, 750-760.

Ochi, M. K. and E. N. Hubble (1976): Six-parameter wave spectra. *Coastal Engineering*, 301-328.

Phillips, O. M. and M. L. Banner (1974): Wave breaking in the presence of wind drift and swell. *J. Fluid Mech.*, **66**, 625-640.

Pierson, W. J. (1964): The interpretation of wave spectrums in terms of the wind profile of the wind measured at a contant height. *J. Geophys. Res.*, **69**, 5191-5203.

Pierson, W. J., and L. Moskowitz (1964): A proposed spectral form for fully developed wind seas based on the similarity theory of S. A. Kitaigorodskii. *J. Geophys. Res.*, **69**, 5181-5190.

Plant, W. J. and J. W. Wright (1977): Growth and equilibrium of short gravity waves in a wind-wave tank. *J. Fluid Mech.*, **28**, 767-793.

Reid, J. S. (1995): Observational evidence of the interaction of ocean wind-sea with swell. *Mar. Freshwater Res.*, **46**, 419-425.

Rieder, K. F., J. A. Smith and R. A. Weller (1994): Observed directional characteristics of the wind, wind stress, and surface waves on the open ocean. *J. Geophys. Res.*, **99**, 22589-22596.

Toba, Y., M. Hatori, Y. Imai, and M. Tokuda (1983): Experimental study of elementary processes in wind-waves using wind over regular waves. *Elementary Processes in Wind-Waves*, 117-127.

Young, I. R., S. Hasselmann and K. Hasselmann (1987): Computations of the response of a wave spectrum to a sudden change in wind direction. *J. Phys. Oceanogr.*, **17**, 1317-1338.

Wright, J. W. (1976): The wind drift and wave breaking. *J. Phys. Oceanogr.*, **6**, 402-405.

Appendix: Computation of the Wave Spectrum

The sensor system of the Directional Waverider consists of one vertical accelerometer for measuring wave height and two horizontal accelerometers, in the north and west directions, for measuring wave direction. The vertical accelerometer is mounted on a stabilized disc suspended in a plastic sphere filled with water whereas the horizontal coils are attached to the plastic sphere. After integration of the acceleration signals, the displacement time series are processed by a fast Fourier transform algorithm to produce the wave spectra.

To calculate the one-dimensional energy spectrum, the heave time series is represented by a Fourier series:

$$\zeta(t) = \sum_{n}^{N} A_n e^{i\,2\pi nt/T} \qquad \text{Eq. 20}$$

where ζ is the surface elevation, T is the duration of the series, and A_n are the Fourier components;

$$A_n = \tfrac{1}{2}(a_n + ib_n)$$

where the coefficients a_n and b_n are given by

$$a_n = \frac{2}{T}\sum_{t}^{T}\zeta(t)\cos(2\pi nt/T)\Delta t$$

$$b_n = \frac{2}{T}\sum_{t}^{T}\zeta(t)\sin(2\pi nt/T)\Delta t\,.$$

The spectral density C_{VV} is given by

$$C_{VV} = \frac{1}{2\Delta f}\sum_{n}(a_n^2 + b_n^2). \qquad \text{Eq. 21}$$

To extract the directional information, the auto-spectra and the cross spectra of the horizontal translations need to be calculated. The time series of the horizontal translations are analyzed as above to determine the Fourier components for the north and west measurements. The auto-spectra and quadrature spectra are computed similarly to the computation of the energy spectra (Eq. 21)

$$\begin{aligned} C_{WW}(f) &= \frac{1}{2\Delta f}\sum(a_{WN}^2 + b_{WN}^2) \\ C_{NN}(f) &= \frac{1}{2\Delta f}\sum(a_{NN}^2 + b_{NN}^2) \\ Q_{VW}(f) &= \frac{1}{2\Delta f}\sum(a_{VN}b_{WN} - b_{VN}a_{WN}) \\ Q_{VN}(f) &= \frac{1}{2\Delta f}\sum(a_{VN}b_{NN} - b_{VN}a_{NN}) \end{aligned} \qquad \text{Eq. 22}$$

where C_{WW} and Q_{VW} are the auto- and quad-spectra, and the indices V, N and W denote the heave, north and west components, respectively. As given in the Directional Waverider Manual (Datawell), the direction of wave propagation is determined to be

$$\Theta = \tan^{-1}\left(\frac{Q_{VW}}{Q_{VN}}\right) \qquad \text{Eq. 23}$$

and the directional spread angle is

$$D = \left(x^2 + y^2\right)^{1/2} \qquad \text{Eq. 24}$$

where

$$x = \frac{Q_{VN}}{\left(C_{NN} + C_{WW} + C_{VV}\right)^{1/2}}$$

and

$$y = \frac{Q_{VW}}{\left(C_{NN} + C_{WW} + C_{VV}\right)^{1/2}}.$$

The energy spectrum given by C_{VV} is the omnidirectional frequency wave spectrum $\Phi(f)$ of Section 1.2. The wave spectrum can be expanded into the two-dimensional spectrum if the mean direction and the directional spread distribution are known.

The frequency spectrum can be converted to a wavenumber spectrum by

$$\int \Phi(k,\theta)\, dk\, d\theta = \int \Phi(f,\theta)\, df\, d\theta \qquad \text{Eq. 25}$$

or

$$\Phi(k,\theta) = \Phi(f,\theta)\frac{df}{dk} \qquad \text{Eq. 26}$$

where $\frac{df}{dk}$ is obtained from differentiation of the linear dispersion relation for deep water conditions

$$(2\pi f)^2 = gk\ .$$

REPORT DOCUMENTATION PAGE

Form Approved
OPM No. 0704-0188

1. AGENCY USE ONLY *(Leave blank)*	2. REPORT DATE	3. REPORT TYPE AND DATES COVERED
	March 1998	Technical

4. TITLE AND SUBTITLE
Observations on the Directional Development of Wind-Waves in Mixed Seas

5. FUNDING NUMBERS
N00039-91-C-0072
N00014-96-1-0325

6. AUTHOR(S)
Dung Nguy

7. PERFORMING ORGANIZATION NAME(S) AND ADDRESS(ES)
Applied Physics Laboratory
University of Washington
1013 NE 40th Street
Seattle, WA 98105-6698

8. PERFORMING ORGANIZATION REPORT NUMBER
APL-UW TR9802

9. SPONSORING / MONITORING AGENCY NAME(S) AND ADDRESS(ES)
Office of Naval Research
800 N. Quincy Street
Arlington, VA 22217-5660

10. SPONSORING / MONITORING AGENCY REPORT NUMBER

11. SUPPLEMENTARY NOTES

12a. DISTRIBUTION / AVAILABILITY STATEMENT
Approved for public release;
distribution is unlimited.

12b. DISTRIBUTION CODE

13. ABSTRACT *(Maximum 200 words)*

Sea surface measurements recorded by a Directional Waverider buoy, deployed in the Gulf of Mexico, served as the basis of this investigation into the evolution of wind-waves in mixed seas. Five events of mixed seas were selected and examined in detail. These events chronicled the growth of new wind-seas in the presence of background swell during periods of high wind forcing. Under sufficiently high wind forcing, the wind-sea system developed similarly to cases of pure wind-waves. Wind-wave systems under wind action were found to grow at an angle to the wind vector and away from the mean direction of the low frequency wave system. Under low winds, the wind-sea evolution was dominated by interactions with swell. Situations of mixed seas showed that coupling between wave systems had a stabilizing effect of reducing a multimodal energy spectrum to a unimodal wave spectrum. Coupling between wave systems was observed to occur over local frequencies as predicted by the weakly nonlinear wave-wave interaction theory, and also over a wider frequency range. In cases where the energy spectrum of swell and wind-sea was distinctly bimodal, an equivalent wind-sea was partitioned from the long wave components to allow for a comparison with the growth of pure wind-waves. The directionality of the wind-sea and swell systems was found to influence the development of wind-waves. The directional spread distribution of mixed seas exhibited features different from those of pure wind-seas. The minimum angular spread of wind-seas was generally located at or above the wind-wave peak frequency. Finally, this modest collection of data supported the current hypothesis that opposed swell intensifies wind-wave growth, whereas an aligned swell attenuates wave growth.

14. SUBJECT TERMS
Directional wave spectra, angular spreading of waves, wind-waves

15. NUMBER OF PAGES
119

16. PRICE CODE

17. SECURITY CLASSIFICATION OF REPORT	18. SECURITY CLASSIFICATION OF THIS PAGE	19. SECURITY CLASSIFICATION OF ABSTRACT	20. LIMITATION OF ABSTRACT
Unclassified	Unclassified	Unclassified	SAR